DIAGNOSIS OF ACID PLACEMENT FROM DOWNHOLE TEMPERATURE MEASUREMENTS

A Dissertation

by

XUEHAO TAN

Submitted to the Office of Graduate Studies of
Texas A&M University
in partial fulfillment of the requirements for the degree of

DOCTOR OF PHILOSOPHY

August 2012

Major Subject: Petroleum Engineering

Diagnosis of Acid Placement from Downhole Temperature Measurements

Copyright 2012 Xuehao Tan

DIAGNOSIS OF ACID PLACEMENT FROM DOWNHOLE TEMPERATURE MEASUREMENTS

A Dissertation

by

XUEHAO TAN

Submitted to the Office of Graduate Studies of
Texas A&M University
in partial fulfillment of the requirements for the degree of

DOCTOR OF PHILOSOPHY

Approved by:

Co-Chairs of Committee,	A. Daniel Hill
	Ding Zhu
Committee Members,	Akhil Datta-Gupta
	Charles Glover
Head of Department,	A. Daniel Hill

August 2012

Major Subject: Petroleum Engineering

ABSTRACT

Diagnosis of Acid Placement from Downhole Temperature

Measurements. (August 2012)

Xuehao Tan, B.S., Tsinghua University;

M.S., Texas A&M University

Co-Chairs of Advisory Committee: Dr. A. Daniel Hill
Dr. Ding Zhu

Placement of a sufficient volume of acid in all desired zones is critical for a successful acid stimulation treatment. Particularly in thick, highly heterogeneous carbonate formations, the acid distribution is crucial for optimal stimulation results. A variety of diversion methods are applied in acidizing treatments to evenly place acid along the well, but the effectiveness of these diversion methods is generally only inferred from the rate and pressure behavior during the treatment, and is not known with any certainty. Recently, distributed temperature sensing technology has enabled us to observe dynamic temperature profiles along the wellbore during and immediately following an acid treatment. This technology allows us to monitor and evaluate treatments and diversion methods in real-time and to capture a sequence of temperature profiles at different times during and after acid injection.

We developed a transient thermal model for reservoir, coupled with a wormhole penetration model. Then the reservoir model is combined with a vertical well temperature model as the forward model, which can predict the temperature behavior

inside formation and wellbore during and after a treatment. We applied the forward model in a synthetic two-layer example, and it shows that the temperature increase caused by the reaction between acid and carbonate rock indicates the acid distribution.

An inversion model was also developed to analyze the temperature data measured after treatments to obtain the acid flow profile for a vertical well. The inversion method applied in this work is Markov chain Monte Carlo (MCMC) method, which is a stochastic method to search globally for possible results. We discuss the approach to realize the inversion procedure and to make the inversion more efficient.

We also applied the comprehensive thermal model for hypothetical cases and field cases. The results from the inverse model give us quantitative understanding of acid distribution, which helps us to confirm the success of the acid treatment and diversion methods.

DEDICATION

To my parents,

Fengke Tan and Chao Jin

my wife,

Jiajing Lin

for their love and support

ACKNOWLEDGEMENTS

I would like to thank my co-advisors, Dr. Hill and Dr. Zhu for their support, patience and encouragement throughout my graduate studies. They also gave me innumerable lessons and insights on the workings of academic research in general, which will benefit my future research and work.

I also thank my committee members, Dr. Datta-Gupta and Dr. Glover, for spending time in discussion with me and every precious advice throughout the course of this research.

Thanks also go to my friends and colleagues and the department faculty and staff for making my time at Texas A&M University a great experience.

Finally, thanks to my parents for their encouragement and to my wife for her patience and love.

NOMENCLATURE

A	constant defined in Eq. 2.92
A_j	area of the j^{th} surface
$\bar{A}$	average area
$B(V_i)$	function of interstitial velocity
C^0_{HCl}	concentration of HCl
$\mathbf{C_n}$	covariance matrix
C_{pf}	heat capacity of the wellbore fluid
C_{ps}	heat capacity of acid solution
C_{pR}	heat capacity of rock
$c(t)$	time-dependent function for estimating injection temperature
D	depth
$D(t)$	time function in the wormhole model
D_{total}	total depth of the wellbore section
$\mathbf{d}$	observed data vector
$\mathbf{e}$	residual vector
e_k	specific kinetic energy
e_p	specific potential energy
e_R	specific internal energy of rock
e_s	specific internal energy of acid solution
E	energy

$E_{reaction}$	energy released by reaction in the control volume
f	objective function
$f(t)$	time-dependent function in Ramey's equation
$\mathbf{G}$	sensitivity matrix
$\mathbf{g}$	forward model
g	standard gravity
g_G	geothermal gradient
h	thickness of the layer
h_j	heat transfer coefficient for the j^{th} surface
H	heat for formation
$\mathbf{H}$	Hessian matrix
$\hat{H}$	specific enthalpy of acid solution
$\mathbf{I}$	identity matrix
$\mathbf{J}$	Jacobian matrix
k	permeability
M_R	molecular mass of rock
n_{HCl}	mole of HCl
N_{AC}	acid capacity number
p	pressure
PV_{bt}	pore volumes to break through
$PV_{bt\text{-}opt}$	optimum pore volumes to break through
q_i	injection rate

$\dot{q}_r$	heat flux caused by conduction in radial direction
$\dot{q}_z$	heat flux caused by conduction in vertical direction
Q_{reac}	reaction heat released by consuming unit mole $CaCO_3$ or HCl
R_i	reaction term in formation thermal model
r	radius
s	skin factor
t	time
T	temperature
T_m	measured temperature data
U	overall heat transfer coefficient for the completion
u	velocity of acid solution in the formation
u_w	velocity of fluid in the wellbore
V	volume
V_i	interstitial velocity
$V_{i\text{-}opt}$	optimum interstitial velocity
$\bar{V}_j$	the specific cumulative volume injected into the j^{th} layer
V_{wh}	velocity of wormhole growth
V_{worm}	volume of newly-created wormhole region in one time step
w	mass rate of fluid inside wellbore
W_B	constant in wormhole model
W_{eff}	constant in wormhole model
W_t	time delay constant

x	parameter vector
Z	Z factor for Ramey's equation
z	coordinate in vertical direction

Subscript

a	acid
accu	accumulation
b	surface
d	damaged
dis	dissolved
e	reservoir
f	fluid
G	geothemal
i	injection
in	input
m	number of grid
out	output
p	production
R	reservoir
rw	radial direction at the wellbore radius
s	damaged
w	wellbore

wf	wellbore
wh	wormhole

Superscript

p	number of time step

Greek

β	angle of slanted well
β_F	dissolve power of acid
δx	upgrading parameter
η	wormhole efficiency
λ	average thermal conductivity of acid solution and rock
λ_c	thermal conductivity of cement
λ_e	thermal conductivity of earth
λ_f	thermal conductivity of fluid
λ_s	thermal conductivity of steel
μ	viscosity
ρ_R	density of rock
ρ_s	density of acid solution
ϕ	porosity
ϕ_i	initial porosity
Δ	prefix for difference

TABLE OF CONTENTS

Page

LIST OF FIGURES

Page

Page

Page

LIST OF TABLES

1. INTRODUCTION

1.1 Background

In carbonate formations, matrix acidizing is commonly applied to enhance well performance by removing the near-wellbore formation damage and creating wormholes inside the formation. For a successful acid stimulation treatment, placement of a sufficient volume of acid in all desired zones is critical. Particularly in thick, heterogeneous carbonate formations, acid distribution is crucial for optimal stimulation results. Meanwhile, a variety of diversion methods are applied to evenly place the acid along the well, but the effectiveness of these diversion methods is generally only inferred from the rate and pressure behavior during the treatment, and is not known with any certainty. Therefore, diagnosis of acid flow profile has important impact on optimizing acid treatments and evaluating diversion results.

Recently, distributed temperature sensing technology (DTS) has enabled us to observe dynamic temperature profiles along the wellbore during and immediately following an acid treatment. This technology allows us to monitor and evaluate treatments and diversion methods in real-time and to capture a sequence of temperature profiles at different times. These temperature profiles contain information related to formation properties, treatment effectiveness and acid distribution. It is possible to reveal the acid distribution from the interpretation of downhole temperature measurements.

This dissertation follows the style of *SPE Journal.*

During acidizing treatments, acid solution reacts with carbonate rock and releases the reaction heat, which causes the temperature of the acid solution and rock inside the formation to increase. After treatments, this temperature increase caused by reaction heat also influences the temperature behavior in the wellbore during shut-in and flow-back periods. Reaction heat is strongly dependent on the amount of acid that has been injected. Therefore, the temperature increase by heat of reaction may provide us a mechanism to interpret the acid flow profile from temperature data.

1.2 Literature Review

1.2.1 Downhole Temperature Monitoring

Recently, distributed temperature sensors (DTS) have been widely applied in the field to provide accurate and continuous downhole temperature measurements during production period as well as during the entire acid stimulation treatment (injection, shut-in and flow-back periods).

DTS with optical fibers is based on optical time-domain reflectometry (Carnahan, et al., 1999). A pulsed laser is coupled to an optical fiber that is the sensing element. The light is backscattered as the pulse propagates through the fiber owing to density and composition as well as to molecular and bulk vibrations. Some of the backscattered light is guided back to the light source and split off by a directional coupler to a receiver. Under ideal conditions, the intensity of the backscattered light decays exponentially with time. As the speed of the light within the fiber is known, the distance that the light has passed can be derived from the time along the decay curve.

The backscattered light consists of several spectral components: Rayleigh, Brillouin and Raman bands (**Fig. 1.1**). The Raman spectral band is caused by thermally influenced molecular vibrations. Therefore, the Raman spectral band can be used to obtain information about the distribution of temperature along the fiber. There are two components for the Raman backscattered light, Stokes and Anti-Stokes, one being only weakly dependent on temperature and the other being strongly affected by temperature. The relative intensities between the Stokes and Anti-Stokes are a function of temperature at which the backscattering occurred. Therefore, temperature can be determined at a remote point in the optical fiber.

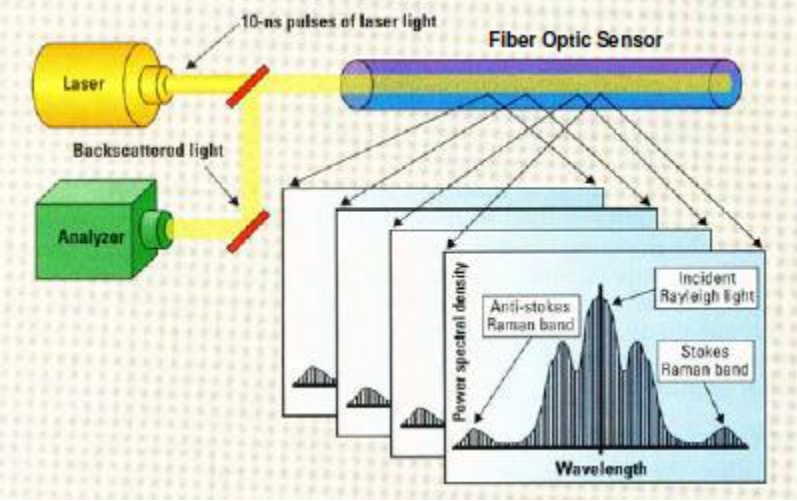

Fig. 1.1—Mechanism of Fiber Optic Temperature Monitoring (Ouyang et al., 2004)

This technology has broad applications. Tolan et al. (2001) showed the application of DTS combined with remotely operated hydraulic interval control valves

(ICVs) as an economical management tool for controlling water encroachment. Johnson et al. (2004) discussed the possibility of using DTS to monitor steam breakthrough in oil and gas producing wells. Johnson et al. (2006) interpreted DTS data to obtain the flow profile for gas wells in a multilayer formation. Huckabee (2009) summarized applications of DTS technology for monitoring hydraulic fracturing stimulation and evaluating well performance for unconventional gas reservoirs.

DTS technology has shown its potential for real-time monitoring well performance and delivering qualitative analysis during production and stimulation. Furthermore, if quantitative analysis of DTS data is available, it will be extremely helpful for understanding downhole flow conditions and optimizing production and stimulation. At this point, temperature models for different flow conditions need to be developed.

1.2.2 Temperature Modeling and Interpretation

Ramey (1962) presented an approximate solution to simulate the transfer of heat between fluid in the wellbore and the earth due to the difference between fluid and formation temperatures. The analytical solution gave an estimation of temperature of fluid, tubing and casing as a function of depth and time during injection of hot or cold fluid. It is assumed that the heat transfer in the wellbore is steady-state and heat transfer to the formation is unsteady radial conduction. Hasan and Kabir (2002) extended Ramey's model to a slanted wellbore. Besides, their model can simulate the fluid temperature in the wellbore during production or injection, as well as two-phase flow inside the wellbore. They introduced the relaxation length parameter depending on the

mass rate in the wellbore, the outer radius of casing, the overall heat transfer coefficient for completion and a time-dependent function. However, these models only considered the fluid flowing inside the wellbore without fluid communicating between wellbore and formation.

Izgec et al. (2006) presented a transient wellbore simulator coupled with a semi-analytical temperature model to simulate wellbore-fluid-temperature profiles in flowing and shut-in wells. The wellbore/reservoir simulator entails simultaneous solution of mass, momentum, and energy balance equations. Furthermore, Sui et al. (2008) developed a coupled wellbore/reservoir thermal model showing that the combination of transient temperature and pressure is sufficiently sensitive to individual layer properties to determine layer permeability and skin values in multilayered systems. Both wellbore and reservoir thermal models are transient. The model requires a multilayer transient testing relying on a series of step changes in surface flow rate with acquisition of stabilized rate profiles before each rate change. Ochi et al. (2008) applied a coupled flow and thermal model to interpret the downhole temperature and pressure data and determined the gas production profile and water flow rate. They assumed that the flow in the reservoir is steady state and the inflow from the reservoir is one-dimensional. The reservoir is segmented and each segment has only single-phase flow. Li and Zhu (2009) used a streamline simulation method to solve the flow problem in the reservoir for fast track of reservoir flow. Then a transient, three-dimensional multiphase reservoir thermal model was developed to calculate the reservoir temperature. Both the reservoir flow model and thermal model were integrated with a horizontal well temperature model to

predict the pressure and temperature distribution in a horizontal well system. The results of their model show that the temperature features in a horizontal well can detect the location and amount of water breakthrough.

All of the above reservoir models are during the production period. However, during acid injection, a reservoir thermal model is also required to simulate the temperature behavior inside the formation with heat of reaction included. Medeiros and Trevisan (2006) simulated the temperature profiles in a sandstone formation during acid treatments. They included the reaction heat in their numerical model and predicted temperature profiles inside the formation. Their results (**Fig. 1.2**) showed that the formation temperature was increased 3-4 K by the contribution of reaction between acid and calcite. They assumed that 8.8% of the rock is calcite and 20% of the calcite will be removed after acidizing. In a carbonate formation, a higher temperature anomaly caused by reaction should be expected.

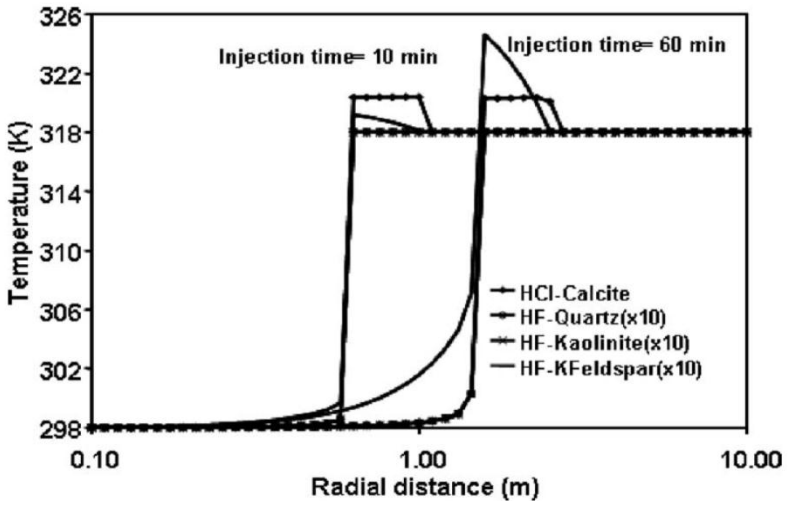

Fig. 1.2—Temperature response in the formation with a constant injection temperature (298 K) (Medeiros and Trevisan, 2006)

1.2.3 Flow Profiling by DTS Data

Based on these temperature models, measured temperature data can be interpreted to diagnose fluid flowing profile during both production and injection. Wang et al. (2008) developed a model based on the steady-state energy balance equation to determine the production profile for a reservoir with multiple production zones. The model is applicable for both gas and oil wells and it contains two parts: forward simulation and flow profiling. The forward simulation calculates temperature behavior for a given production profile by considering geothermal profile, fluid properties, formation properties, well completion as wells as Joule-Thomson effects. The flow profiling part estimates the production profile based on measured temperature data. Yoshioka et al. (2005) discussed their thermal model to determine the inflow profiles of oil, gas and water in horizontal, multilateral and multi-branching wells. The interpretation mainly depends on Joule-Thomson effects. In the model, the reservoir is separated into finite segments. For each segment, the flow is assumed to be single phase, steady state flow, and an analytical solution is used to simulate reservoir fluid flow. Li and Zhu (2009) further developed Yoshioka's model. They used streamline simulation method to solve the flow problem in the reservoir. A transient, three-dimensional, multiphase reservoir thermal model and a horizontal wellbore thermal model were developed to calculate reservoir temperature and wellbore temperature.

Some research has been conducted regarding the determination of the flow profile during water or acid injection. Gao and Jalali (2005) presented a wellbore temperature model based on an analytical solution to interpret distributed temperature

data in horizontal wells. The model can be applied to determine the injection profile for water-injection wells. Clanton et al. (2006) discussed the possibility of using a fiber-optic DTS system for real-time monitoring of acid stimulation treatments. Based on a qualitative analysis of the temperature data, they discussed the application of DTS for monitoring the acid front movement, volume of acid leaking off into the formation, cross-flow during shut-in, and also effectiveness of diversion methods. Glasbergen et al. (2007 and 2009) presented both qualitative and quantitative analysis of temperature data during an acid treatment. They concluded that a qualitative evaluation of continuous wellbore temperature can provide an assessment of fluid placement, diversion effects and the existence of cross flow of fluid between zones within the wellbore. Regarding the quantification of the flow distribution, they first analyzed the effect of flow distribution on the temperature profile by solving the forward problem. Then the results of analysis were applied to quantify the acid distribution from the temperature data, as the inversion problem. For cases in which the temperature profile has a characteristic that can lead to a unique solution, they suggested to solve the inversion problem and obtain the flow profile. When the inversion problem is not unique, they suggested the tracer slug to quantify the flow distribution. To apply the tracer slug concept, they intentionally made a sequence of temperature disturbances and tracked the movement of a fluid slug. Applying this method, the velocity of the fluid slug in the wellbore and consequently the acid leakoff profile can be determined. However, there are some limitations of this tracer slug concept. To obtain the flow profile throughout a treatment, the method requires frequent change in the operation and a sequence of temperature

disturbances needs to be created repeatedly. Meanwhile, the tracer slug may lose its temperature signature with time due to the heat transfer with surroundings.

To realize the interpretation from measured temperature data to flow profile, an inversion method is always necessary to minimize the least-square difference between the forward model results and the observed data. Yoshioka et al. (2005) and Sui et al. (2008) used the gradient-based method, Levenberg-Marquardt method in their inversion models. Li and Zhu (2009) applied the traditional Markov Chain Monte Carlos (MCMC) method, which is a stochastic method searching the solution domain globally and judge the acceptance of samples by the Metropolis-Hastings (M-H) algorithm.

1.3 Objective

The objective of this study is to determine the acid distribution along a vertical well in a multi-layer carbonate formation by using downhole temperature measurements. Based on the acid flow distribution, we can evaluate the efficiency of treatments and improve the design of diverting methods. The interpretation depends on the forward model that is a reservoir thermal model coupled with a wellbore thermal model. The reservoir thermal model is a transient and single phase model by assuming the flow in the formation is 1D radial flow. Convection, conduction and heat of reaction are considered in the reservoir model. Wormhole propagation is also included. For the wellbore thermal model, we include convection and conduction inside wellbore, as well as the thermal effect caused by fluid transporting between the reservoir and the wellbore. The temperature behavior in the wellbore and formation is simulated with the forward model during acid injection, shut-in and flow-back periods.

With the forward model, we can interpret the downhole temperature data measured during shut-in and flow-back periods to the acid injection profile by developing an inversion model. The inversion model can also be used to determine layer properties such as permeability, damaged skin and damage radius from temperature data. We also apply the model to field cases, using temperature data to determine acid distribution and confirm the success of acid treatments and diversion methods.

2. FORWARD MODEL*

2.1 Introduction

In this section, a forward model is developed to predict downhole temperature behavior as a function of acid distribution in a multilayer carbonate reservoir. The forward model consists of a reservoir thermal model and a wellbore thermal model.

The reservoir model is a transient thermal model by assuming the flow inside the formation is 1D, radial and single phase flow. It considers the wormhole growth, convection, conduction and heat of reaction. The reservoir model can calculate the temperature behavior inside formation for different layers during acid injection, shut-in and flow-back periods if the acid distribution is given.

The wellbore model can simulate the transient temperature response inside the wellbore during acid injection, shut-in and flow-back. For the injection period, an analytical solution is applied to simulate the heat transfer between the fluid inside the wellbore and formation. For shut-in and flow-back periods, the governing equations are derived from energy balance for a control volume. The wellbore thermal model considers convection and conduction inside the wellbore, convection from the reservoir to the wellbore and conduction between the formation and the wellbore fluid.

All of the wellbore model equations and the reservoir model equations are coupled and discretized to be solved numerically. With this combined model, we can

---

*Part of this section is reprinted with permission from "Determining Acid Distribution Using Distributed Temperature Measurements" by X. Tan, D. Zhu and A.D. Hill, 2009. Paper SPE 124743.

predict the temperature behavior in both the formation and the wellbore during the entire acid stimulation treatment.

2.2 Reservoir Model

Reservoir thermal model is developed to calculate the temperature inside the reservoir during acid injection, shut-in and flow-back periods. The model considers conduction and convection as well as the heat of reaction, and is developed based on the energy balance over a control volume in the formation. A wormhole propagation model is also required to calculate the position of the wormhole front and determine the heat of reaction.

2.2.1 Reservoir Thermal Model during Acid Injection

The physical system assumed to develop the reservoir thermal model is illustrated in **Fig. 2.1**. Wormholes are assumed to develop from the wellbore. At the front of this wormhole region, we assumed a small reaction region defined as the newly-created wormhole region during a unit time. Beyond the wormhole region and the reaction region, we also have the spent acid region and the formation region. In the spent acid region, the fluid is water containing reaction products, calcium chloride and CO_2. The formation region has not been affected by the acid and is filled with original formation fluid.

Assuming radial flow of an incompressible fluid in the near-wellbore region and instantaneous thermal equilibrium between acid and rock, the formation thermal model for vertical wells can be derived by considering conduction and convection in the near

wellbore formation. Besides, we need to consider the reaction between acid and carbonate rocks which releases heat and results in a temperature increase. Applying an energy balance over the control volume in the near-wellbore region (**Fig. 2.2**), we have

$$E_{accu} = E_{in} - E_{out} + E_{reaction} \quad \text{.....(2.1)}$$

where E_{accu} is the energy accumulation in the control volume, E_{in} is the energy flowing into the control volume, E_{out} is the energy flowing out of the control volume, and $E_{reaction}$ is the energy released by reaction between acid and rock.

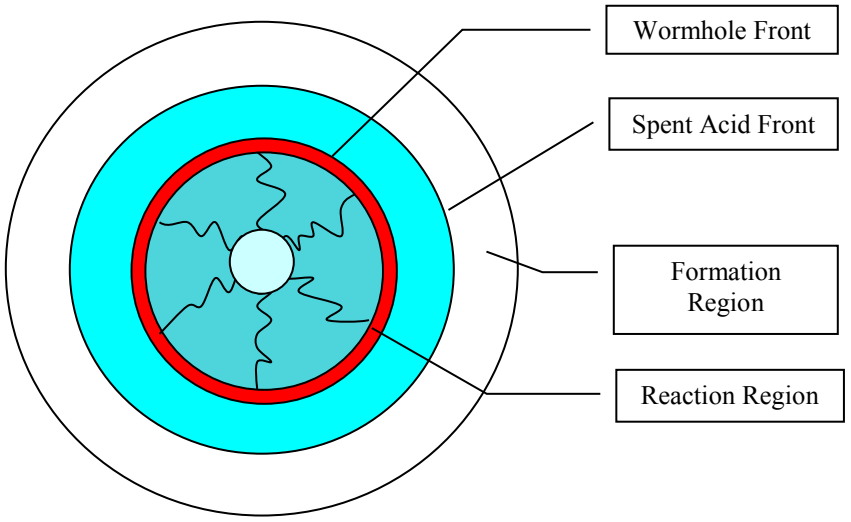

Fig. 2.1—Physical system assumed to develop the formation thermal model

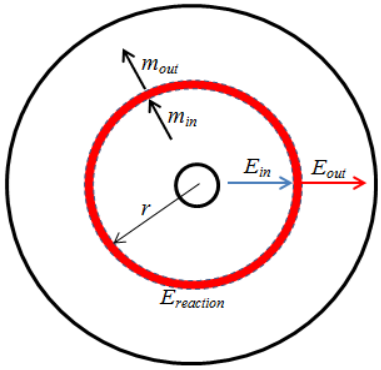

Fig. 2.2—Energy and mass transfer over a control volume of the near-wellbore region

The energy that accumulates in the control volume is

$$E_{accu} = \left\{\left[\rho_s \phi(\hat{u}_s + e_k + e_p)\right]_{t+\Delta t} - \left[\rho_s \phi(\hat{u}_s + e_k + e_p)\right]_t\right\} \times 2\pi r \Delta r \Delta z$$

$$+ \left\{\left[\rho_R (1-\phi)\hat{u}_R\right]_{t+\Delta t} - \left[\rho_R (1-\phi)\hat{u}_R\right]_t\right\} \times 2\pi r \Delta r \Delta z \quad \text{..... (2.2)}$$

In the above equation, ρ_s and ρ_R are densities of solution and rock, respectively, ϕ is the average porosity in the treated region, e_k is the specific kinetic energy, e_p is the specific potential energy, $\hat{u}_s$ is the specific internal energy of acid solution and $\hat{u}_R$ is the specific internal energy of rock. The energy that flows into the control volume is

$$E_{in} = \left[\rho_s u\left(\hat{H} + e_k + e_p\right)\right]_r \times 2\pi r \Delta z \Delta t + \dot{q}_r \times 2\pi r \Delta z \Delta t \quad \text{..... (2.3)}$$

where $\hat{H}$ is the specific enthalpy of the fluid, u is the velocity of fluid, $\dot{q}_r$ is the heat flux caused by heat conduction. The energy that flows out of the control volume is

$$E_{out} = \left[\rho_s u\left(\hat{H} + e_k + e_p\right)\right]_{r+\Delta r} \times 2\pi (r+\Delta r) \Delta z \Delta t + \dot{q}_{r+\Delta r} \times 2\pi (r+\Delta r) \Delta z \Delta t \quad \text{..... (2.4)}$$

The energy released by reaction is

$$E_{reaction} = R_i \times 2\pi r \Delta r \Delta z \Delta t \,, \quad \text{..... (2.5)}$$

where R_i is the reaction heat released in a unit volume of formation during a unit time.

Then the energy balance equation for the control volume is

$$\begin{aligned}
&\Delta\left[\rho_s \phi\left(\hat{u}_s + e_k + e_p\right)\right] \times 2\pi r \Delta z \Delta r + \Delta\left[\rho_R (1-\phi)\hat{u}_R\right] 2\pi r \Delta r \Delta z \\
&= -\Delta\left[\rho_s u\left(\hat{H} + e_k + e_p\right)\right] \times 2\pi r \Delta z \Delta t - \rho_s u\left(\hat{H} + e_k + e_p\right)_{r+\Delta r} 2\pi \Delta r \Delta z \Delta t \\
&\quad - \Delta \dot{q}_r \times 2\pi r \Delta z \Delta t - \dot{q}_{r+\Delta r} 2\pi \Delta r \Delta z \Delta t \\
&\quad + R_i \times 2\pi r \Delta r \Delta z \Delta t \quad \text{..... (2.6)}
\end{aligned}$$

Dividing Eq. 2.6 with $2\pi r \Delta r \Delta z \Delta t$, we have

$$\begin{aligned}
\frac{\Delta\left[\rho_s \phi\left(\hat{u}_s + e_k + e_p\right)\right]}{\Delta t} + \frac{\Delta\left[\rho_R (1-\phi)\hat{u}_R\right]}{\Delta t} &= -\frac{\Delta\left[\rho_s u\left(\hat{H} + e_k + e_p\right)\right]}{\Delta r} - \frac{\rho_s u\left(\hat{H} + e_k + e_p\right)_{r+\Delta r}}{r} \\
&\quad - \frac{\Delta \dot{q}_r}{\Delta r} - \frac{\dot{q}_{r+\Delta r}}{r} + R_i \quad \text{..... (2.7)}
\end{aligned}$$

Taking the limits, $\Delta t \to 0, \Delta r \to 0$, Eq. 2.7 becomes

$$\begin{aligned}
\frac{\partial\left[\rho_s \phi\left(\hat{u}_s + e_k + e_p\right)\right]}{\partial t} + \frac{\partial\left[\rho_R (1-\phi)\hat{u}_R\right]}{\partial t} &= -\frac{\partial\left[\rho_s u\left(\hat{H} + e_k + e_p\right)\right]}{\partial r} - \frac{\rho_s u\left(\hat{H} + e_k + e_p\right)_{r+\Delta r}}{r} \\
&\quad - \frac{\partial \dot{q}_r}{\partial r} - \frac{\dot{q}_{r+\Delta r}}{r} + R_i \quad \text{..... (2.8)}
\end{aligned}$$

After reorganization, the governing equation is

$$\frac{\partial\left[\rho_s \phi\left(\hat{u}_s + e_k + e_p\right)\right]}{\partial t} + \frac{\partial\left[\rho_R (1-\phi)\hat{u}_R\right]}{\partial t} = -\frac{1}{r}\frac{\partial\left[r\rho_s u\left(\hat{H} + e_k + e_p\right)\right]}{\partial r} - \frac{1}{r}\frac{\partial\left(r\dot{q}_r\right)}{\partial r} + R_i \quad \text{..... (2.9)}$$

In Eq. 2.9, e_k can be neglected because the difference between the velocity flowing in and velocity flowing out is small. The change of e_p is zero since the fluid is flowing horizontally in radial direction. Then we have

$$\frac{\partial(\rho_s\phi\hat{u}_s)}{\partial t}+\frac{\partial[\rho_R(1-\phi)\hat{u}_R]}{\partial t}=-\frac{1}{r}\frac{\partial(r\rho_s u\hat{H})}{\partial r}-\frac{1}{r}\frac{\partial(r\dot{q}_r)}{\partial r}+R_i \quad \text{.....(2.10)}$$

If a constant injection rate is also assumed, we have

$$q=2\pi hr_w u_w=2\pi hru \quad \text{.....(2.11)}$$

The product of r and u is a constant. Besides, if ρ_s and ρ_R and ϕ are assumed to be constants, Eq. 2.10 becomes

$$\rho_s\phi\frac{\partial\hat{u}_s}{\partial t}+\rho_R(1-\phi)\frac{\partial\hat{u}_R}{\partial t}=-\frac{1}{r}\rho_s r_w u_w\frac{\partial\hat{H}}{\partial r}-\frac{1}{r}\frac{\partial(r\dot{q}_r)}{\partial r}+R_i \quad \text{.....(2.12)}$$

If the fluid is assumed to be incompressible, we can assume

$$d\hat{H}\approx d\hat{u}_s\approx C_{ps}dT \quad \text{.....(2.13)}$$

$$d\hat{u}_R\approx C_{pR}dT\ . \quad \text{.....(2.14)}$$

In Eqs. 2.13 and 2.14, C_{ps} and C_{pR} are the heat capacities of acid solution and rock, respectively. T is the temperature.

$\dot{q}_r$ in Eq. 2.12 is the heat flux caused by radial heat conduction in the formation and can be calculated by

$$\dot{q}_r = -\lambda \frac{\partial T}{\partial r} \quad \text{.....(2.15)}$$

where λ is the average thermal conductivity for both acid solution and rock, and can be considered as a constant. Substituting Eq. 2.13-Eq. 2.15 into Eq. 2.12, we have the energy balance equation as,

$$\rho_s \phi \frac{\partial (C_{ps} T)}{\partial t} + \rho_R (1-\phi) \frac{\partial (C_{pR} T)}{\partial t} = -\frac{1}{r} \rho_s r_w u_w \frac{\partial (C_{ps} T)}{\partial r} + \frac{1}{r} \frac{\partial}{\partial r} \left(r \lambda \frac{\partial T}{\partial r} \right) + R_i \quad \text{.....(2.16)}$$

We can assume that heat capacities of acid solution and rock, C_{ps} and C_{pR}, are constants, then we have

$$\rho_s \phi C_{ps} \frac{\partial T}{\partial t} + \rho_R (1-\phi) C_{pR} \frac{\partial T}{\partial t} = -\frac{1}{r} \rho_s r_w u_w \frac{\partial T}{\partial r} + \frac{1}{r} \frac{\partial}{\partial r} \left(r \lambda \frac{\partial T}{\partial r} \right) + R_i \quad \text{.....(2.17)}$$

To solve this partial differential equation, the reaction term, R_i, needs to be determined, which will be introduced in the next section.

2.2.2 Determination of the Reaction Term

Because the reaction between carbonate rock and acid is exothermic, reaction heat has significant effect on the temperature behavior. The heat of reaction is shown as a source term in the energy balance equation, the last term on the RHS in Eq. 2.17. To determine the reaction term in the energy balance equation, we need to know two parameters. The first is the reaction heat released when a unit mole of acid is consumed. The second is

the amount of acid consumed during injection, which also indicates the amount of rock that is dissolved.

Assuming the reservoir rock is limestone with $CaCO_3$ as the main composition and the acid used is hydrochloric acid, the reaction formula is

$$CaCO_3 + 2HCl \rightarrow CaCl_2 + H_2O + CO_2 \quad \text{.....(2.18)}$$

The heat of reaction for consuming one mole of hydrochloric acid can be calculated by

$$Q_{reac} = \sum|\Delta H(\text{resultants})| - \sum|\Delta H(\text{reactants})| \quad \text{.....(2.19)}$$

ΔH here is the heat of formation of a certain substance. The heat of formation of reactants and resultants are listed in **Table 2.1**.

TABLE 2.1—HEAT OF FORMATION OF THE REACTANTS AND RESULTANTS FOR LIMESTONE (Perry et al. 1963)

Substance	ΔH, kcal/mol
$CaCO_3$	-289.5
HCl	-39.85
$CaCl_2$	-209.15
H_2O	-68.32
CO_2	-94.05

The heat of reaction for consuming one mole of acid is

$$Q_{reac} = \left|-209.15-68.32-94.05\right| - \left|-289.5-2*39.85\right| \\ = 2.32 kcal/(molCaCO_3) \\ = 1.16 kcal/(molHCl) \quad \text{.....(2.20)}$$

In the SI unit system, we have

$$Q_{reac} = 9.71 kJ/(molCaCO_3) = 4.855 kJ/(molHCl) \quad \text{.....(2.21)}$$

In order to formulate the reaction term, R_i, we need to track the wormhole growth by applying a wormhole model. In the newly-created wormhole region, the volume fraction of dissolved rock and consequently the amount of rock dissolved can be determined by applying wormhole models. In addition, a wormhole model is also required to track the wormhole penetration into the formation because the propagation of wormholes indicates the position of the reaction region. In this work, we applied the wormhole model developed by Buijse and Glasbergen (2006) to simulate the wormhole growth. In their model, the growth rate of the wormhole front, V_{wh}, is given by

$$V_{wh}(r_{wh}) = W_{eff} \cdot V_i(r_{wh})^{2/3} \cdot B(V_i(r_{wh}) \quad \text{.....(2.22)}$$

where V_i is the interstitial velocity of the acid, r_{wh} is the radius of wormhole front, W_{eff} is a constant, and $B(V_i)$ is a function of V_i, defined by

$$B(V_i) = \left(1 - \exp\left(-W_B V_i^2\right)\right) \quad \text{.....(2.23)}$$

and W_B is a constant. W_{eff} and W_B are defined by

$$W_{eff} = \frac{V_{i-opt}^{1/3}}{PV_{bt-opt}} \quad \text{.....(2.24)}$$

$$W_B = \frac{4}{V_{i-opt}^2} \quad \text{.....(2.25)}$$

$V_{i\text{-}opt}$ and $PV_{bt\text{-}opt}$ in the above equations are the optimum interstitial velocity and the optimum pore volumes to breakthrough, respectively. They can be obtained empirically from core flow tests (**Fig. 2.3**).

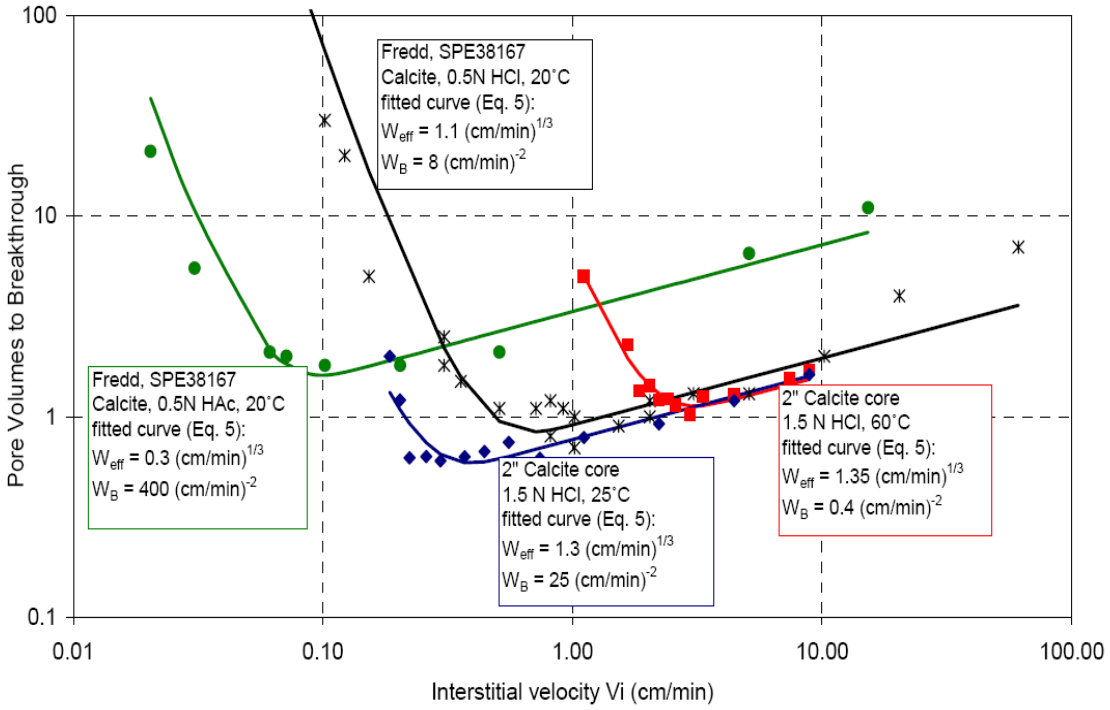

Fig. 2.3—Core flow test results. Pore volumes to breakthrough as a function of injection rate (Buijse and Glasbergen, 2006)

Economides et al. (1994) presented the wormhole efficiency which can be calculated by

$$\eta(t) = N_{AC} PV_{bt}(t) \quad \text{.....(2.26)}$$

Wormhole efficiency is the volumetric fraction of rock that is dissolved in the wormhole region. In Eq. 2.26, PV_{bt} is the pore volume to breakthrough, and N_{AC} is the acid capacity number. They can be calculated by

$$PV_{bt}(t) = \frac{V_i(t)}{V_{wh}(t)} = \frac{V_i(t)^{1/3}}{W_{eff} B(V_i)} \quad \text{.....(2.27)}$$

$$N_{AC} = \frac{\phi_i \beta_F C^0_{HCl} \rho_s}{(1-\phi_i)\rho_R} \quad \text{.....(2.28)}$$

In Eq.2.27, both V_i and V_{wh} are functions of time. As a result, PV_{bt} is also a function of time. In Eq. 2.28, β_F is the dissolving power of the acid, C^0_{HCl} is acid concentration in weight fraction, and ϕ_i is the initial porosity. The volume of rock in the newly-created wormhole region in one time step is given by

$$V_{worm}(t) = \pi\left[r_{wh}(t+\Delta t)^2 - r_{wh}(t)^2\right] \cdot h(1-\phi_i) \quad \text{.....(2.29)}$$

Multiplying the wormhole efficiency to Eq. 2.29, we obtain the volume of dissolved rock in one time step,

$$V_{dis}(t) = \eta(t) \cdot \pi\left[r_{wh}(t+\Delta t)^2 - r_{wh}(t)^2\right] \cdot h(1-\phi_i) \quad \text{.....(2.30)}$$

The number of moles of HCl consumed in one time step is

$$n_{HCl}(t) = \frac{2 \cdot V_{dis}(t) \cdot \rho_R}{M_R} \quad \text{.....(2.31)}$$

where M_R is the molecular weight of $CaCO_3$. Then, the reaction term in the Eq. 2.17 is defined by

$$R_i(t) = \frac{V_{dis}(t)\rho_R Q_{reac}}{M_R \pi r \Delta r \Delta z \Delta t} \quad \text{.....(2.32)}$$

In Eq. 2.32, Q_{reac} is the reaction heat released by dissolving unit mole of HCl.

2.2.3 Reservoir Thermal Model during Shut-In and Flow-Back

After the acid treatments, the well is generally shut down for a short period and temperature data can be measured within this time period. During a shut-in period, we assume that fluid in the formation and wellbore stays static and cross-flow does not exist. We also assume that no reaction happens during the shut-in period. Therefore, the conduction in the formation and wellbore will be the only heat transfer phenomenon to change the temperature. The governing equation for the shut-in period in the formation is

$$\rho_s \phi C_{ps} \frac{\partial T}{\partial t} + \rho_R (1-\phi) C_{pR} \frac{\partial T}{\partial t} = \frac{1}{r} \frac{\partial}{\partial r}\left(r\lambda \frac{\partial T}{\partial r} \right) \quad \text{.....(2.33)}$$

In Eq. 2.33, the terms on the LHS are accumulation terms for acid solution and rock, respectively. On the RHS, the only term is the heat conduction term in radial direction.

When a stimulated well is put back on production after acid stimulation and shut-in period, the fluid inside the formation flows back into the wellbore. The fluid with higher temperature due to the reaction heat will enter the well eventually, causing a temperature anomaly in the wellbore. During this flow-back period, the convection dominates the heat transfer and we also assume that no reaction happens during the flow-back period. The governing equation for the flow-back period is

$$\rho_s \phi C_{ps} \frac{\partial T}{\partial t} + \rho_R (1-\phi) C_{pR} \frac{\partial T}{\partial t} = -\frac{1}{r} \rho_s r_w u_w \frac{\partial T}{\partial r} + \frac{1}{r} \frac{\partial}{\partial r} \left(r\lambda \frac{\partial T}{\partial r} \right) \quad \text{..... (2.34)}$$

The only difference between Eq. 2.33 and Eq. 2.34 is the convection term on the RHS in Eq. 2.34.

Reservoir thermal models for injection, shut-in and flow-back periods have been developed. We can use these models to simulate temperature behavior in the reservoir during the entire acidizing treatment. Meanwhile, to predict the temperature profile in the wellbore, a wellbore thermal model is also necessary.

2.3 Wellbore Model

Since most of the DTS can measure the temperature of fluid inside the wellbore, it is necessary to develop a wellbore thermal model to calculate the temperature in the well during different periods. The wellbore model needs to be coupled with the previously developed formation thermal model to capture the effect of all significant thermal processes involved during the acid stimulation treatment, shut-in and flow-back periods, including heat of reaction, conduction and convection.

2.3.1 Estimation of Injection Temperature

To estimate the acid temperature right before it enters the formation, we need to calculate the temperature of acid when it flows through the non-perforated wellbore as a function of time. Ramey (1962) introduced an analytical method to calculate the temperature behavior in the wellbore during acid injection by considering the heat transfer between the fluid inside the wellbore with lower temperature and the formation

with higher geothermal temperature. However, before acid treatments, it is common that wells are on production for several months. The temperature in the wellbore at the end of the production is higher than the geothermal temperature at the same depth, since the hotter fluid from lower producing zones is flowing upwards in the well. Therefore, the temperature of the near-wellbore formation is heated up and deviates from the original geothermal temperature. Thus, we first need to calculate the wellbore temperature at the end of the production period, and consider this temperature as the new near-wellbore formation temperature for the injection period. Then, Ramey's model will be applied to predict the wellbore temperature during acid injection. With the new higher near-wellbore formation temperature, the acid will be heated up faster compared with the original geothermal temperature.

During production, based on the model developed by Hasan & Kabir (2002), we have

$$T_{wp} = T_R - g_G \sin\beta\left[(D_{total} - D) - \left(1 - e^{(D-D_{total})/z_p}\right)Z_p\right] \quad \text{.....(2.35)}$$

For vertical wells, β=90˚, Eq. 2.35 can be reduced to

$$T_{wp} = T_R - g_G\left[(D_{total} - D) - \left(1 - e^{(D-D_{total})/z_p}\right)Z_p\right] \text{.....(2.36)}$$

where T_{wp} is the wellbore temperature during production period, T_R is the reservoir temperature at the bottomhole, g_G is the geothermal gradient, D_{total} is the total depth of the well above the producing zones, D is the depth, and Z_p is a coefficient for the production period, which is calculated by

$$Z_p = \frac{wC_{pf}\left[\lambda_e + f(t)r_1U\right]}{2\pi\lambda_e r_1 U} \quad \text{.....(2.37)}$$

where w is the mass flow rate inside the wellbore, C_{pf} is the heat capacity of the wellbore fluid, λ_e is the thermal conductivity of the formation, r_1 is the inner radius of the tubing, U is the overall heat transfer coefficient for completion, and f(t) is a time-dependent function that depends on the boundary condition assumed for the heat conduction problem.

To calculate the overall heat transfer coefficient, the completion for non-perforated section can be simplified as **Fig. 2.4**. In Fig. 2.4, S means steel, and is for tubing and casing. W means the water in the annulus, and C stands for cement. r_1 is the inner radius of tubing, r_2 is the outer radius of tubing, r_3 is the inner radius of the casing, r_4 is the outer radius of the casing and r_5 is the outer radius of cement. The thermal conductivity of steel, water and cement are summarized in **Table 2.2** to calculate the overall heat transfer coefficient of the completion.

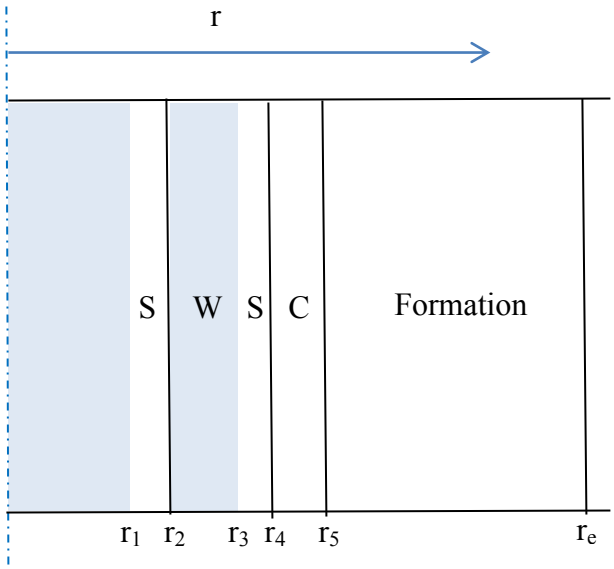

Fig. 2.4—Completion schematic for non-communicating section

TABLE 2.2—THERMAL CONDUCTIVITIES FOR COMPLETION MATERIALS	
Substance	Thermal conductivity, W/(m·K)
Steel	43
Water	0.58
Cement	4

The overall heat transfer coefficient U can be determined by Eq. 2.38 (McAdams, 1942)

$$\frac{1}{U}=\frac{A_1}{h_1A_1}+\frac{x_1A_1}{\lambda_s\overline{A}_1}+\frac{A_1}{h_2A_2}+\frac{A_1}{h_3A_2'}+\frac{x_3A_1}{\lambda_s\overline{A}_3}+\frac{x_4A_1}{\lambda_c\overline{A}_4} \quad \text{.....(2.38)}$$

In Eq. 2.38, x_i is the thickness of the i^{th} layer, h_i is the heat transfer coefficient for the i^{th} surface, A_i is the area of the i^{th} inner surface, A_i' is the area of the i^{th} outer surface, and $\overline{A}_i$ is the average area of the i^{th} layer. These areas can be calculated as

$$A_1 = 2\pi r_w D_{total} \quad \text{.....(2.39)}$$

$$A_2 = 2\pi r_2 D_{total} \quad \text{.....(2.40)}$$

$$A_2^{'} = 2\pi r_3 D_{total} \quad \text{.....(2.41)}$$

$$\overline{A} = \frac{A^{'} - A}{\ln(A^{'} / A)} \quad \text{.....(2.42)}$$

After several months of production, the temperature of the near-wellbore formation is no longer the original geothermal temperature. It is almost the same as the wellbore temperature at the end of the production. During the injection, we assume that the near-wellbore region temperature is the wellbore temperature at the end of production and heat transfer between wellbore and formation is controlled by the difference between the wellbore fluid temperature and the near-wellbore formation temperature. During injection, from Ramey's equation (Ramey, 1962), we have

$$\frac{dT_{wi}}{dD} = -\frac{T_{wi}}{Z_i} + \frac{T_G}{Z_i} \quad \text{.....(2.43)}$$

where T_G is the geothermal temperature, T_{wi} is the wellbore temperature during injection period, and Z_i is a coefficient for injection period, which can be calculated by Eq. 2.37. Instead of using T_G, we use T_{wp} as the temperature of the near-wellbore formation in the equation, then Eq. 2.43 becomes

$$\frac{dT_{wi}}{dD} = -\frac{T_{wi}}{Z_i} + \frac{T_{wp}}{Z_i} \quad \text{.....(2.44)}$$

Multiplying $e^{D/Z}$ on both sides, we have

$$\frac{dT_{wi}}{dD}e^{D/Z_i} = -\frac{T_{wi}}{Z_i}e^{D/Z_i} + \frac{T_{wp}}{Z_i}e^{D/Z_i} \quad \text{.....(2.45)}$$

After reorganization, Eq. 2.45 becomes

$$\frac{dT_{wi}}{dD}e^{D/Z_i} + \frac{T_{wi}}{Z_i}e^{D/Z_i} = \frac{T_{wp}}{Z_i}e^{D/Z_i} \quad \text{.....(2.46)}$$

The two terms on the left-hand side can be combined as

$$\frac{d}{dD}\left(T_{wi}e^{D/Z_i}\right) = \frac{T_{wp}}{Z_i}e^{D/Z_i} \quad \text{.....(2.47)}$$

Integrating Eq. 2.47 with D on both sides,

$$T_{wi}e^{D/Z_i} = \int \frac{T_{wp}}{Z_i}e^{D/Z_i}dD + C(t) \quad \text{.....(2.48)}$$

Then substituting T_{wp} (Eq. 2.36) into the Eq. 2.48 and reorganizing, the final solution is

$$\begin{aligned} T_{wi} &= (T_R - g_G D_{total} + g_G Z_p - g_G Z_i) + g_G D \\ &\quad - \frac{g_G Z_p^2 e^{-D_{total}/Z_p}}{Z_p + Z_i}e^{D/Z_p} + C(t)e^{-D/Z_i} \end{aligned} \quad \text{.....(2.50)}$$

Applying the boundary condition that the wellbore temperature is the same as the injection temperature at the surface, $T_{wi}=T_i$ at D=0, we have

$$T_i = (T_R - g_G D_{total} + g_G Z_p - g_G Z_i) - \frac{g_G Z_p^2 e^{-D_{total}/Z_p}}{Z_p + Z_i} + C(t) \quad \text{.....(2.51)}$$

And the constant C(t) is given by

$$C(t) = T_i - (T_R - g_G D_{total} + g_G Z_p - g_G Z_i) + \frac{g_G Z_p^2 e^{-D_{total}/Z_p}}{Z_p + Z_i} \quad \text{.....(2.52)}$$

We combine Eq. 2.50 and Eq. 2.52, and after simplification, the final solution is

$$T_{wi} = (T_b + g_G Z_p - g_G Z_i) + g_G D - \frac{g_G Z_p^2 e^{-D_{total}/Z_p}}{Z_p + Z_i} e^{D/Z_p} + \left[T_i - T_b - g_G Z_p + g_G Z_i + \frac{g_G Z_p^2 e^{-D_{total}/Z_p}}{Z_p + Z_i} \right] e^{-D/Z_i} \quad \text{.....(2.53)}$$

where T_b is the geothermal temperature at the surface, which can be calculated by

$$T_b = T_R - g_G D_{total} \quad \text{.....(2.54)}$$

2.3.2 Wellbore Thermal Model during Flow-Back and Shut-In

Fig. 2.5 illustrates the energy and mass transfer over a control volume of a communicating section of the wellbore during the flow-back period in a vertical well.

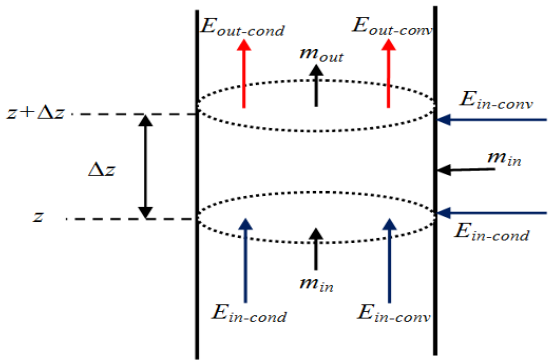

Fig. 2.5—Energy and mass transfer over a control volume of a vertical well during the flow-back period

The wellbore models can be derived by applying energy and mass balances over this control volume. For a vertical well during the flow-back period, the energy balance equation for communicating sections is

$$E_{accu} = E_{in} - E_{out} \quad \text{.....(2.55)}$$

The accumulation energy in the control volume is

$$E_{accu} = \left\{ \left[\rho_s (\hat{u}_s + e_k + e_p) \right]_{t+\Delta t} - \left[\rho_s (\hat{u}_s + e_k + e_p) \right]_t \right\} \times \pi r_w^2 \Delta z \quad \text{.....(2.56)}$$

In the above equation, ρ_s is the density of wellbore fluid, e_k is the specific kinetic energy, e_p is the specific potential energy, and $\hat{u}_s$ is the specific internal energy of fluid. The energy that flows into the control volume is

$$\begin{aligned} E_{in} = & \left[\rho_s u_w \left(\hat{H} + e_k + e_p \right) \right]_z \times \pi r_w^2 \Delta t + \dot{q}_z \times \pi r_w^2 \Delta t \\ & + \left[\rho_s u_{rw} \left(\hat{H}_r + e_k + e_p \right) \right]_{r_w} \times 2\pi r_w \Delta z \Delta t + \dot{q}_r \times 2\pi r_w \Delta z \Delta t \end{aligned} \quad \text{.....(2.57)}$$

where $\hat{H}$ is the specific enthalpy of the fluid, u_w is the velocity of fluid inside the wellbore, $\dot{q}_z$ is the heat flux caused by heat conduction in z direction, u_{rw} is the velocity of fluid at the wellbore radius flowing into the wellbore from the reservoir, $\hat{H}_r$ is the specific enthalpy of the formation fluid entering the well, and $\dot{q}_r$ is the heat flux of heat conduction from the formation to the wellbore. The energy that flows out of the control volume is

$$E_{out} = \left[\rho_s u_w \left(\hat{H} + e_k + e_p \right) \right]_{z+\Delta z} \times \pi r_w^2 \Delta t + \dot{q}_{z+\Delta z} \times \pi r_w^2 \Delta t \quad \text{.....(2.58)}$$

Then after each term is substituted into the energy balance equation, we have

$$\begin{aligned}
&\left\{\left[\rho_s(\hat{u}_s + e_k + e_p)\right]_{t+\Delta t} - \left[\rho_s(\hat{u}_s + e_k + e_p)\right]_t\right\} \times \pi r_w^2 \Delta z \\
&= \left[\rho_s u_w \left(\hat{H} + e_k + e_p\right)\right]_z \times \pi r_w^2 \Delta t + \dot{q}_z \times \pi r_w^2 \Delta t \\
&+ \left[\rho_s u_{rw} \left(\hat{H}_r + e_k + e_p\right)\right]_{r_w} \times 2\pi r_w \Delta z \Delta t \\
&+ \dot{q}_r \times 2\pi r_w \Delta z \Delta t - \left[\rho_s u_w \left(\hat{H} + e_k + e_p\right)\right]_{z+\Delta z} \times \pi r_w^2 \Delta t \\
&- \dot{q}_{z+\Delta z} \times \pi r_w^2 \Delta t \quad \text{..... (2.59)}
\end{aligned}$$

Dividing Eq. 2.59 with $\pi r_w^2 \Delta z \Delta t$, it becomes

$$\begin{aligned}
\frac{\Delta\left[\rho_s\left(\hat{u}_s + e_k + e_p\right)\right]}{\Delta t} &= -\frac{\Delta\left[\rho_s u_w \left(\hat{H} + e_k + e_p\right)\right]}{\Delta z} - \frac{\Delta \dot{q}_z}{\Delta z} \\
&+ \left[\rho_s u_{rw} \left(\hat{H}_r + e_k + e_p\right)\right]_{r_w} \times \frac{2}{r_w} + \frac{2\dot{q}_r}{r_w} \quad \text{..... (2.60)}
\end{aligned}$$

Taking the limits, $\Delta t \to 0$ and $\Delta z \to 0$, we have

$$\begin{aligned}
\frac{\partial\left[\rho_s\left(\hat{u}_s + e_k + e_p\right)\right]}{\partial t} &= -\frac{\partial\left[\rho_s u_w \left(\hat{H} + e_k + e_p\right)\right]}{\partial z} - \frac{\partial \dot{q}_z}{\partial z} \\
&+ \left[\rho_s u_{rw} \left(\hat{H}_r + e_k + e_p\right)\right]_{r_w} \times \frac{2}{r_w} + \frac{2\dot{q}_r}{r_w} \quad \text{..... (2.61)}
\end{aligned}$$

If the fluid is assumed to be incompressible, we can assume

$$d\hat{H} \approx d\hat{u}_s \approx C_{ps} dT \quad \text{..... (2.62)}$$

$$e_k = \frac{1}{2} u^2 \quad \text{..... (2.63)}$$

$$e_p = gz \quad \text{..... (2.64)}$$

After substitution, we have

$$\frac{\partial\left[\rho_s\left(C_{ps}T + \frac{1}{2}u_w^2 + gz\right)\right]}{\partial t} = -\frac{\partial\left[\rho_s u_w\left(C_{ps}T + \frac{1}{2}u_w^2 + gz\right)\right]}{\partial z} - \frac{\partial \dot{q}_z}{\partial z}$$

$$+\left[\rho_s u_{rw}\left(C_{ps}T_{rw}+\frac{1}{2}u_{rw}^2+gz\right)\right]\times\frac{2}{r_w}+\frac{2\dot{q}_r}{r_w} \quad \text{.....(2.65)}$$

where T is the fluid temperature inside the wellbore, T_{rw} is the arriving temperature, ρ_s is the density of the acid solution and C_{ps} is the heat capacity of the acid solution. Both ρ_s and C_{ps} are considered to be constants.

In Eq. 2.65, the term on the LHS accounts for the accumulated energy in the control volume. On the RHS, the first term is convection in the z direction, the second term is conduction in the wellbore, the third term represents the energy from the formation to the wellbore by convection and the last term is the energy transferred from the formation to the wellbore by conduction. In Eq. 2.65, both T_{rw} and $\dot{q}_r$ can be calculated from the reservoir thermal model.

If the flow rate is constant, u_w does not change with time, we have

$$\frac{\partial u_w}{\partial t}=0 \quad \text{.....(2.66)}$$

And for the control volume, gz is a constant, we have

$$\frac{\partial(gz)}{\partial t}=0 \quad \text{.....(2.67)}$$

Besides, the heat flux caused by conduction in the z direction is

$$\dot{q}_z=-\lambda_f\frac{\partial T}{\partial z} \quad \text{.....(2.68)}$$

where λ_f is the thermal conductivity of the wellbore fluid.

Then Eq. 2.65 becomes

$$\rho_s C_{ps}\frac{\partial T}{\partial t} = -\rho_s C_{ps} u_w \frac{\partial T}{\partial z} - \rho_s C_{ps} T \frac{\partial u_w}{\partial z} - \frac{3}{2}\rho_s u_w^2 \frac{\partial u_w}{\partial z} - \rho_s g u_w - \rho_s g \frac{\partial u_w}{\partial z} z + \lambda_f \frac{\partial^2 T}{\partial z^2} + \left[\rho_s u_{rw}\left(C_{ps}T_{rw} + \frac{1}{2}u_{rw}^2 + gz\right)\right]\times\frac{2}{r_w} + \frac{2\dot{q}_r}{r_w} \quad \text{(2.69)}$$

For communicating sections, u_w and u_{rw} are related by

$$u_{wz}\pi r_w^2 + u_{rw} 2\pi r_w \Delta z = u_{wz+\Delta z}\pi r_w^2 \quad \text{(2.70)}$$

After simplification, we have

$$\frac{\partial u_w}{\partial z} = u_{rw}\frac{2}{r_w} \quad \text{(2.71)}$$

Substituting Eq. 2.71 to Eq. 2.69, we get

$$\rho_s C_{ps}\frac{\partial T}{\partial t} = -\rho_s C_{ps} u_w \frac{\partial T}{\partial z} - \rho_s C_{ps} T u_{rw}\frac{2}{r_w} - \frac{3}{2}\rho_s u_w^2 u_{rw}\frac{2}{r_w} - \rho_s g u_w - \rho_s g u_{rw}\frac{2}{r_w} z + \lambda_f \frac{\partial^2 T}{\partial z^2} + \left[\rho_s u_{rw}\left(C_{ps}T_{rw} + \frac{1}{2}u_{rw}^2 + gz\right)\right]\times\frac{2}{r_w} + \frac{2\dot{q}_r}{r_w} \quad \text{(2.72)}$$

After reorganization, we have

$$\rho_s C_{ps}\frac{\partial T}{\partial t} = -\rho_s C_{ps} u_w \frac{\partial T}{\partial z} + \lambda_f \frac{\partial^2 T}{\partial z^2} - 3\rho_s u_w^2 u_{rw}\frac{1}{r_w} - \rho_s g u_w - \rho_s g u_{rw}\frac{2}{r_w} z + \left[\rho_s u_{rw}\left(C_{ps}T_{rw} + \frac{1}{2}u_{rw}^2 + gz\right)\right]\times\frac{2}{r_w} + \frac{2\dot{q}_r}{r_w} \quad \text{(2.73)}$$

For non-communicating sections, since there is no fluid entering the wellbore from the formation, the heat only can be transferred between the wellbore and the

formation by conduction through the completion. The governing equation Eq. 2.73 is reduced to

$$\rho_s C_{ps} \frac{\partial T}{\partial t} = -\rho_s C_{ps} u_w \frac{\partial T}{\partial z} + \lambda_f \frac{\partial^2 T}{\partial z^2} - 3\rho_s u_w^2 u_{rw} \frac{1}{r_w} - \rho_s g u_w - \rho_s g u_{rw} \frac{2}{r_w} z + \frac{2\dot{q}_r}{r_w} \quad \text{.....(2.74)}$$

During a shut-in period, it is assumed that fluid stays static both in the formation and wellbore. We also assumed no cross-flow happens during shut-in period. In this case, u_w and u_{rw} are equal to zero in Eq. 2.74. The energy balance equation is reduced to

$$\rho_s C_{ps} \frac{\partial T}{\partial t} = \lambda_f \frac{\partial^2 T}{\partial z^2} + \frac{2\dot{q}_r}{r_w} \quad \text{.....(2.75)}$$

2.4 Injection Distribution and Layer Properties

In the previous section, our forward model is to predict the temperature behavior with a given injection distribution. Furthermore, the injection rate distribution is dependent on layer properties, such as original permeability, damaged permeability and damage radius. If we extend our forward model to calculate the temperature response from layer properties, rather than the injection profile, we may invert these layer properties from temperature measurements directly.

Economides et al. (1994) introduced a set of equations to calculate the acid distribution based on pressure difference and layer properties, as Eqs. 2.76-2.80.

$$\frac{d\bar{V}_j}{dt} = \frac{\left(2.066 \times 10^{-4}\right)\left(p_{wf} - p_e\right)k_j}{\mu[\ln\left(r_e / r_w\right) + s_j + c_{1,j}\bar{V}_j]} \quad \text{.....(2.76)}$$

In Eq. 2.76, $\overline{V}_j$ is the specific cumulative volume injected into the j^{th} layer (gal/ft), p_{wf} is the wellbore pressure, p_e is the reservoir pressure, r_e is the reservoir radius, r_w is the wellbore radius, k_j is the permeability of the j^{th} layer and s_j is the skin factor for the j^{th} layer. $c_{1,j}$ is defined as

$$c_{1,j} = \frac{2.26*10^{-4}\alpha c_{da}\rho_{da}k_j}{r_w^2} \quad \text{.....(2.77)}$$

$c_{1,j}$ represents the skin effect caused by filter cake. If we assume that there is no filter cake, $c_{1,j}=0$.

The skin effect during acid injection for a layer with damaged zone is

$$s = \frac{k}{k_s}\ln\frac{r_s}{r_{wh}} - \ln\frac{r_s}{r_w} \quad \text{.....(2.78)}$$

where k_s is the damaged permeability, r_s is the damaged radius and r_{wh} is the wormhole radius.

For layers without damaged zone or the wormholes penetrating beyond the damaged region, the skin is

$$s = -\ln\frac{r_{wh}}{r_w} \quad \text{.....(2.79)}$$

In Eq. 2.78 and Eq. 2.79, the wormhole radius is calculated by the Buijse and Glasbergen's wormhole model.

Eq. 2.76 cannot be solved explicitly for $\overline{V}_j$, so an iterative method must be used to solve for $\overline{V}_j$ as a function of injection time. Then we can get the injection rate for each layer as a function of time by

$$q_j = \frac{\Delta \overline{V}_j}{\Delta t} \quad \text{.....(2.80)}$$

Combining this part with our previous developed forward model gives us a new forward model, from which we can calculate the temperature response by knowing the layer properties.

2.5 Forward Model Solution

The developed forward model, including the reservoir model and wellbore thermal model needs to be discretized and solved numerically since the equations are nonlinear and include source terms. The solution of the forward model will show the relationship between the temperature behavior and thermal properties of rock and acid, total injection rate and acid distribution. In this section, both the reservoir thermal model and wellbore thermal model are also validated by comparing with analytical solutions and some numerical simulation results.

2.5.1 Finite Difference Equation for Reservoir Thermal Model

To illustrate the finite difference procedure for the reservoir thermal model, we use the governing equation (Eq. 2.17) during acid injection as an example. The accumulation terms on the LHS are discretized by backward differencing. On the RHS, the convection term with first-order derivative is discretized by the upwind scheme and the conduction

term with second-order derivative is discretized by central differences. The discretized energy balance equation is

$$\rho_s \phi C_{ps} \frac{T_m^{p+1} - T_m^p}{\Delta t} + \rho_R (1-\phi) C_{pR} \frac{T_m^{p+1} - T_m^p}{\Delta t} = -\frac{1}{r_m} \cdot r_w u_w \rho_s C_{ps} \frac{T_m^{p+1} - T_{m-1}^{p+1}}{\Delta r} + \frac{\lambda}{r_m} \frac{T_m^{p+1} - T_{m-1}^{p+1}}{\Delta r} + \lambda \frac{T_{m+1}^{p+1} - 2T_m^{p+1} + T_{m-1}^{p+1}}{\Delta r^2} + R_i \quad \text{.....(2.81)}$$

In Eq. 2.81, m denotes the m^{th} grid and p represents the p^{th} time step.

The numerical solution uses an implicit method to achieve better accuracy, numerical stability and flexibility for time step size compared with explicit method. For each grid, one equation like Eq. 2.81 will be generated, and in total we have n-2 equations. n is the number of grids. These equations combined with two boundary conditions will be solved together to get the temperature at each grid for one time step.

To solve this discretized equation, two boundary conditions and one initial condition are required. The boundary conditions during acid injection are

$$\begin{aligned} T|_{r=r_w} &= T_a \\ T|_{r=r_e} &= T_G \end{aligned} \quad \text{.....(2.82)}$$

where Ta is the acid temperature before it enters the formation, calculated from the analytical injection temperature solution (Eq. 2.53), and T_G is the geothermal temperature at a certain depth. For the initial condition, we assume that temperature

everywhere in the formation is equal to the geothermal temperature at t=0, and it can be written as

$$T|_{t=0,r} = T_G \quad \text{.....(2.83)}$$

2.5.2 Finite Difference Equation for Wellbore Thermal Model

Following the same finite difference procedure as for the reservoir thermal model, the discretized wellbore thermal model during flow-back is

$$\rho_s C_{ps}\frac{T_m^{p+1}-T_m^{p}}{\Delta t} = -\rho_s C_{ps}u_w\frac{T_m^{p+1}-T_{m-1}^{p+1}}{\partial z} + \lambda\frac{T_{m+1}^{p+1}-2T_m^{p+1}+T_{m-1}^{p+1}}{\Delta z^2} - 3\rho_s u_w^2 u_{rw}\frac{1}{r_w} - \rho_s g u_w - \rho_s g u_{rw}\frac{2}{r_w}z + \left[\rho_s u_{rw}\left(C_{ps}T_{rw}+\frac{1}{2}u_{rw}^2+gz\right)\right]\times\frac{2}{r_w}+\frac{2\dot{q}_r}{r_w} \quad \text{.....(2.84)}$$

To solve this equation, boundary conditions are required. At the bottomhole, the temperature equals to the geothermal temperature at the same depth (T_G), and at the bottom of the non-communicating section ($z=D_p$), the temperature in the wellbore is the acid temperature (T_a). T_a is calculated from the injection temperature estimation part. The boundary conditions can be written as

$$\begin{aligned} T|_{z=D_p} &= T_a \\ T|_{z=0} &= T_G \end{aligned} \quad \text{.....(2.85)}$$

The initial condition for the wellbore model is also necessary. We assume that at t=0, the wellbore temperature is a constant that equals to T_a, which is related to the

production rate and production time before the acid stimulation, as well as the injection rate and injection time.

2.5.3 Forward Model Solution Procedure

To simulate the temperature response for a multilayer carbonate formation during the entire acid treatment, we need to solve the coupled formation and wellbore thermal model according to the following procedure:

1. Use the analytical solution (Eq. 2.53) to get the temperature profile in the wellbore after certain time of production and injection. From the solution, we can obtain T_w as a function of depth at the end of the injection and consider it as the initial condition for the wellbore thermal model during shut-in and flow-back. The wellbore temperature at the depth of producing layers, T_a, also can be calculated to be one boundary condition for the reservoir thermal model.
2. Solve the discretized reservoir energy balance equation for acid injection for each layer during the entire injection time. The temperature profile in the formation at the end of injection is considered as the initial condition for shut-in or flow-back reservoir thermal model.
3. Solve the discretized reservoir energy balance equation for each layer during shut-in or flow-back periods. We can obtain the arriving temperature T_{rw} for each time step and each layer.
4. Solve the discretized wellbore energy balance equation during shut-in or flow-back with the temperature profile from step 1 as the initial condition

2.6 Forward Model Validation

In this section, we will validate our forward model by comparing the simplified formation thermal model with analytical solutions and comparing the formation thermal model with the reaction term with published numerical simulation results. For the wellbore thermal model, we will verify the injection temperature estimation part by comparing with FLUENT simulation results with the same simulation conditions.

2.6.1 Compare Reservoir Thermal Model with Analytical Solution

When we neglect the conduction term and reaction heat term in the reservoir thermal model, Eq. 2.17 becomes

$$\frac{\partial(\rho_s \phi C_{ps} T)}{\partial t} + \frac{\partial[\rho_R (1-\phi) C_{pR} T]}{\partial t} = -\frac{1}{r}\frac{\partial(r \rho_s u C_{ps} T)}{\partial r} \quad \text{.....(2.86)}$$

If a constant injection rate is assumed, we have

$$q = 2\pi h r_w u_w = 2\pi h r u \quad \text{.....(2.87)}$$

The product of r and u can be considered as a constant for constant injection rate case. We assume ρ_s, ϕ, C_{ps}, ρ_R, and C_{PR} are constants. Then Eq. 2.86 can be simplified as

$$\left[\rho_s \phi C_{ps} + \rho_R (1-\phi) C_{pR}\right]\frac{\partial T}{\partial t} = -r_w u_w \rho_s C_{ps}\frac{1}{r}\frac{\partial T}{\partial r} \quad \text{.....(2.88)}$$

After reorganization, we have

$$\frac{\partial T}{\partial t} = -\frac{r_w u_w \rho_s C_{ps}}{[\rho_s \phi C_{ps} + \rho_R (1-\phi) C_{pR}]}\frac{1}{r}\frac{\partial T}{\partial r} \quad \text{.....(2.89)}$$

The partial differential equation in this form has an analytical solution, and results are compared with the numerical solution from our forward model by dropping the conduction and heat of reaction terms.

If we define

$$A = \frac{r_w u_w \rho_s C_{ps}}{[\rho_s \phi C_{ps} + \rho_R (1-\phi) C_{pR}]} \quad \text{.....(2.90)}$$

Eq. 2.89 is reduced to

$$\frac{\partial T}{\partial t} + A \frac{1}{r} \frac{\partial T}{\partial r} = 0 \quad \text{.....(2.91)}$$

Using the method of characteristics, the temperature T is moving with the characteristic velocity:

$$\frac{dr}{dt} = \frac{A}{r} \quad \text{.....(2.92)}$$

Thus, the characteristics are given by

$$r = \sqrt{2At + r_0} \quad \text{.....(2.93)}$$

where r_0 is a constant from integration.

Applying the initial condition,

$$T(r,0) = \begin{cases} T_a, r < r_w \\ T_G, r \geq r_w \end{cases} \quad \text{.....(2.94)}$$

We obtain

$$r_0 = r_w^2 \quad \text{.....(2.95)}$$

Then, the solution is given as

$$T(r,t)=\begin{cases}T_a, r<\sqrt{2At+r_w^2}\\ T_G, r\geq\sqrt{2At+r_w^2}\end{cases} \quad \text{.....(2.96)}$$

This analytical solution can be used to verify the numerical solution when only the convection in the formation is considered. A comparison between the analytical solution and numerical solution is in **Fig. 2.6** for 60 minutes and 120 minutes injection. We assumed that the wellbore temperature is 139 °F throughout the injection, and the geothermal temperature is 170 °F. The injection rate is 1 bbl/min and remains constant during the injection. Other parameters used to simulate this example are summarized in **Table 2.3**. In Fig. 2.6, the numerical results show good agreement with the analytical solutions. The numerical results can capture the location of temperature front with acceptable numerical dispersion.

TABLE 2.3—INPUT DATA FOR RESERVOIR THERMAL MODEL VALIDATION		
Wellbore radius	3.5	in
Injection rate	1	bbl/min
Layer thickness	10	ft
Density of acid solution	1070	kg/m^3
Density of rock	2710	kg/m^3
Heat capacity of acid solution	4187	J/(kg·K)
Heat capacity of rock	1040	J/(kg·K)
Acid temperature	139	°F
Geothermal temperature	170	°F
Porosity	0.2	fraction

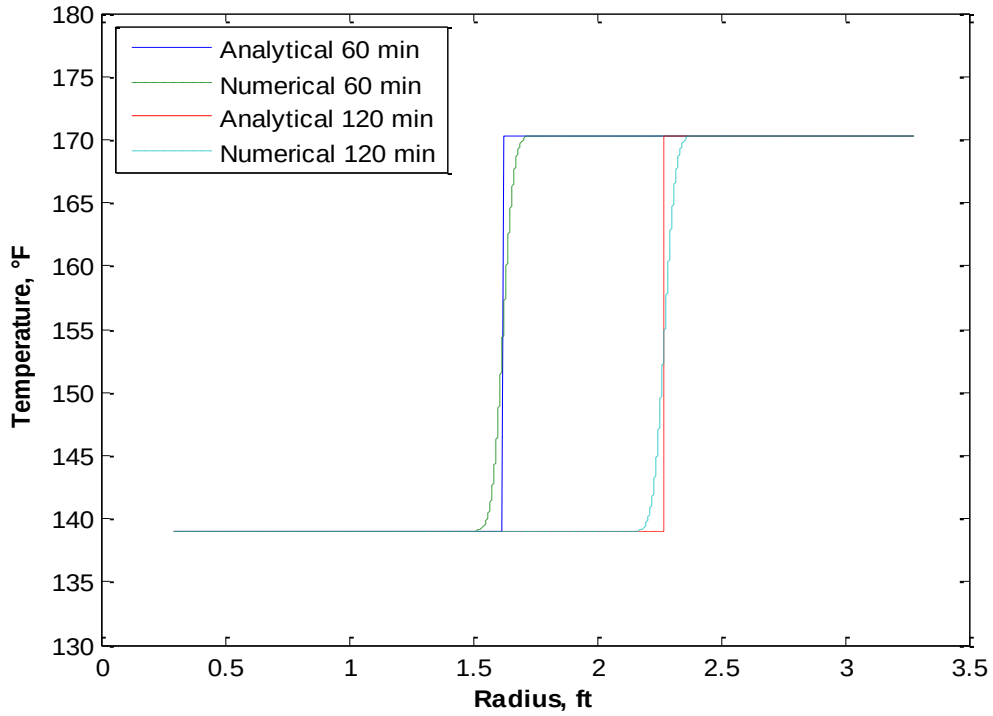

Fig. 2.6—Comparison between analytical solution and simplified numerical solution

2.6.2 Compare Reservoir Thermal Model with Numerical Results

To validate our reservoir thermal model with convection and heat of reaction, we compare the results with Medeiros and Trevisan (2006) numerical solutions. We use the same simulation conditions as their work. The injection temperature is 298 K, and the formation temperature is 318 K. They assumed that 8.8% of the rock is calcite and 20% of calcite will be removed after acidizing. Only the effect of reaction between calcite and acid is shown in **Fig. 2.7**.

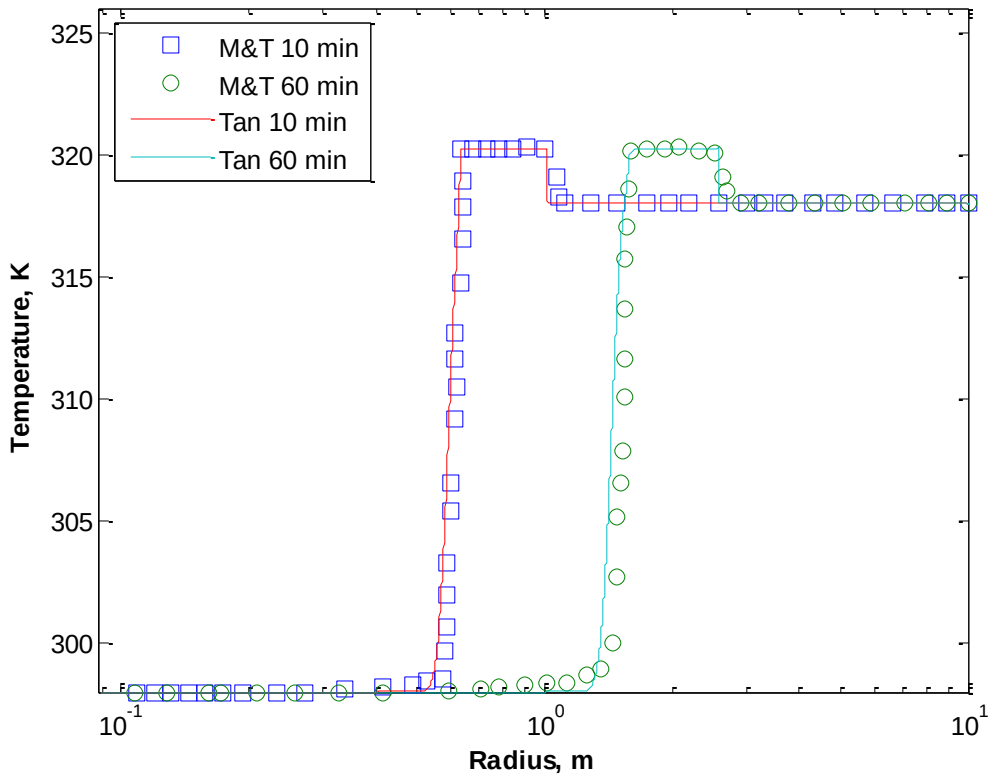

Fig. 2.7—Comparison between numerical solution with heat of reaction and Medeiros and Trevisan's solution

We can see from Fig. 2.7 that our numerical simulation results capture the position of temperature front as well as the shape of the temperature peak caused by reaction. The heights of temperature peaks are also matched. This validates our reservoir thermal model with convection, conduction and reaction terms. Other parameters used to calculate these temperature profiles are listed in **Table 2.4**.

TABLE 2.4—INPUT DATA FOR RESERVOIR THERMAL MODEL VALIDATION WITH MEDEIROS AND TREVISAN'S SOLUTION		
Wellbore radius	3.5	in
Injection rate	1	bbl/min
Layer thickness	3	m
Density of acid solution	1080	kg/m^3
Density of rock	2150	kg/m^3
Heat capacity of acid solution	4180	J/(kg·K)
Heat capacity of rock	1960	J/(kg·K)
Acid temperature	298	K
Geothermal temperature	318	K
Porosity	0.15	fraction

2.6.3 Compare Injection Temperature Estimation with FLUENT Results

To estimate the injection temperature in the wellbore, we applied an analytical solution by combining Hasan & Kabir's solution with Ramey's solution. To validate this solution, we run FLUENT to numerically simulate the temperature behavior in the wellbore with the same injection and production conditions, as well as the same completion configuration. We assumed a 7000 ft long wellbore without inflow or outflow to the formation and acid is injected at the surface. The surface temperature is 100 °F, and the geothermal gradient is 0.01 °F/ft. The other input parameters are listed in **Table 2.5**. **Fig. 2.8** shows the comparison between the results from this work and FLUENT results after 2 months of production at 3000 B/D and 1 hour injection at 5 bbl/min for the 7000 ft wellbore. The results from analytical model and FLUENT have good agreement for both the temperature profile at the end of production and the temperature profile after 1 hour injection, which verifies our combined analytical model.

TABLE 2.5—INPUT DATA FOR ESTIMATION OF INJECTION TEMPERATURE		
Casing O.D.	7	in
Casing I.D.	6.366	in
Tubing O.D.	4.5	in
Tubing I.D.	3.958	in
Surface temperature	100	˚F
Reservoir temperature	170	˚F
Geothermal gradient	0.01	˚F/ft
Earth thermal diffusivity	0.04	ft^2/hr
Earth thermal conductivity	1.4	Btu/(hr·ft·˚F)
Production time	2	months
Production rate	3000	B/D
Injection time	60	minutes
Injection rate	5	bbl/min

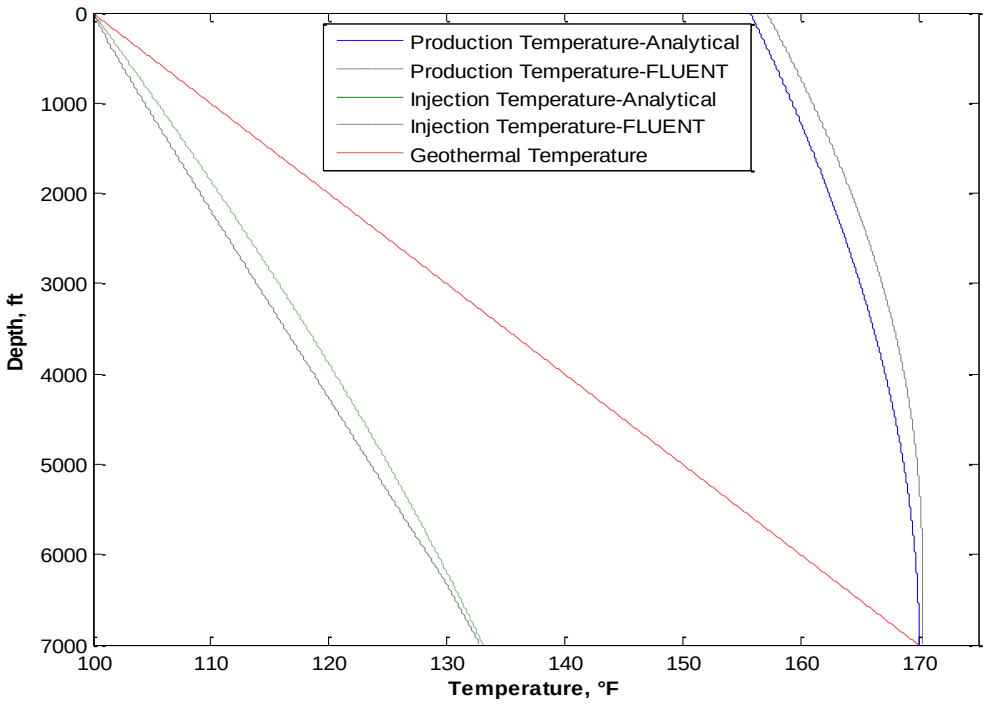

Fig. 2.8—Comparison between analytical solution and FLUENT solution for injection temperature estimation

3. FORWARD MODEL RESULTS AND DISCUSSION*

3.1 Introduction

In this section, the developed forward model will be applied for a hypothetical example throughout the entire acidizing treatment to study the effect of acid distribution and layer properties on the temperature behavior. The objective is to determine if the dynamic temperature response will provide enough information to quantify the acid profile or determine the layer properties. The example we set up is shown in **Fig. 3.1**. The wellbore depth is 7000 ft and there are two 50 ft-thick producing zones. The two layers are separated by a non-producing zone with a thickness of 50 ft.

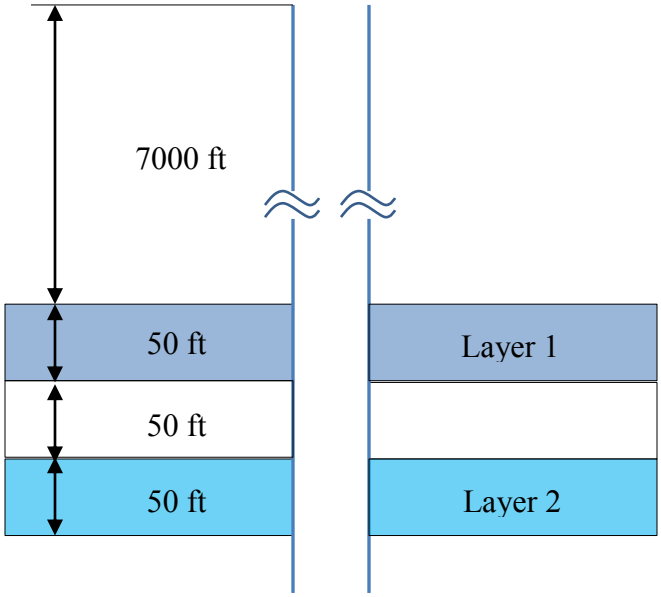

Fig. 3.1—Two-layer example for illustration of the forward model

*Part of this section is reprinted with permission from "Measurement of Acid Placement with Temperature Profiles" by X. Tan, M. Tabatabaei, D. Zhu and A.D. Hill, 2011. Paper SPE 144194.

3.2 Temperature Behavior in the Wellbore during Acid Injection

To estimate the temperature of acid when it enters each layer, we need to calculate the temperature of acid when it flows through the long wellbore section (7000 ft). The completion configuration and other parameters assumed are listed in **Table. 3.1**. Firstly, we calculate the temperature in the wellbore after 2 months of production, as shown in **Fig. 3.2**. In Fig. 3.2, the red dashed line is the geothermal temperature and the blue curve is the temperature in the wellbore after 2 months of production. Since it takes 21 minutes for acid to reach the top productive zone, we calculate the temperature in the well after 21 minutes injection as the green curve in Fig. 3.2. At 7000 ft, the temperature of the acid is 139 ˚F, and that will be used as the acid temperature for the reservoir thermal model.

TABLE 3.1—PARAMETERS FOR ESTIMATION OF INJECTION TEMPERATURE IN THE TWO-LAYER EXAMPLE

Casing O.D.	7	in
Casing I.D.	6.366	in
Tubing O.D.	4.5	in
Tubing I.D.	3.958	in
Surface temperature	100	˚F
Reservoir temperature	170	˚F
Geothermal gradient	0.01	˚F/ft
Earth Thermal diffusivity	0.04	ft^2/hr
Earth Thermal conductivity	1.4	Btu/(hr·ft·˚F)
Production time	2	months
Production rate	3000	B/D
Injection time	21	minutes
Injection rate	5	bbl/min

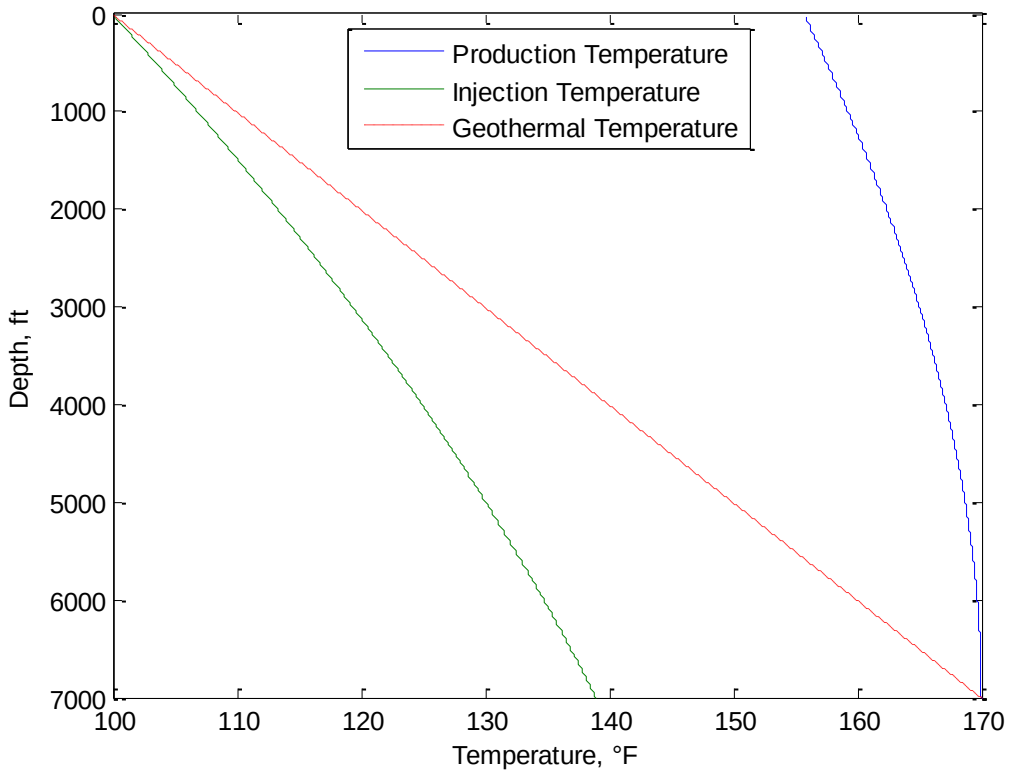

Fig. 3.2—Temperature profiles in the wellbore after 2 months of production and 21 minutes of injection

3.3 Temperature Behavior in the Reservoir during Acid Injection

In the example shown in Fig. 3.1, the two layers have different permeabilities, porosities, and damage conditions. The combination of these reservoir properties and damage conditions controls the volume of injected acid into each layer. Layer properties are assumed and listed in Table. All the other input data are listed in **Tables 3.2** and **3.3** for this example. In Table 3.3, C_{HCl} is the acid concentration, M_R is the molecular weight of carbonate rocks, Q_{reac} is the heat of reaction generated by consuming a unit mole of

acid, T_{G1} and T_{G2} are the geothermal temperature for Layer 1 and Layer 2, respectively, and T_a is the injected acid temperature, which is 139 °F in this case.

TABLE 3.2 —FORMATION PROPERTIES IN THE TWO-LAYER EXAMPLE

	Layer 1	Layer 2
Permeability	10 md	20 md
Damaged permeability	5 md	10 md
Damage radius	1 ft	0.5 ft
Thickness	50 ft	50 ft

TABLE 3.3 — PARAMETERS FOR THE FORWARD MODEL IN THE TWO-LAYER EXAMPLE

Parameters	Values	Units
C_{HCl}	15%	weight fraction
C_{pR}	1040	J/(kg·K)
C_{ps}	4186.8	J/(kg·K)
M_R	0.1	kg/mol
Q_{reac}	4855	J/(molHCl)
r_w	0.3	ft
T_{G1}	170.3	°F
T_{G2}	171.25	°F
T_a	139	°F
ρ_R	2710	kg/m^3
ρ_s	1080	kg/m^3
λ	3.6	W/(m·K)
$V_{i\text{-}opt}$	0.9	cm/min
$PV_{bt\text{-}opt}$	0.95	fraction
ϕ_i	0.2	fraction

With assumed layer properties, we can apply Eqs. 2.76-2.80 to generate the injection rate profile under the constant pressure injection with the Buijse and Glasbergen's wormhole model, as shown in **Fig. 3.3**. For this constant pressure injection case, it is assumed that the pressure difference between the injection pressure and the reservoir pressure is 1000 psi. Each layer has an increasing injection rate due to the propagation of wormholes and the reduction of the skin factor. However, Layer 2, with lower initial skin factor, accepts more acid than Layer 1 during the 20 minutes of injection.

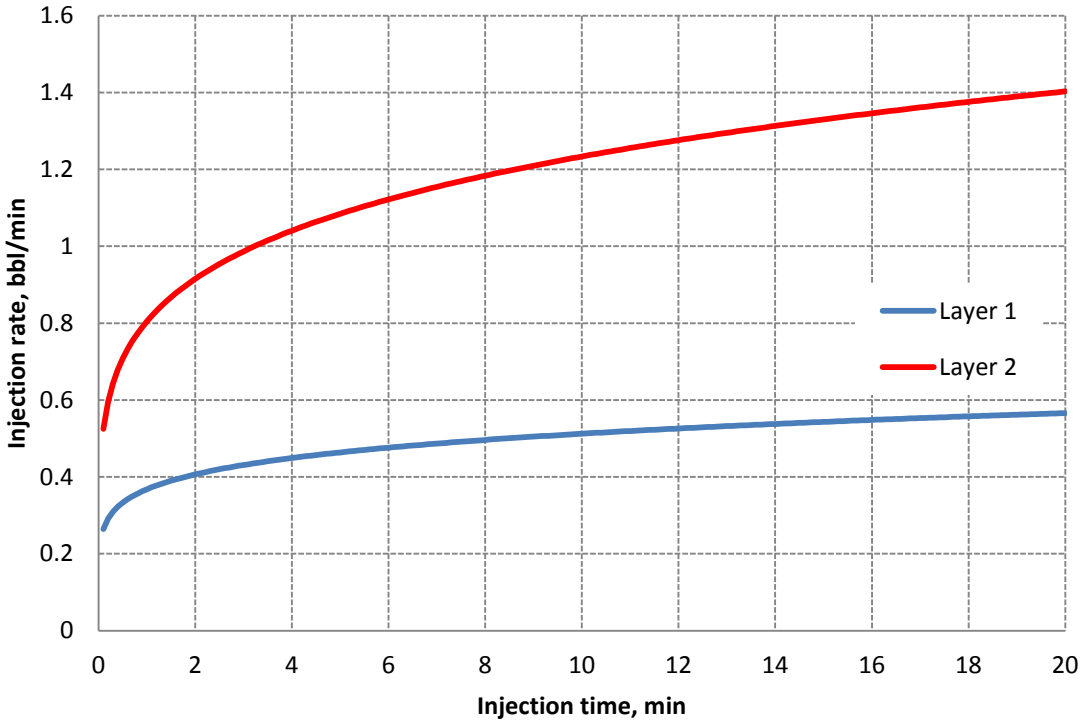

Fig. 3.3—Injection rate distribution for the two-layer example during 20 minutes of constant pressure injection

During acid injection, we simulated the temperature in the formation for both layers, and the result in Layer 1 after 20 minutes injection is plotted in **Fig. 3.4**. There are three sections of these temperature profiles: the low-temperature section near the wellbore is the acid temperature section, the middle high temperature section is the reaction temperature section and the final section is the reservoir temperature section. In the first section, the acid enters the formation and keeps the original injection temperature. In the third section where the formation has not been touched by the acid, the temperature keeps the original geothermal temperature, which is 170.3 ℉ in this case. In the second section, the temperature is increased significantly, which is because a large amount of heat has been released due to the reaction between acid and carbonate rocks.

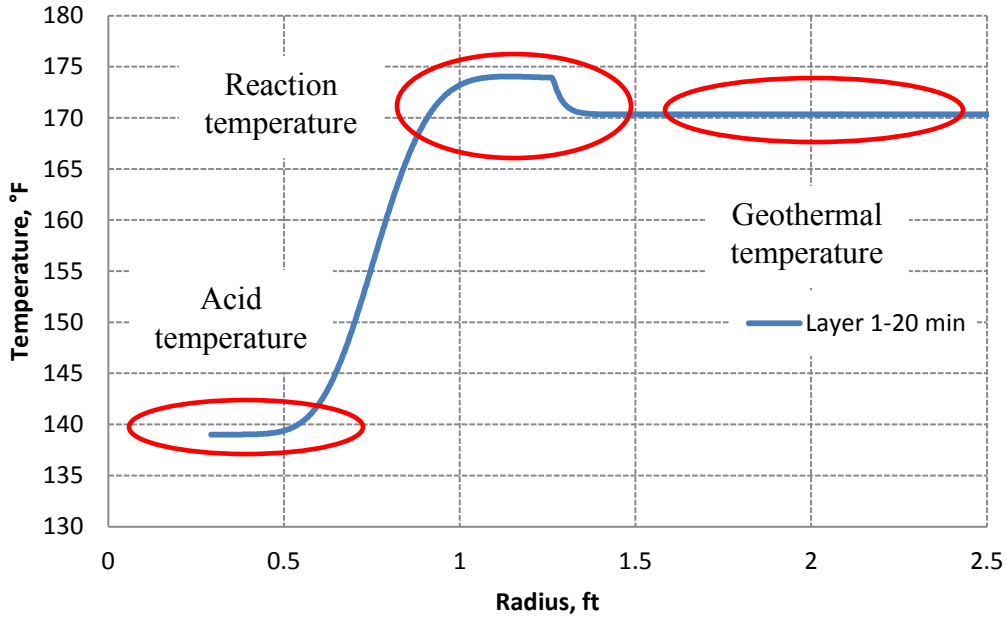

Fig. 3.4—Temperature profile in the formation for layer 1 after 20 minutes of injection

If we continue injecting acid for another 20 minutes, the temperature profile in the formation at the end of 40 minutes is plotted in **Fig. 3.5** as the red curve. Obviously, after another 20 minutes of injection, acid penetrates deeper into the formation. Meanwhile, the shape of temperature peak is also changed due to the dispersion caused by conduction. The change of shape is also because that the fast moving wormhole front, where the reaction happens, stretches the temperature peak.

The comparison of temperature behaviors in layer 1 and layer 2 at the end of 20 minutes injection is shown in **Fig. 3.6**. In Layer 2, acid penetrates deeper than in layer 1 since a larger volume of acid has been injected. Layer 2, with higher injection rate, also has higher temperature in the reaction section (increased 6℉) and Layer 1 has relatively lower temperature in the reaction section (increased 4℉).

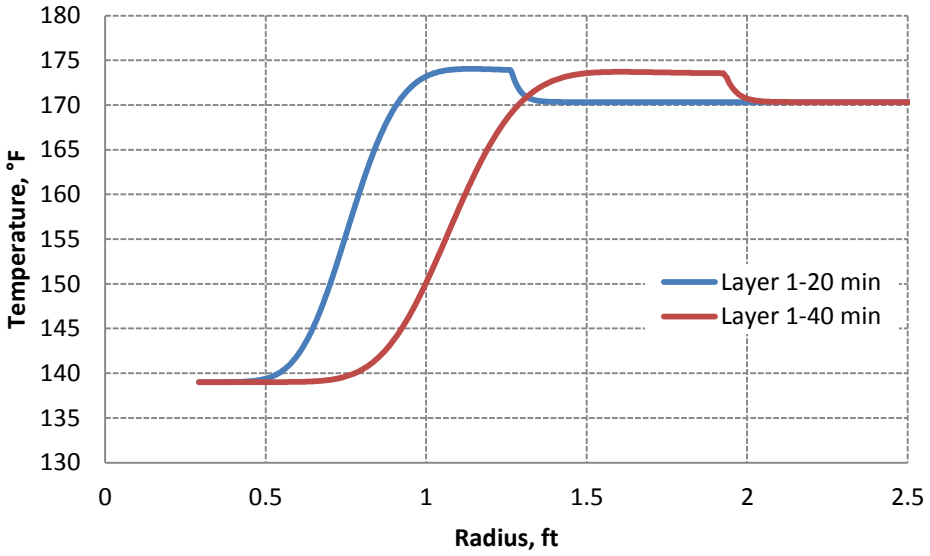

Fig. 3.5—Temperature profiles in the formation for layer 1 after 20 and 40 minutes of injection

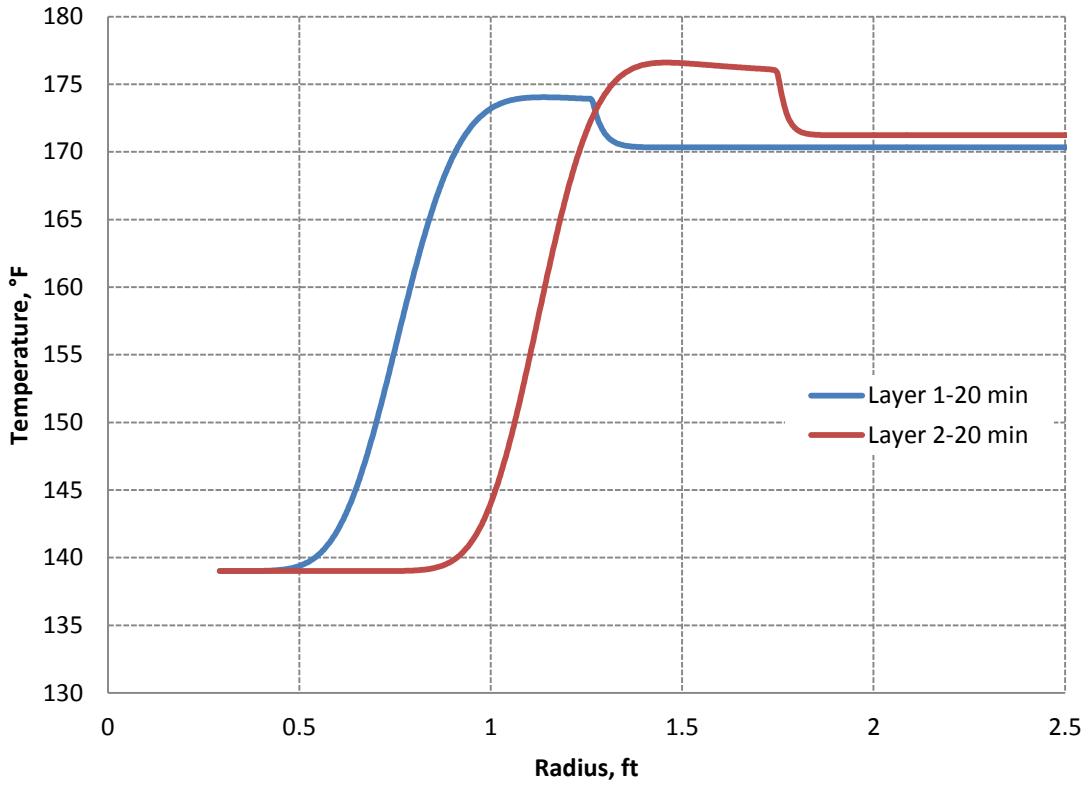

Fig. 3.6—Temperature profiles in the formation for layer 1 and layer 2 after 20 minutes of injection

In previous examples, we assumed that the carbonate rock only consists of limestone. However, in reality, dolomite commonly exists in carbonate reservoirs. If acid is injected into the formation, the reaction between dolomite and HCl can be expressed as

$$CaMg(CO_3)_2 + 4HCl \rightarrow CaCl_2 + MgCl_2 + 2CO_2 + 2H_2O \quad \text{.....(3.1)}$$

Then the reaction heat released is different from the reaction between acid and limestone. The reaction heat is determined by the same approach as limestone.

The reaction heat is calculated by

$$Q_{reac} = \sum|\Delta H(\text{resultants})| - \sum|\Delta H(\text{reactants})| \quad \text{.....(3.2)}$$

The heat of formation of each reactant and resultant is listed in **Table 3.4**.

TABLE 3.4—HEAT OF FORMATION OF THE REACTANTS AND RESULTANTS FOR DOLOMITE (Perry et al. 1963)

Substance	ΔH, kcal/mol
$CaMg(CO_3)_2$	-558.8
HCl	-39.85
$CaCl_2$	-209.15
$MgCl_2$	-189.76
H_2O	-68.32
CO_2	-94.05

Then reaction heat released by acid reacting with dolomite is calculated as

$$\begin{aligned} Q_{reac} &= |-209.15 - 189.76 - 2*68.32 - 2*94.05| - |-558.8 - 4*39.85| \\ &= 5.45 kcal/(molCaMg(CO_3)_2) \\ &= 1.36 kcal/(molHCl) \end{aligned} \quad \text{.....(3.3)}$$

In the SI unit system, we have

$$Q_{reac} = 22.8 kJ/\left(molCaMg\left(CO_3\right)_2\right) = 5.7 kJ/(molHCl) \quad \text{.....(3.4)}$$

We notice that this reaction heat is slightly larger than that of limestone. However, the reaction between the acid and the dolomite is much slower than the reaction between the acid and the calcite. Therefore, the pore volume to breakthrough in a dolomite formation is much larger than that in a limestone formation, which means wormholes may not exist or wormholes are very short and penetrate very slowly in a dolomite formation.

3.4 Temperature Behavior in the Reservoir during Shut-in and Flow-Back

After the acid injection, the well is shut down for a short time or flowed back immediately. During these periods, the temperature increase caused by heat of reaction will be dispersed due to the heat transfer with surroundings. We use the temperature profile in the formation at the end of injection as the initial condition for shut-in and flow-back problems.

It is assumed that the well is shut down for 30 minutes after 20 minutes of injection, and other stimulation conditions are the same as Tables 3.2 and 3.3. The temperature profiles in layer 1 and layer 2 are shown as **Fig. 3.7** and **Fig. 3.8**, respectively. During shut-in period, the temperature anomaly caused by heat of reaction is dispersed because of heat conduction inside the formation. After 30 minutes of shut-in, the temperature anomaly is only 1 °F higher than the geothermal temperature for layer 1 (4 °F before shut-in) and 4 °F for layer 2 (6 °F before shut-in). However, we can notice that the temperature gradient at the wellbore radius is changing with shut-in time. For layer 1, the initial temperature gradient at the wellbore radius is 0, since the near-wellbore formation is filled with cold acid. After 30 minutes of shut-in, the temperature gradient at the wellbore radius has increased to 29 °F/ft. For Layer 2, due to the large volume of acid that has been injected into the formation, the temperature gradient at the wellbore radius is still 0 after 30 minutes. This will result in different heat flux from the reservoir to wellbore for different layers, since the heat flux is proportional to the temperature gradient. Consequently, the wellbore temperature has different behaviors during shut-in period at different depths.

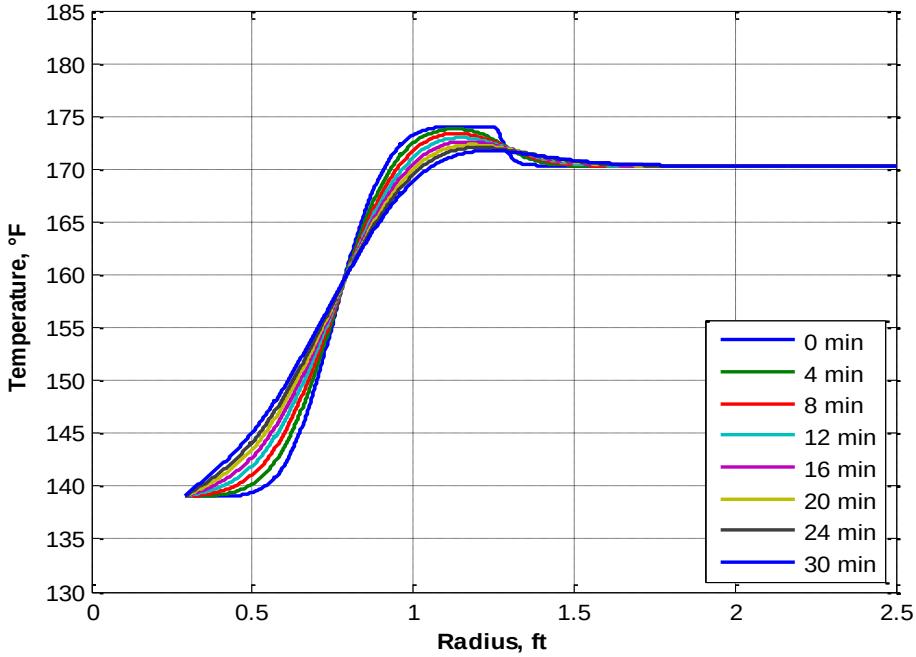

Fig. 3.7—Temperature profiles in the formation for layer 1 during 30 minutes of shut-in

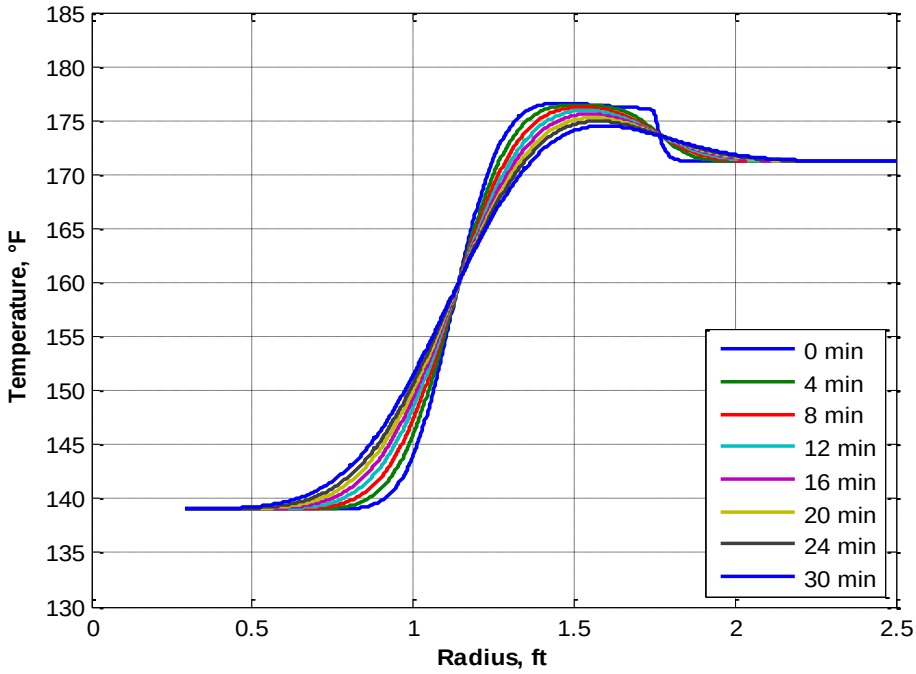

Fig. 3.8—Temperature profiles in the formation for layer 2 during 30 minutes of shut-in

It is also possible that the wellbore is put on production right after the acid injection. In this situation, the temperature anomaly from reaction heat will flow back into the wellbore and be detected by DTS in the wellbore. We assume that the flow-back rate for layer 1 is 0.58 bbl/min and the flow-back rate for layer 2 is 1.4 bbl/min. The temperature profiles in the formation after 10 minutes of flow-back are shown in **Fig. 3.9** and **Fig. 3.10** for layer 1 and 2, respectively. We can observe that the temperature anomaly caused by reaction flows back to the wellbore in both layers. In layer 1, after 10 minutes, the hot fluid caused by reaction already flows into the wellbore. In layer 2, it takes almost the same amount of time for the temperature anomaly to flow into the wellbore since the flow-back rate for layer 2 is higher. These fluids with higher temperature from both layers will be detected by DTS placed inside the wellbore.

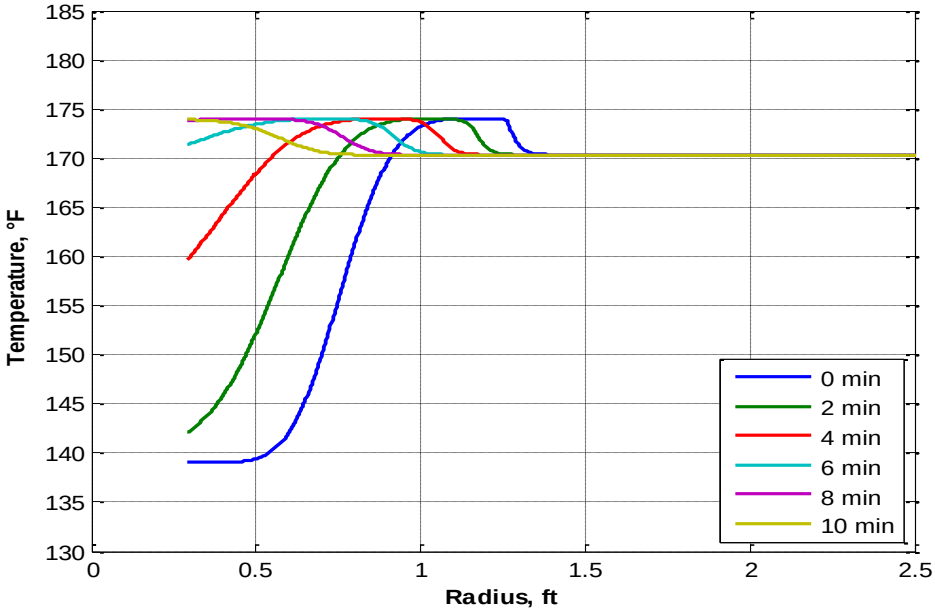

Fig. 3.9—Temperature profiles in the formation for layer 1 during 10 minutes of flow-back

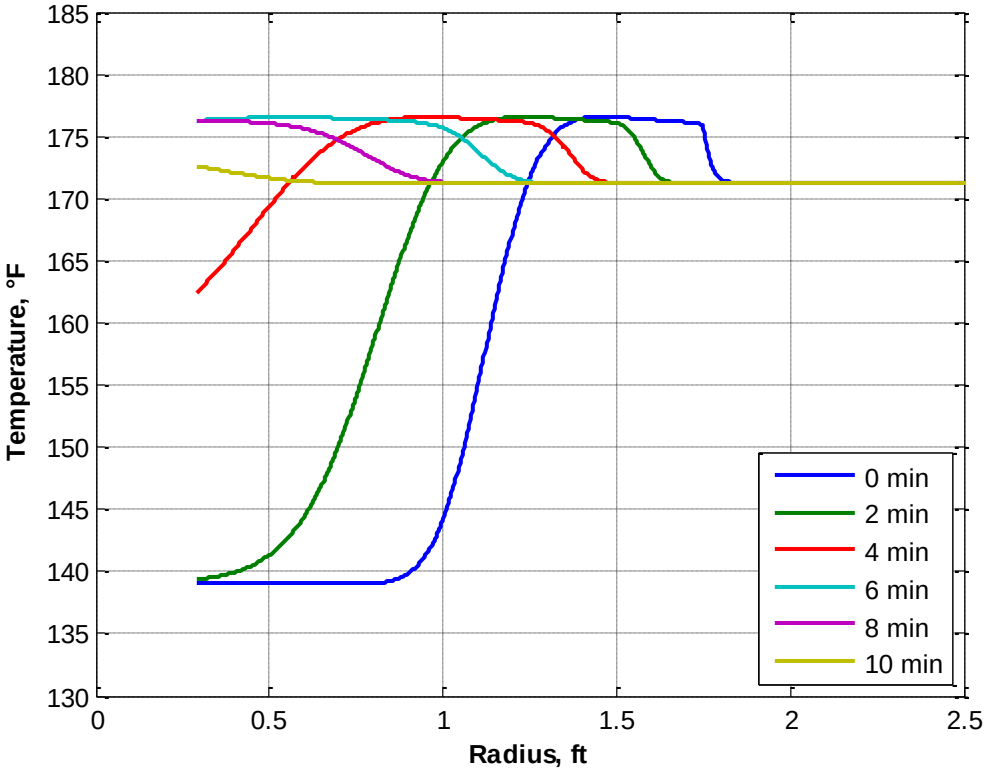

Fig. 3.10—Temperature profiles in the formation for layer 2 during 10 minutes of flow-back

3.5 Temperature Behavior in the Wellbore during Shut-in and Flow-Back

During shut-in period, we assume there is no fluid flowing in the reservoir or wellbore, and no cross-flow happens. Therefore, conduction inside wellbore and conduction from the formation to the wellbore are the only heat transfer phenomena. For the acid stimulation shown in Table 3.2, after 30 minutes shut-in, the wellbore temperature is shown in **Fig. 3.11**. The shaded areas indicate the production layers.

From Fig. 3.11, we can observe that non-communicating sections are warmed by the geothermal temperature, which is the normal warm-back. For the top layer, since

acid was taken during acid injection, it initially shows a lower temperature compared with non-communicating sections. After 22 minutes, the top layers starts to be warmed up by conduction from the formation, which is because the temperature gradient at the wellbore radius is greater than 0 in the top layer after 20 minutes (Fig. 3.7), which will cause a heat flux from the formation to the wellbore and heat up the wellbore fluid. For the bottom layer, due to the large amount of acid that has been injected, after 30 minutes of shut-in, Fig. 3.8 shows that the temperature gradient at the wellbore radius is still 0. Therefore, the heat flux is 0 and the wellbore temperature keeps the original acid temperature during the 30 minute shut-in period.

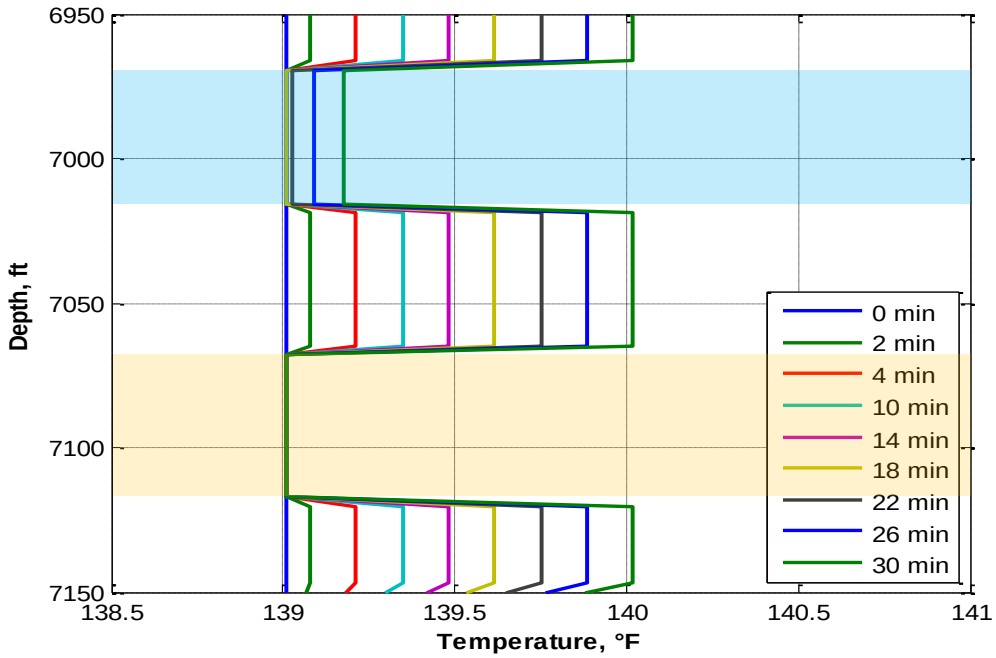

Fig. 3.11—Temperature profiles in the wellbore during 30 minutes of shut-in

If the well is shut down for a longer time, 90 minutes, the temperature profiles in the wellbore are shown in **Fig. 3.12**. After 30 minutes, the fluid in the wellbore at the bottom layer starts to be heated up due to heat flux caused by conduction. Meanwhile, at the top layer, the temperature is also increasing but slower than the bottom layer since less acid has been injected in to the top layer and the temperature increase caused by reaction is less. At 90 minutes, both layers show higher temperature than non-communicating zones, and the bottom layer with more acid injected has the highest temperature. These different temperature behaviors during shut-in depends on the amount of acid that has been injected into different layers and the temperature anomaly caused by reaction, providing us a mechanism to quantify the acid profile from the temperature data measured during shut-in period.

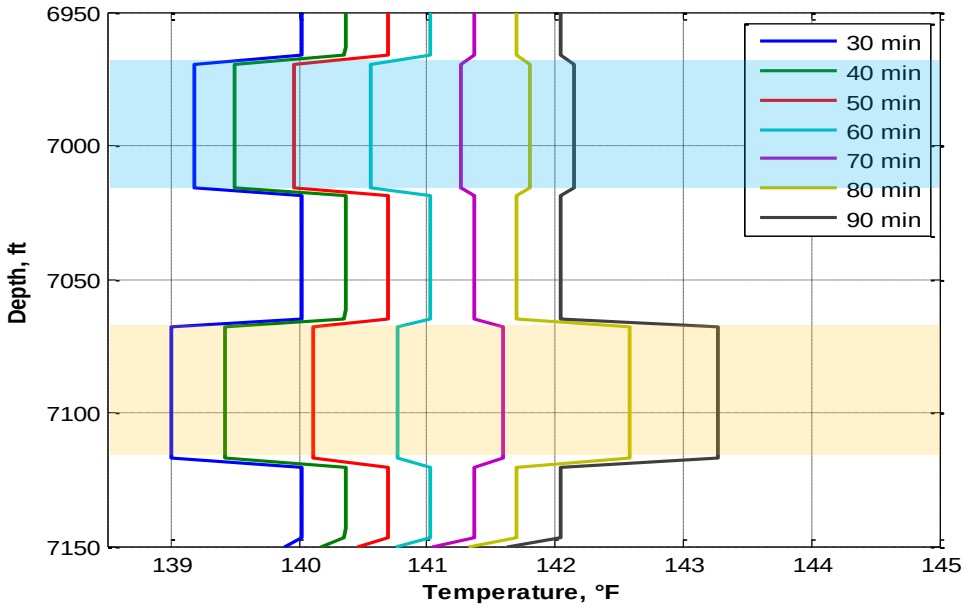

Fig. 3.12—Temperature profiles in the wellbore during 90 minutes of shut-in

When the well starts to produce again following acid injection, the fluid in the formation will flow back into the wellbore. The higher temperature due to the reaction heat will be detected by the sensor. Since the reservoir fluid will mix with the fluid inside the wellbore, the temperature signal is dispersed by this mixing process depending on the amount of reaction heat generated during the injection. If the reaction heat just increased the temperature slightly, there is a possibility that the temperature increase disappears in the wellbore. If the reaction heat generated is significant, the temperature peak may still be detectable after the mixing. **Fig. 3.13** shows the temperature in the wellbore for different flow-back times. Although the mixing of the formation fluid with the wellbore fluid can dissipate the temperature signal, we still detect that at both layer 1 and layer 2, after 3 minutes, there are high temperature anomalies in the wellbore due to the large amount of reaction heat released and the anomaly is flowing upward in the wellbore with time. At 10 minutes, the temperature anomaly from the bottom layer arrives at the upper layer, and mixes with the fluid entering the wellbore from the upper layer. The mixing process changes the shape of the temperature anomaly. This unique phenomenon enables the quantitative determination of the acid distribution during a flow-back period.

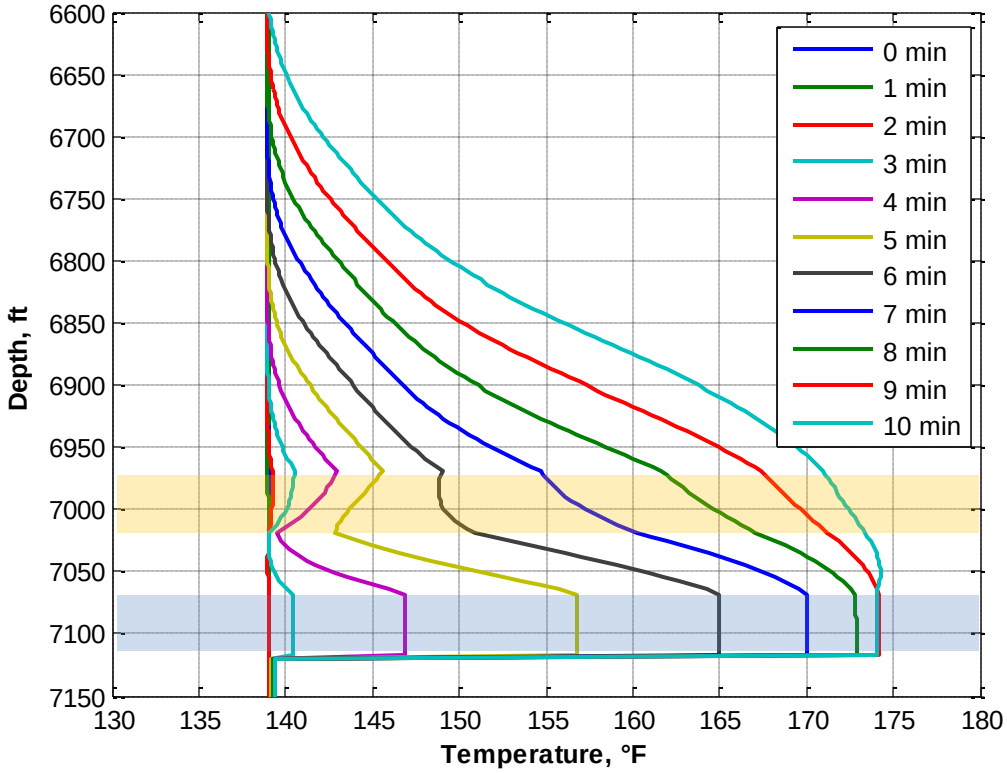

Fig. 3.13—Temperature profiles in the wellbore after 10 minutes of flow-back

4. INVERSION METHOD*

4.1 Introduction

The inversion procedure is required to interpret the measured temperature data to obtain the injection distribution. Inversion models can search a particular domain and find the solution by minimizing the objective function. The objective function for this problem is defined by

$$f = \sum \left(T_m^i - T_{cal}^i \right)^2 \quad \text{.....(4.1)}$$

where T_m is the observed temperature data, and T_{cal} is the temperature calculated by the forward model which is a function of injection distribution.

4.2 Inversion Algorithm

In general there are two types of inversion methods, stochastic methods and gradient-based methods. Gradient-based inversion methods calculate the search vector using the gradient or the Hessian of the objective function. This requires the calculation of parameter sensitivities, which are partial derivatives of the observed data with respect to model parameters (injection rate for this work). Generally, the gradient-based methods provide faster convergence. However, this method may result in local minima when there are many parameters to invert. In such a case, a unique solution is not guaranteed. Stochastic methods can avoid the local minimum problem because they can search the

*Part of this section is reprinted with permission from "Measurement of Acid Placement with Temperature Profiles" by X. Tan, M. Tabatabaei, D. Zhu and A.D. Hill, 2011. Paper SPE 144194.

global parameter space. The main drawback of stochastic methods is that when the parameter number is large, computation becomes expensive, which hinders its application in some cases.

4.2.1 Levenberg-Marquardt's Method

Since the gradient-based inversion methods are relatively faster than the stochastic methods, we started with solving the inverse problem by applying the Levenberg-Marquardt's method (Marquardt, 1963), which is a gradient-based inversion algorithm.

In Levenberg-Marquardt's method, we define the error or residual vector, $\mathbf{e}$ between observation $\mathbf{d}$ and model calculation $\mathbf{g}(\mathbf{x})$ as

$$\mathbf{e} = \mathbf{C}_m^{-1/2}(\mathbf{d} - \mathbf{g}(\mathbf{x})) \quad \text{.....(4.2)}$$

The objective function can be written as

$$\mathbf{f}(\mathbf{x}) = \frac{1}{2}\mathbf{e}^T\mathbf{e} \quad \text{.....(4.3)}$$

For a gradient based method, the objective function is minimized by updating the parameter vector $\mathbf{x}$ by adding a gradient-relative term at each step:

$$\mathbf{x}_{n+1} = \mathbf{x}_n + \delta\mathbf{x}_n \quad \text{.....(4.4)}$$

The update rule for the Levenberg-Marquardt method is

$$\delta\mathbf{x}_n = -(\mathbf{H} + \lambda\mathbf{I})^{-1}\mathbf{w} = -(\mathbf{J}^T\mathbf{J} + \lambda\mathbf{I})^{-1}\mathbf{J}^T\mathbf{e} \quad \text{.....(4.5)}$$

where $\mathbf{w}$ is the gradient of $\mathbf{f}(\mathbf{x})$,

$$\mathbf{w} = \nabla\mathbf{f}(\mathbf{x}) = \mathbf{J}^T\mathbf{e} \quad \text{.....(4.6)}$$

$\mathbf{J}$ is the Jacobian matrix of vector $\mathbf{e}$,

$$\mathbf{J} = \nabla \mathbf{e} = \begin{bmatrix} \frac{\partial e_1}{\partial x_1} & \frac{\partial e_1}{\partial x_2} & \cdots & \frac{\partial e_1}{\partial x_n} \\ \frac{\partial e_2}{\partial x_1} & \frac{\partial e_2}{\partial x_2} & \cdots & \frac{\partial e_2}{\partial x_n} \\ \vdots & \vdots & \vdots & \vdots \\ \frac{\partial e_m}{\partial x_1} & \frac{\partial e_m}{\partial x_2} & \cdots & \frac{\partial e_m}{\partial x_n} \end{bmatrix} \quad \text{.....(4.7)}$$

$\mathbf{H}$ is the Hessian matrix of $\mathbf{f}(\mathbf{x})$, and rigorous solution of Hessian matrix is

$$\mathbf{H} = \mathbf{J}^T \mathbf{J} + \sum_{j=1}^{m} e_j T_j \quad \text{.....(4.8)}$$

where m is the number of elements in **e**, **T** is the Hessian matrix of **e**. For lower residuals or a quasi-linear system, $\mathbf{H}$ can be approximated as

$$\mathbf{H} = \mathbf{J}^T \mathbf{J} \quad \text{.....(4.9)}$$

This approximation does not affect the final minimum but only the search procedure.

The Jacobian matrix, $\mathbf{J}$ can be obtained by

$$\mathbf{J} = \nabla \mathbf{e} = \nabla \left[\mathbf{C}_m^{-1/2} \left(\mathbf{d} - \mathbf{g}(\mathbf{x}) \right) \right] = -\mathbf{C}_m^{-1/2} \cdot \nabla \mathbf{g}(\mathbf{x}) = -\mathbf{C}_m^{-1/2} \cdot \mathbf{G} \quad \text{.....(4.10)}$$

where $\mathbf{G}$ is the sensitivity matrix of forward model $\mathbf{g}$. So, it can be calculated from forward model by giving a small perturbation of $\mathbf{x}$. If we use injection rate, q, as the parameter, the sensitivity matrix is:

$$\mathbf{G} = \nabla \mathbf{g}(\mathbf{x}) = \begin{bmatrix} \frac{\partial T_1}{\partial q_1} & \frac{\partial T_1}{\partial q_2} & \cdots & \frac{\partial T_1}{\partial q_n} \\ \frac{\partial T_2}{\partial q_1} & \cdots & \cdots & \frac{\partial T_2}{\partial q_n} \\ \vdots & \vdots & \vdots & \vdots \\ \frac{\partial T_j}{\partial q_1} & \cdots & \cdots & \frac{\partial T_j}{\partial q_n} \end{bmatrix} \quad \text{.....(4.11)}$$

The sensitivity is determined by

$$\frac{\partial T_j^{cal}}{\partial q_i} = \frac{T_j^{cal}(q_1,\cdots,q_i+\delta q_i,\cdots,q_N) - T_j^{cal}(q_1,\cdots,q_i,\cdots,q_N)}{\delta q_i} \quad \text{.....(4.12)}$$

We use the perturbation $\delta q_i \approx 0.01 q_i$. For a system with N parameters, we need calculate the forward model N times to obtain the sensitivity in one update step.

Therefore, we can calculate the update parameter $\delta \mathbf{x}_n$ by

$$\delta \mathbf{x}_n = -(\mathbf{H}+\lambda \mathbf{I})^{-1}\mathbf{w} = -\left(\mathbf{G}^T\mathbf{C}_m^{-1}\mathbf{G}+\lambda \mathbf{I}\right)^{-1}\mathbf{G}^T\mathbf{C}_m^{-1}(\mathbf{d}-\mathbf{g}(\mathbf{x})) \quad \text{.....(4.13)}$$

Starting from an initial guess $\mathbf{x}_0$, we can use Eq. 4.13 to calculate the update parameter $\delta \mathbf{x}$ iteratively. The iteration will stop when the objective function converges by using the following criteria:

$$\mathbf{f}(\mathbf{x}_n) - \mathbf{f}(\mathbf{x}_{n+1}) < \varepsilon_1 \quad \text{.....(4.14)}$$

Or

$$\frac{\mathbf{f}(\mathbf{x}_n) - \mathbf{f}(\mathbf{x}_{n+1})}{\mathbf{f}(\mathbf{x}_n)} < \varepsilon_2 \quad \text{.....(4.15)}$$

where ε_1 and ε_2 are relative small residuals.

However, we discovered that this method is inefficient especially for the cases with more than 2 parameters to be inverted. For many cases we have run, this method caused the searching path to be trapped in the local minima and we were not able to determine the true injection distribution. In addition, we observed that the Levenberg-Marquardt's inversion method is highly dependent on the initial guess.

4.2.2 Markov Chain Monte Carlo Method

In our study, we interpreted the measured temperature data by using Markov Chain Monte Carlo (MCMC) method (Wadsley, 2005). MCMC method is a stochastic inversion algorithm which works well for non-linear problems like this one. The general idea of MCMC method is to construct a Markov chain by sampling from a proposed distribution. In our case, the proposed distribution is uniform because all the samples have the same probability without any prior information. In this work, we choose the acid injection rate for each time period as the parameter and use the traditional Metropolis-Hastings (M-H) MCMC algorithm (Metropolis et al., 1953 and Hastings, 1970) to minimize the objective function. The MCMC inversion procedure is as follows:

1. Obtain the observed data.
2. Propose an initial guess of acid distribution.
3. Use the initial guess to run the forward model, and get the temperature response.
4. Calculate the objective function, f.
5. Generate a new acid distribution based on a random sampler. In this work, we use the uniform distribution to sample.
6. Run the forward model again and get the new temperature data and new objective function.
7. Use M-H algorithm to decide the acceptance of the new acid distribution.
8. If the new acid distribution is accepted, store it and go to step 2, else, go to step 5.

The M-H algorithm follows these steps:

1. Calculate $R(x_1, x_2) = \dfrac{f(x_2)q(x_1|x_2)}{f(x_1)q(x_2|x_1)}$.

2. Because we use uniform distribution for Step 5, so $R(x_1, x_2) = \dfrac{f(x_2)}{f(x_1)}$

3. $\rho = \min\{1, \quad R(x_1, x_2)\}$, if $\rho > 1$, accept the new injection rates, else

4. Draw u from uniform $U = (0,1)$, if $u \le \rho$, accept the new injection rates, else, keep the old injection rates in the chain.

After testing the MCMC method, we observe that although it takes more time to find the solution for the inversion problem, MCMC method works perfectly for the cases with several parameters, and is able to locate the global minimum of the objective function.

4.3 Hypothetical Examples for Inversion Method

4.3.1 Inversion Results for Constant Pressure Injection Case

The same two-layer example used to test the forward model is applied to show the results of the inverse model. The injection rate for each layer is assumed to be Fig. 3.3. The objective is to invert the injection rate of each layer from temperature "measurements". In this synthetic case, Fig. 3.13 is considered as the measured temperature data to start the inversion procedure. Other input parameters are listed in Table 3.3. We run the inverse model by applying the MCMC method. Without any prior information, the most reasonable initial guess is that acid distribution is uniform for two layers. With the uniform initial guess, the temperature profiles calculated by forward

model and measured temperature data are plotted in **Fig. 4.1** after 5 and 10 minutes of flow-back. It is obvious that the temperature profile from the forward model does not catch the characteristics of the temperature anomaly at the location of two production layers.

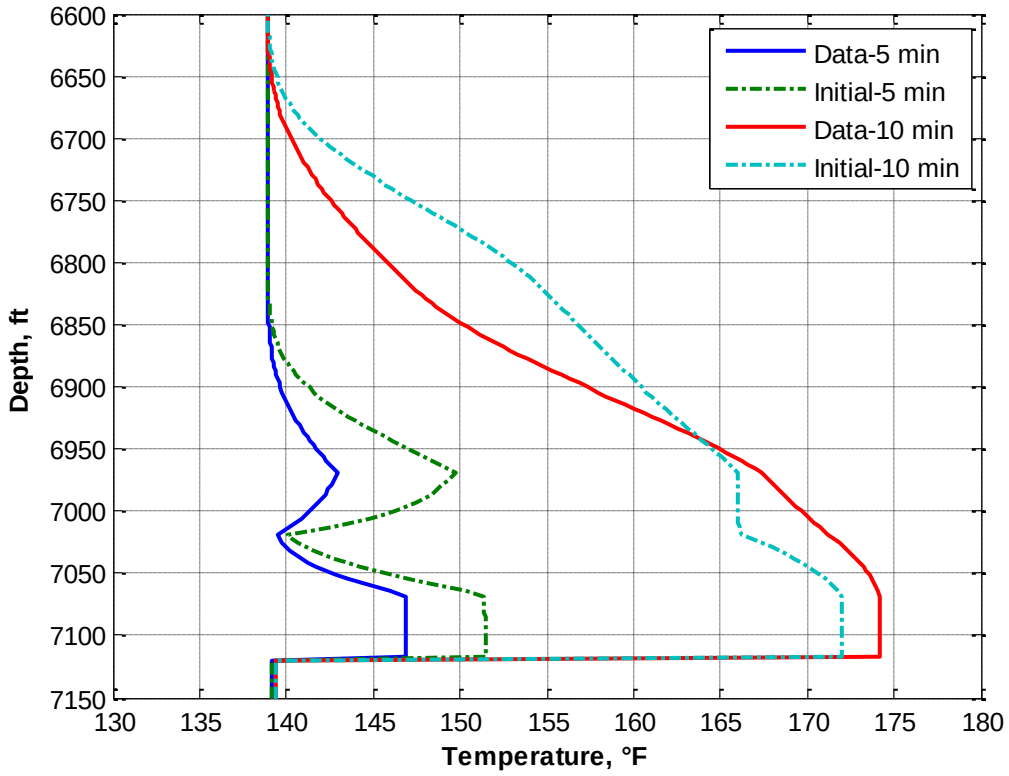

Fig. 4.1—Comparison of temperature profiles calculated with uniform initial guess and temperature data for the case with constant pressure injection

To invert the continuous injection rate distribution, computation is extremely extensive. To save the computational time of the inverse problem, we divided the entire

injection period into several time periods and assign a constant injection rate for each time period (**Fig. 4.2**).

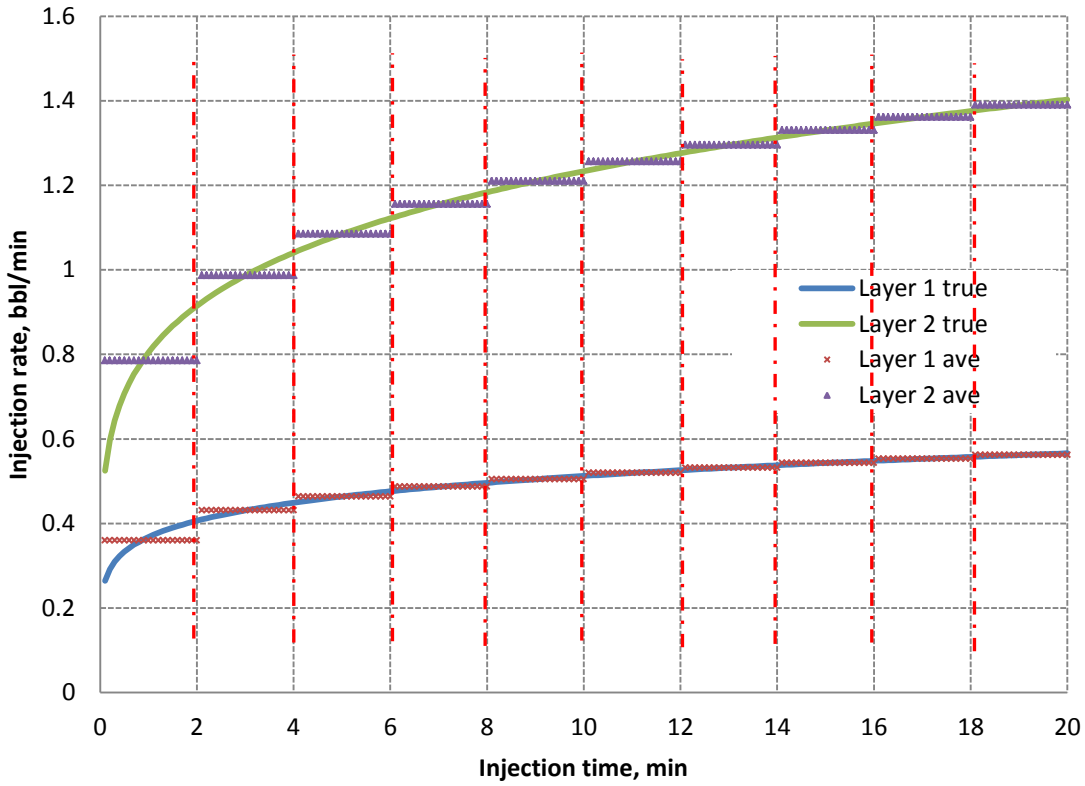

Fig. 4.2—True injection rate profiles and average injection rate of each time period for the case with constant pressure injection

After several trials, we find out that 10 sections for each layer give us acceptable results with reasonable computational time. Using this approach, there are 20 parameters for this two-layer example (10 parameters for each layer). If we define the average rate for each time period as integrating the true distribution over the time period and then dividing by the length of the corresponding time period, the expected result from the

inversion model is that for each time period, the inverted rate is close to the average rate for this period, which will give us a good estimation of the injected acid volume for each layer. The inversion results are shown in **Fig. 4.3**. From Fig. 4.3, although the inverted injection rate for each time period does not match the average injection rate perfectly, the error is small. Thus, we can expect that the inverted volume for each layer can match the true value very well. **Table 4.1** summarizes the inversion results. We invert the injection volume for each layer with little error. The error is introduced by dividing the injection rate history into 10 time periods and approximating the injection rate profile for each time period with one constant injection rate. The match of temperature profiles after running the inversion model is shown in **Fig. 4.4**.

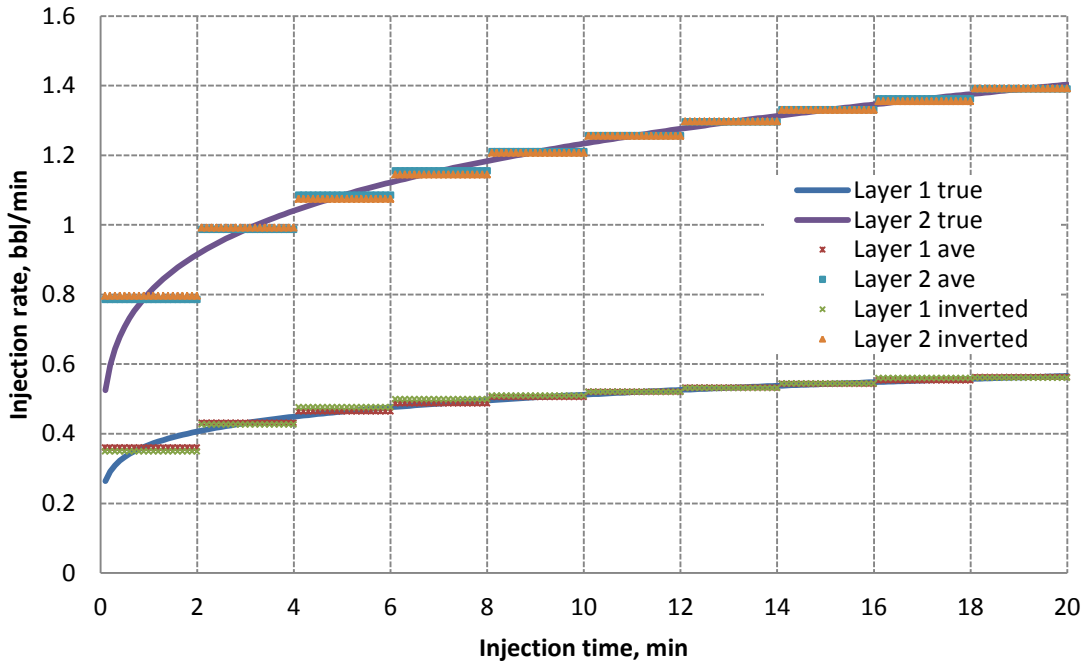

Fig. 4.3—True injection rate profiles, average injection rates and inverted injection rates for the case with constant pressure injection

TABLE 4.1—VOLUME MATCH FOR CONSTANT PRESSURE INJECTION CASE		
	Layer 1	Layer 2
True volume, bbl	9.91	23.72
Inverted volume, bbl	9.95	23.68
Error, %	0.4%	0.2%

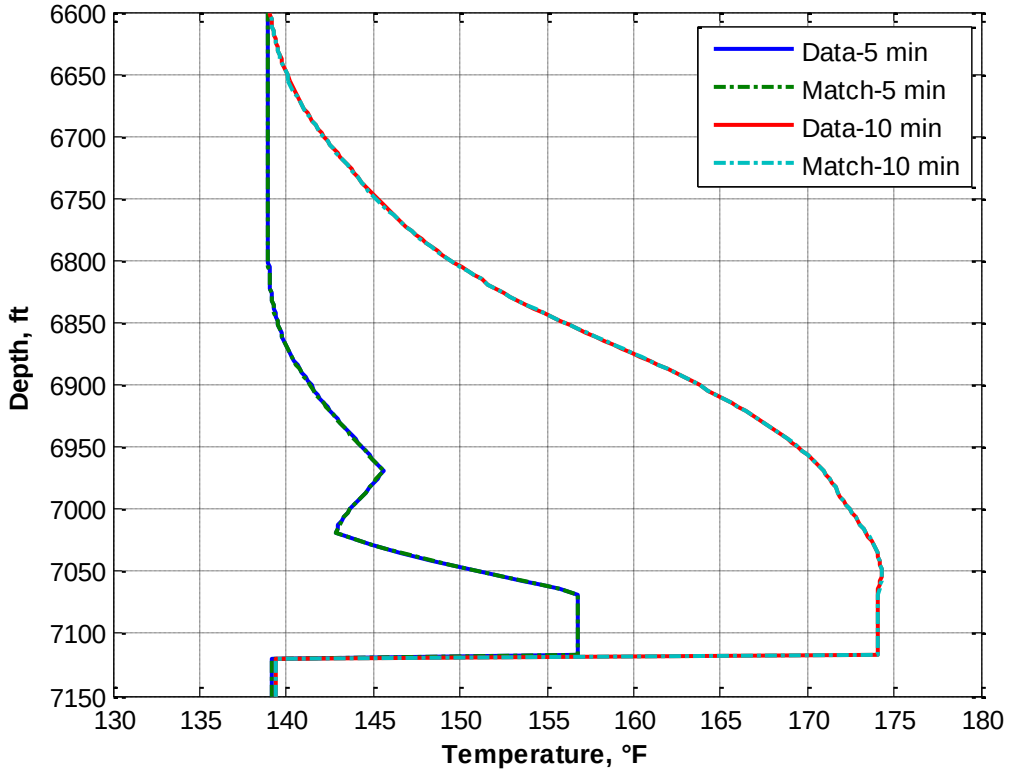

Fig. 4.4—Match between forward-model-calculated temperature profiles and temperature data after running inverse model for the case with constant pressure injection

4.3.2 Inversion Results for Layer Properties

Besides using temperature data to invert the injection distribution, we can apply the inverse model to determine layer properties from temperature measurements, such as permeability, damaged permeability and damage radius. We extended our forward

model by adding the relation between the layer properties and acid distribution (Eq. 2.76 to Eq. 2.80). We still use the previous two layer example, with acid temperature of 139 °F and geothermal temperature of 170.3 °F.

Figure 4.5 shows the measured temperature data and calculated temperature profile with initial guess of layer properties. The mismatch in Fig. 4.5 is significant. The simulated temperature is not able to catch the temperature anomaly in the measured data. **Fig. 4.6** shows the match of temperature profiles after running the inverse model. The temperature profiles calculated by forward model now capture the existence of the temperature anomaly as well as the shape and location. Besides, the forward model results give us an almost perfect match of temperature, which indicates that the estimation of layer properties should be accurate. **Table 4.2** summarizes the comparison between inverted layer properties and true values as well as the initial guess. We can see that after running the inversion model, the inverted layer properties for each layer agree with the true values. This extends the application of our temperature model in the field.

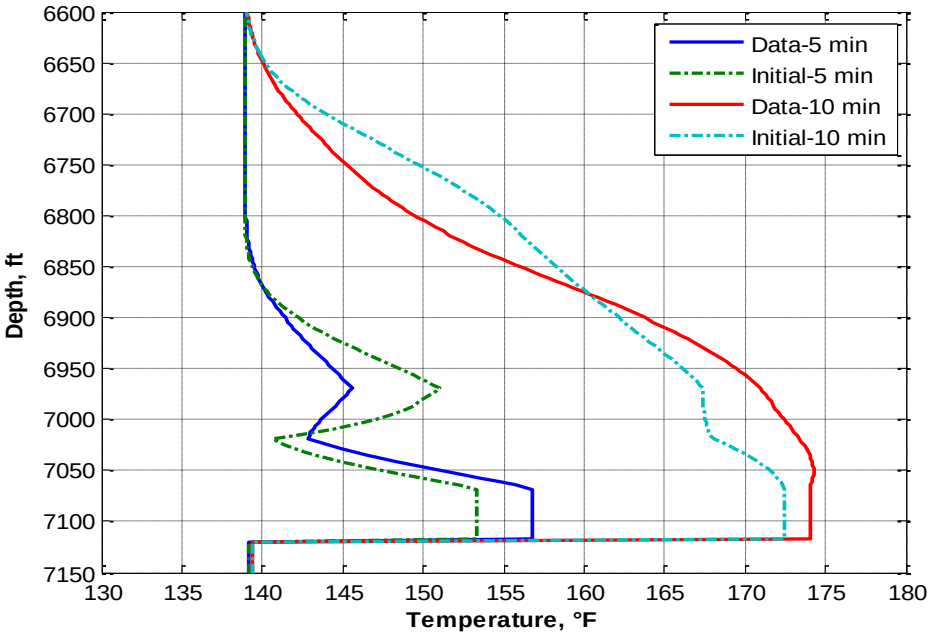

Fig. 4.5— Comparison of temperature profiles calculated with initial guess and temperature data for inversion of layer properties

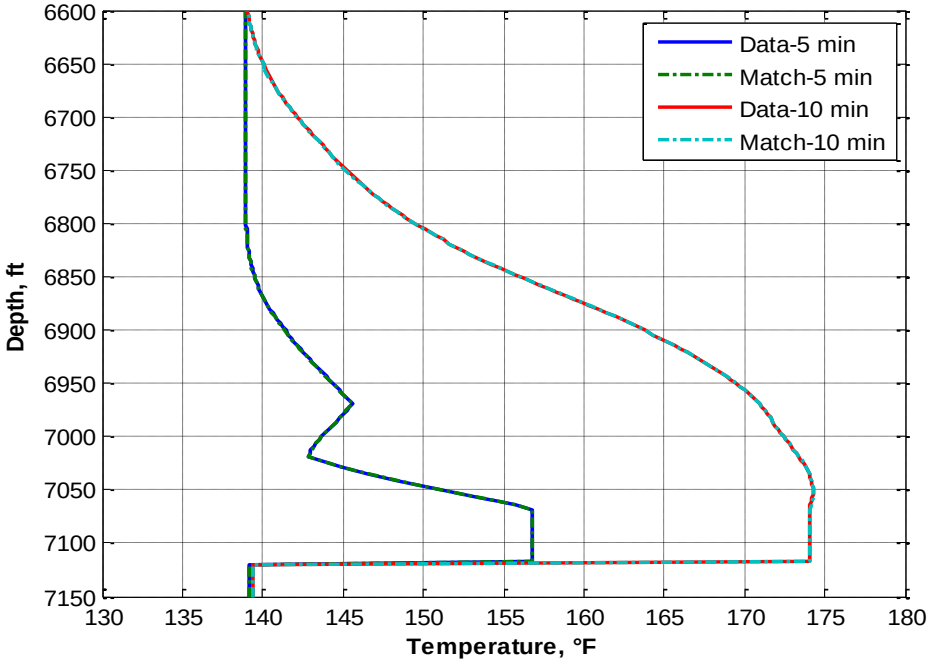

Fig. 4.6— Match between forward-model-calculated temperature profiles and temperature data after running inverse model for inversion of layer properties

TABLE 4.2—INVERSION RESULTS FOR LAYER PROPERTIES

	r_{s1}, ft	K_{s1}, md	k_1, md	r_{s2}, ft	k_{s2}, md	k_2, md
Initial Guess	2	7	15	2	7	15
True Values	1	5	10	0.5	10	20
Inverted Values	0.97	4.85	10.27	0.52	9.8	19.82
Error	3%	3%	2.7%	4%	2%	0.9%

5. APPLICATION OF DOWNHOLE TEMPERATURE MEASUREMENTS

5.1 Introduction

In the previous sections, we have developed a comprehensive thermal model to predict the temperature in the formation and wellbore during the entire acid stimulation, and a hypothetical example was shown to illustrate the application of the model to interpret the downhole temperature measurements to get the acid distribution or layer properties. In this section, we will apply our model to an actual field case, and help to determine the flow profile for different stages, including the pre-stimulation acid wash and the main acid stage. The results will provide us a quantitative understanding of fluid distribution of each zone during different stages, and help us to confirm the success of the acid treatment and the effectiveness of diversion methods.

The field is located in the Middle East area, and the mineral is mainly calcite. The well was completed as a perforated gas producer. The well was stimulated by matrix acidizing with 20% HCl diversion with 2.375 inches coiled tubing, and the perforations were at 7160 ft -7370 ft and 7400 ft -7500 ft. The bottomhole temperature is 214 °F, and surface temperature is 104 °F. Temperature data is measured during the shut-in period after the acid wash and the main acid stage, and can be used to do the interpretation. The well schematic is shown in **Fig. 5.1**. The inner and outer diameter of casings and tubing are listed in **Table 5.1**. The DTS fiber optic is placed inside the coiled tubing, and attached to the inner wall of the coiled tubing, as shown in **Fig. 5.2**. Other input parameters are summarized in **Table 5.2** and **Table 5.3**.

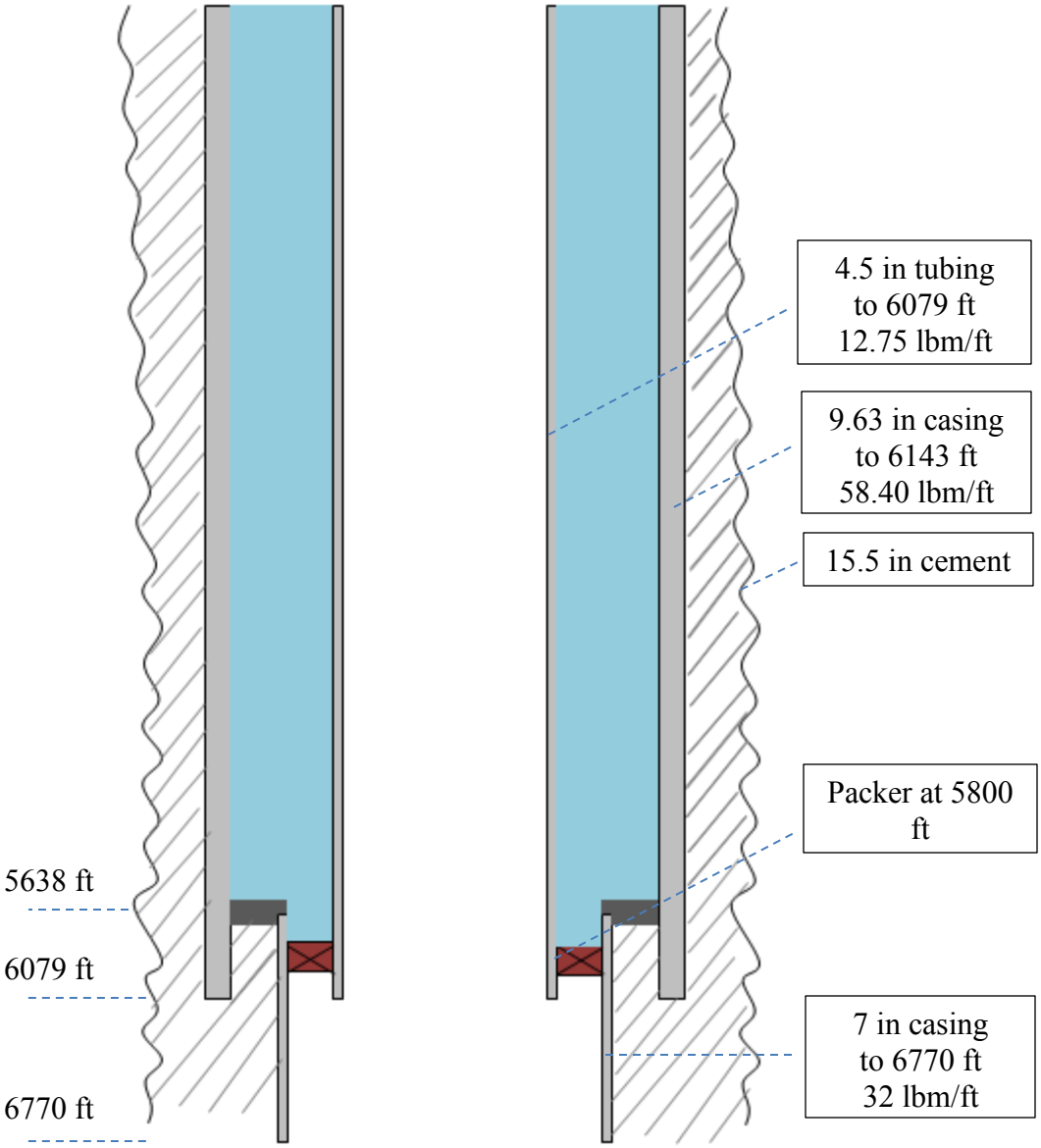

Fig. 5.1—Schematic for a well in the Middle East area

TABLE 5.1—TUBING AND CASING DIAMETERS FOR THE FIELD CASE

	Outer diameter	Inner diameter
4.5 in tubing	4.771 in	4.5 in
7 in casing	7 in	6.094 in
9.63 in casing	9.63 in	8.435 in

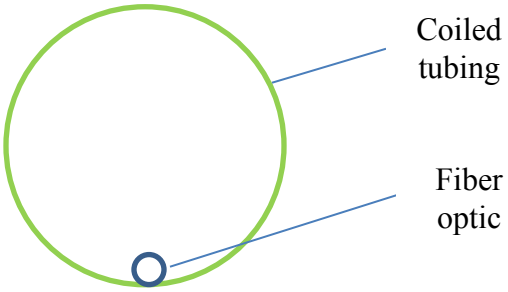

Fig. 5.2—Location of DTS fiber optic

TABLE 5.2—PERFORATION LOCATIONS AND TEMPERATURE FOR THE FIELD CASE		
Perforation intervals	6160-6370	ft
	6400-6500	ft
Bottomhole temperature	214	°F
Surface temperature	104	°F
Geothermal gradient	0.01	°F/ft

TABLE 5.3—INPUT PARAMETERS FOR THE FIELD CASE		
Parameters	Values	Units
C_{HCl}	20%	weight fraction
C_{pR}	1040	J/(kg·K)
C_{ps}	4186.8	J/(kg·K)
M_R	0.1	kg/mol
Q_{reac}	4855	J/(molHCl)
ρ_R	2710	kg/m^3
ρ_s	1080	kg/m^3
$V_{i\text{-}opt}$	0.9	cm/min
$PV_{bt\text{-}opt}$	0.95	fraction
ϕ_i	0.2	fraction

To calculate the heat flux from the formation to the wellbore, the overall heat transfer coefficient for the completion is needed. Due to the injection of acid with the coiled tubing, the heat flux from the formation will go through the completion as well as the coiled tubing. Thus, the coiled tubing also needs to be considered in the calculation of the overall heat transfer coefficient. Since the completion is complicated between 5638 ft and 6079 ft, we separate the completion into three sections: 0 ft – 5638 ft, 5638 ft – 6079 ft and 6079 ft – 6770 ft. Each of these sections has one value for the overall heat transfer coefficient. Eq. 2.38 is applied to calculate these three overall heat transfer coefficients of the completion, and the completion schematics including the coiled tubing for three sections are plotted in **Figs. 5.3-5.5**. In these figures, S means steel, W means water and C means cement. The calculation results are summarized in **Table 5.4**.

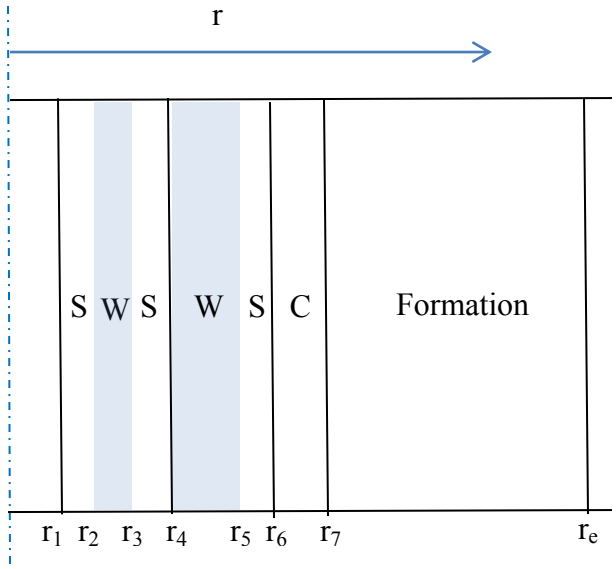

Fig. 5.3—Schematic for the completion and the coiled tubing between 0 ft and 5638 ft

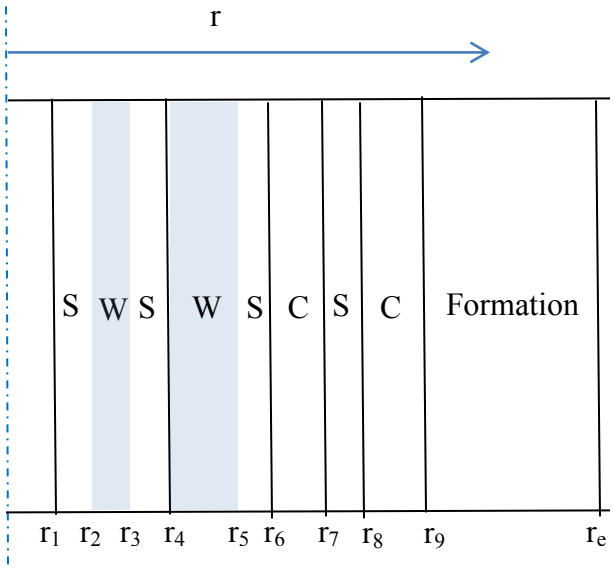

Fig. 5.4—Schematic for the completion and the coiled tubing between 5638 ft and 6079 ft.

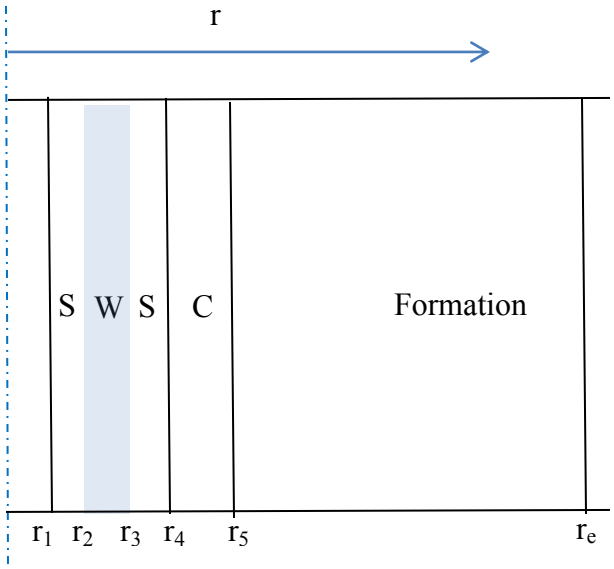

Fig. 5.5—Schematic for the completion and the coiled tubing between 6079 ft and 6770 ft

TABLE 5.4—OVERALL HEAT TRANSFER COEFFICIENTS		
	During injection	During shut-in
0 ft - 5638 ft	19.7 Btu/(hr-ft^2-°F)	14.2 Btu/(hr-ft^2-°F)
5638 ft - 6079 ft	14.6 Btu/(hr-ft^2-°F)	11.3 Btu/(hr-ft^2-°F)
6079 ft - 6770 ft	18.6 Btu/(hr-ft^2-°F)	13.68 Btu/(hr-ft^2-°F)

5.2 Pre-Stimulation Acid Wash

After the preflush stage, the well was washed with 96 barrels of breakdown acid (20% HCl). Then the well was shut down at 21:39. During the shut-in period, the DTS temperature measurements were conducted from 21:53 to 23:05 (72 minutes). In order to determine the acid distribution, we follow the same procedure as for the hypothetical example. The injection rate history is divided into 5 time periods, and we assign the average injection rate for each period to approximate the rate history (**Fig. 5.6**).

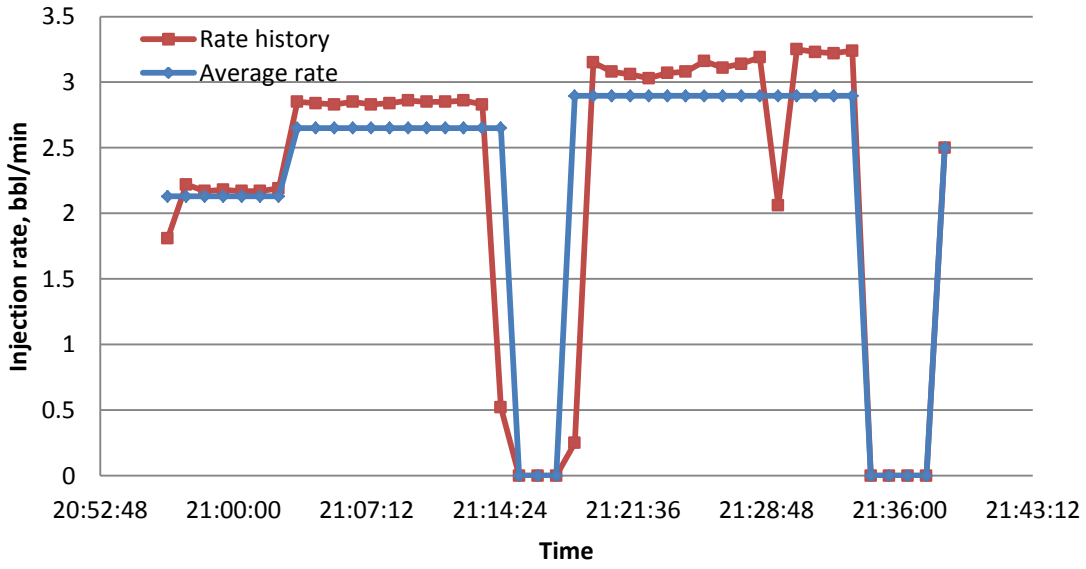

Fig. 5.6—Injection rate history and average injection rates for the acid wash stage

Before the inversion model is applied, the acid temperature in the wellbore when it arrives at the perforated zones needs to be calculated. We apply Ramey's solution (Eq. 2.43) to estimate the injection temperature in the wellbore. The temperature of acid at the surface is 104 °F. The injection temperature profile is plotted in **Fig. 5.7** against the geothermal temperature. This temperature profile is used as the initial condition for the wellbore thermal model during the shut-in period.

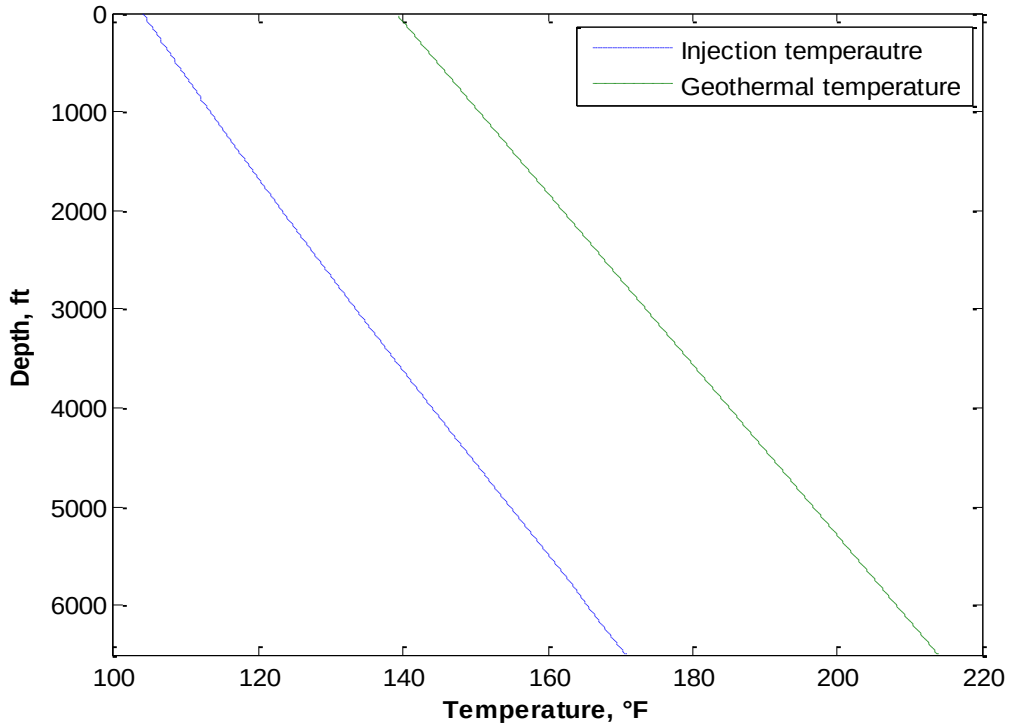

Fig. 5.7—Estimation of acid temperature in the wellbore at the end of injection for the acid wash stage

The DTS data measured at 21:53 and 23:05 is shown in **Fig. 5.8** by red and green curves, respectively. We also plot the wellbore temperature at the beginning of the shut-

in. This temperature profile is the temperature at the end of the injection period. The temperature increase from 21:53 to 23:05 is plotted in **Fig. 5.9**. We can observe that from 5000 ft to 5600 ft, the temperature was warmed back by the geothermal temperature. Between 21:39 and 21:53, the temperature for this section was increased by 3-4 °F, and between 21:53 and 23:05, the temperature for this section was warmed by 8 °F. This normal temperature warm-back will be considered as the base line for the interpretation, and the temperature of other sections will be compared with it. For the section from 5600 ft to 6170 ft, it showed a relative lower temperature at the start of the shut-in period and is warmed back faster from 21:53 to 23:05. The temperature in this section was increased 1-2 °F from 21:39 to 21:53, which is smaller than the temperature increase for the normal warm-back section (5000 ft to 5600 ft). From 21:53 to 23:05, the temperature increase was 13-14 °F, compared with 8 °F for the section from 5000 ft to 5600 ft. The similar temperature behavior can be found for the bottom perforated interval (6400 ft to 6500 ft). The temperature for this section was warmed by 3-4 °F from 21:39 to 21:53, and from 21:53 to 23:05, the temperature increase was 16-17 °F. This temperature behavior indicates the existence of a large amount of acid in these sections. At the beginning of the shut-in period, the wellbore was surrounded by the cold acid, so the temperature was warmed back slowly. During the next 72 minutes of shut-in, the temperature peak caused by reaction in the formation was dispersed and caused a heat flux from the formation towards the wellbore. This heat flux heated up the wellbore fluid and caused a larger temperature increase from 21:53 to 23:05. The temperature profiles indicate that the section from 5600 to 6170 also accepted the acid, although this zone is a

non-perforated section. The acid might flow upwards behind the casing and enter the formation. On the other hand, the top perforation interval (6160 ft to 6370 ft) was showing different temperature behavior. The temperature increase for the top perforated interval was 12-14 °F from 21:39 to 21:53, and from 21:53 to 23:05, the temperature was increased by 8 °F, which is similar to the normal geothermal temperature warm-back during this period of time. The explanation of this temperature behavior is that this zone accepted a small amount of acid. As a result, the acid did not penetrate deeply into the formation. At the beginning of the shut-in period, the temperature caused by reaction inside the formation already had some impact on the wellbore temperature and increased the temperature significantly. From 21:53 to 23:05, the temperature peak in the formation had been completely dispersed, and the wellbore fluid was warmed by the geothermal temperature.

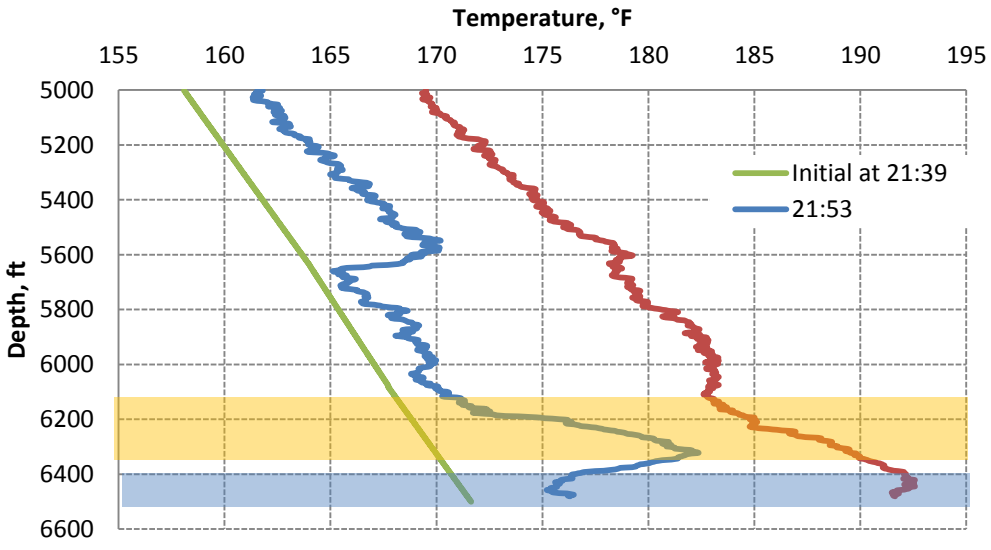

Fig. 5.8—Temperature data during the shut-in period after the acid wash

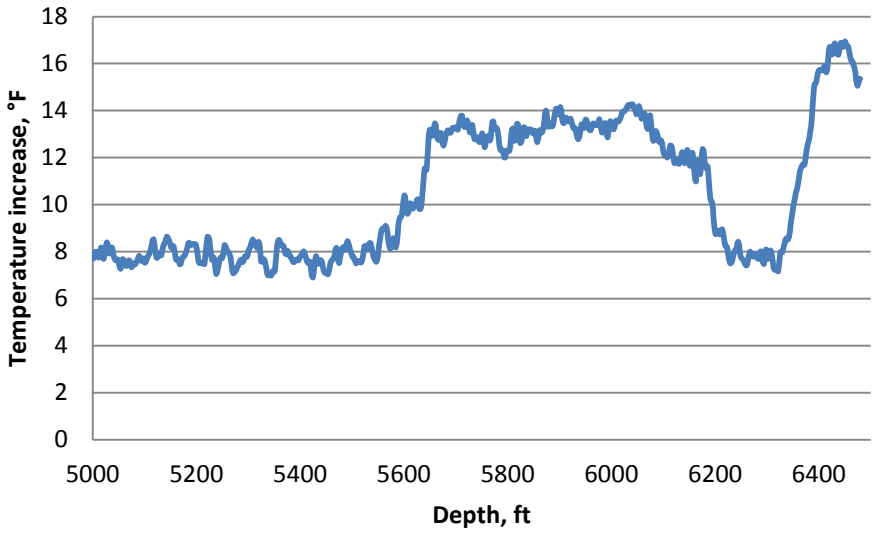

Fig. 5.9—Temperature increase from 21:53 to 23:05 for different depths during the shut-in period after the acid wash

To quantitatively understand the acid distribution, the inversion model developed is applied here, and the match of temperature profiles is plotted in **Fig. 5.10**. To achieve a better match between the calculated temperature and the actual temperature data, we divide the top perforated interval into several small layers. Although the temperature match is not perfect, we capture the characteristic of the temperature behavior for different sections. The percentage of acid for different sections is listed in **Table 5.5**. From the inversion results, 17% of the acid flows into the bottom perforated section, and 9% of the acid is unevenly placed among the top perforated zone. Most of the acid entered the sections from 5600 ft to 6160 ft, indicating that a lot of acid flowed upwards behind the casing and entered this section.

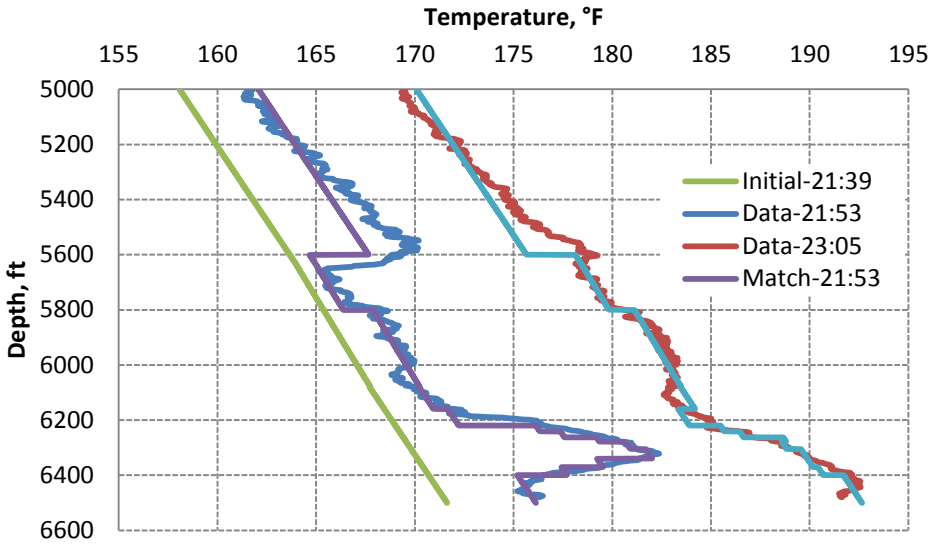

Fig. 5.10—Temperature data and match from 21:53 to 23:05 during the shut-in period after the acid wash

TABLE 5.5—ACID DISTRIBUTION FROM THE INVERSION MODEL FOR THE ACID WASH	
Section	Acid percentage
5600 ft-5800 ft	26%
5800 ft-6160 ft	48%
6160 ft-6370 ft	9%
6400 ft-6500 ft	17%

For better understanding the temperature behavior in the wellbore, we use the inverted acid distribution to calculate the reservoir temperature profiles for different sections at the end of the injection periods, as shown in **Figs. 5.11-5.13**. The temperature behavior in the bottom layer is plotted in Fig. 5.11. We can observe that the acid penetrated into the formation relatively deeper, and the temperature increase caused by reaction was about 10 °F. Therefore, at the beginning of the shut-in period, the

temperature in the well was warmed back slowly, and afterwards, the high temperature peak started to affect the wellbore temperature, causing a faster temperature warm-back. The temperature behavior in the formation for the top layer is plotted in Fig. 5.12. The acid did not penetrate deeply in this layer. When the injection was stopped for a short time, the temperature peak caused by reaction already had effect on the wellbore temperature. Thus, during the first 14 minutes of shut-in period, the temperature in the well for this section was increased significantly. Since the temperature behaviors in the well for the bottom layer and the section from 5600 ft to 5800 ft were similar, so we can expect that the formation temperature at the end of the injection were also similar, as shown in Fig. 5.13. However, in this section, the temperature peak caused by reaction was not as high as that in the bottom layer. The temperature increase from the reaction is about 6 °F, compared with 10 °F for the bottom layers. This is the reason why the wellbore temperature at the bottom layer was increased by 16 °F and the wellbore temperature at the 5600 ft-5800 ft section was increased by 8 °F.

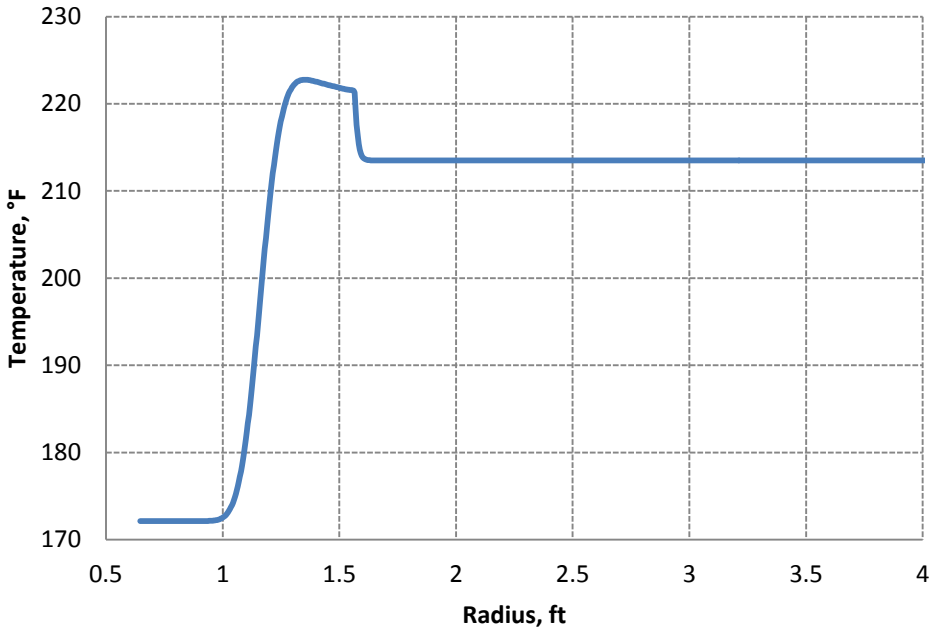

Fig. 5.11—Temperature profile inside the formation for the bottom perforated interval at the end of the acid wash stage

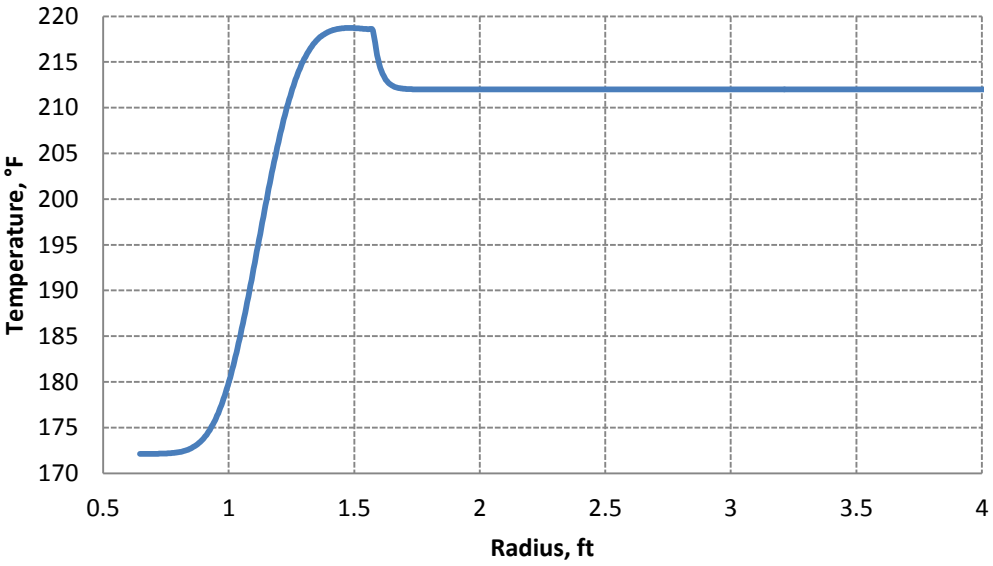

Fig. 5.12—Temperature profile inside the formation for the top perforated interval at the end of the acid wash stage

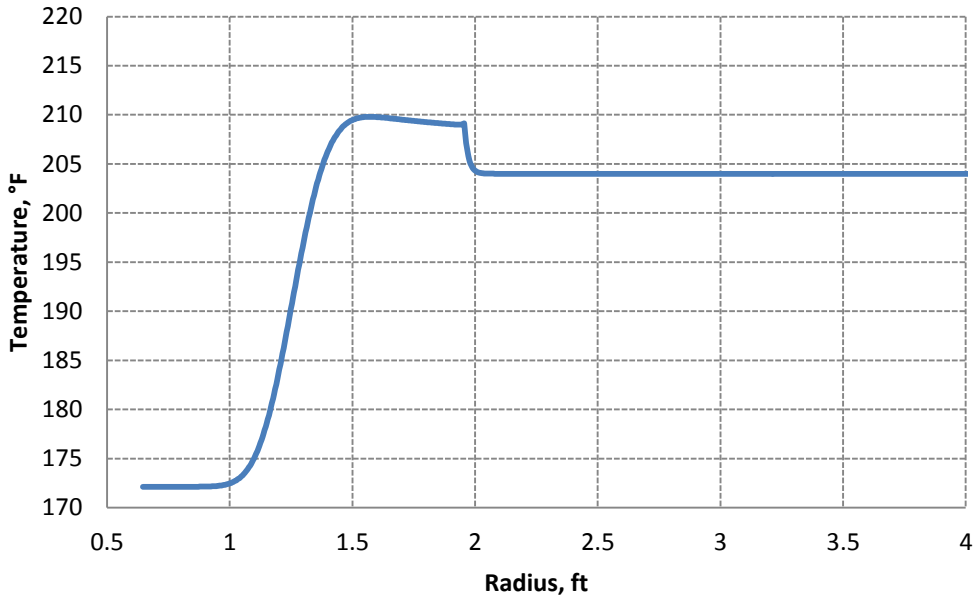

Fig. 5.13—Temperature profile inside the formation for the 5600 ft-5800 ft section at the end of the acid wash stage

5.3 Main Acid Stage

After acid wash, the main stage of acidizing was injected with coiled tubing. In this stage, 156 barrels of acid were pumped. The pumping stopped at 5:15 and the temperature data was measured during the following shut-in period from 5:59 to 7:10. We follow the same analysis procedure as for the pre-stimulation acid wash section. Based on the injection rate history, we also divide it into 3 time periods. For each time period, average injection rate for this time period is used to approximate the rate history (**Fig. 5.14**). The acid temperature in the well before it enters the formation is calculated with Ramey's equation. The injection temperature profile as a function of wellbore depth

is shown in **Fig. 5.15**, and this temperature profile is used as the initial condition for the wellbore model during the shut-in period.

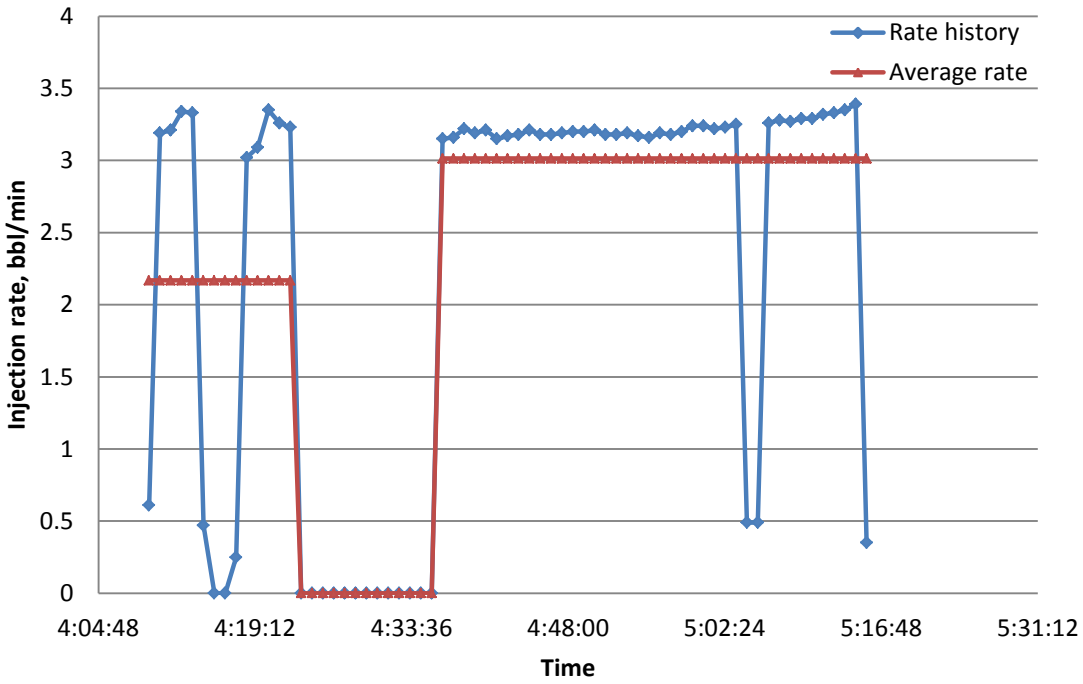

Fig. 5.14—Injection rate history and average injection rates for the main acid stage

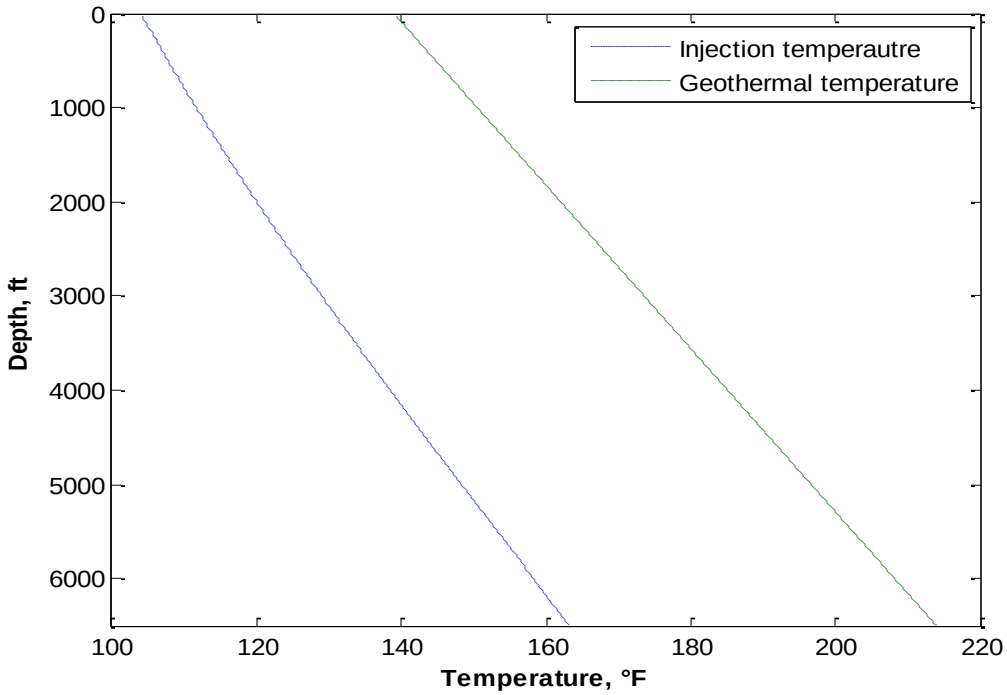

Fig. 5.15—Estimation of acid temperature in the wellbore at the end of injection for the main acid stage

The temperature data at 5:59 and 7:10 are plotted in **Fig. 5.16**. The initial temperature profile in the wellbore at 5:15 is also shown in green curve. The increase of the temperature from 5:59 to 7:10 is shown in **Fig. 5.17**. We can observe that from 5000 ft to 5400 ft, the fluid in the well was warmed by the geothermal temperature. Between 5:15 and 5:59, the temperature for this section was increased by 6 °F, and between 5:59 and 7:10, the temperature was increased by 8-9 °F. For the section from (5400 ft to 5800 ft) and the two perforated intervals, the temperature showed a relatively larger temperature increase (9 °F and 18 °F) compared with the normal geothermal temperature warm-back from 5:15 to 5:59. From 5:59 to 7:10, the temperature of these sections is

only increased by 8 °F, which is similar to the geothermal temperature warm-back during this time period. This temperature behavior is because the effect of reaction inside the formation heated up the wellbore fluid during the first 44 minutes shut-in period. During the next 71 minutes of shut-in, since the effect of reaction had been completely dispersed, the temperature increase was only due to the geothermal temperature warm-back. On the other hand, the section between 5800 ft and 6160 ft had different temperature behaviors. After the first 44 minutes of shut-in, the temperature increase was relatively small (6-7 °F). From 5:59 to 7:10, the temperature warm-back was about 12 °F. The interpretation is that in these zones, the acid penetrated deeper into the formation. At the beginning of the shut-in period, the warm-back was slower due to the cold acid surrounding the wellbore. If the wellbore was shut down for longer time, the temperature peak caused by heat of reaction in the formation would generate a heat flux towards the wellbore and increased the wellbore temperature significantly.

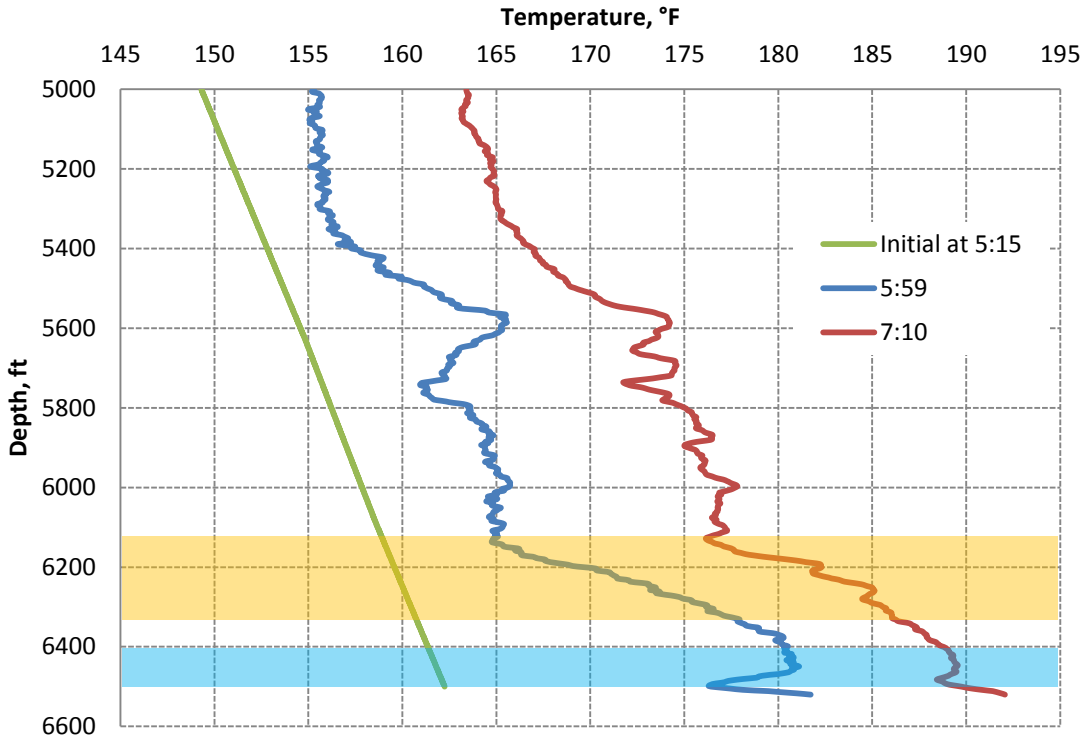

Fig. 5.16—Temperature data during the shut-in period after the main acid stage

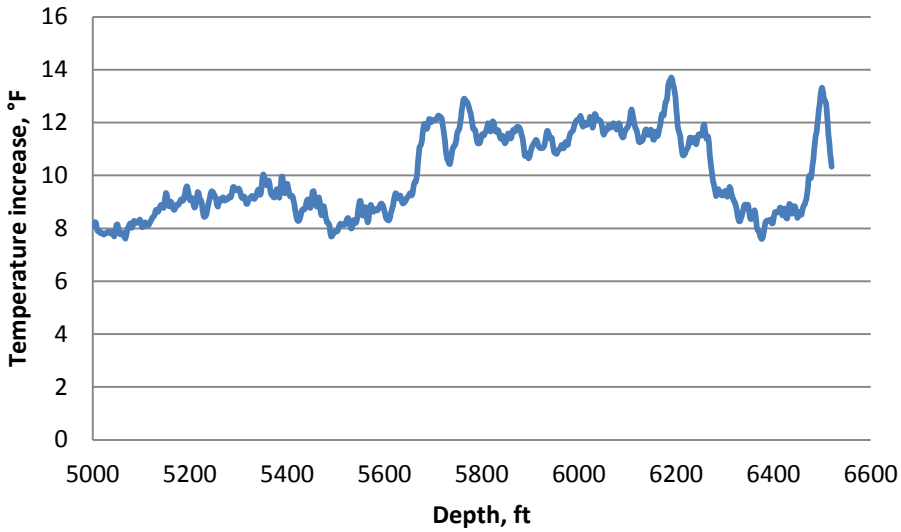

Fig. 5.17—Temperature increase from 5:59 to 7:10 for different depths during the shut-in period after the main acid stage

By applying our inversion model, we can match the temperature data with our forward model (the green and purple curves), as shown in **Fig. 5.18**. We also divide the top perforated interval and the section from 5400 ft to 6160 ft into several small intervals to get a better temperature match. After running the inversion mode, the quantitative analysis of these temperature data is shown in **Table 5.6**. 20% of the acid was injected into the bottom perforated zone and 12% of the acid entered the top perforated interval. The rest of the acid was distributed among the section between 5400 ft to 6170 ft, indicating that most of the acid was flowing upward behind the casing and entered this section.

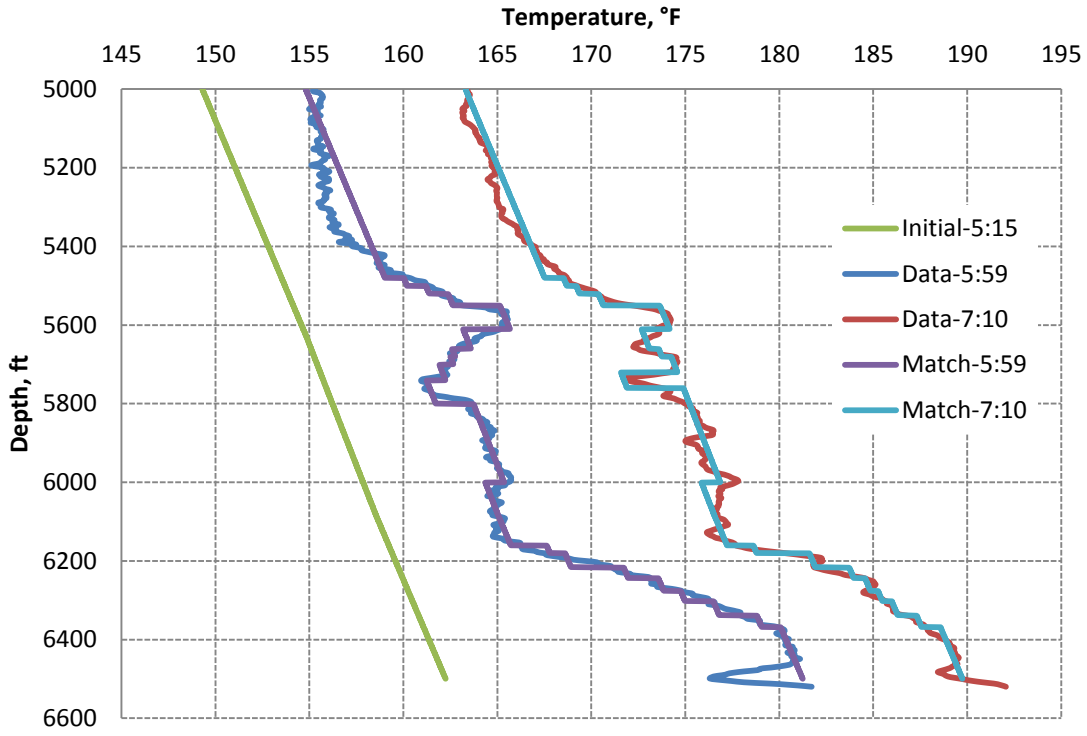

Fig. 5.18—Temperature data and match from 5:59 to 7:10 during the shut-in period after the main acid stage

TABLE 5.6—ACID DISTRIBUTION FROM THE INVERSION MODEL FOR THE MAIN ACID STAGE	
Section	Acid percentage
5400 ft-5800 ft	26%
5800 ft-6160 ft	42%
6160 ft-6370 ft	12%
6400 ft-6500 ft	20%

We use the inverted acid distribution to calculate the reservoir temperature profiles for different sections at the end of the injection periods, as shown in **Figs. 5.19 and 5.20**. The temperature behavior in the bottom layer is plotted in Fig. 5.18. We can observe that the temperature increase caused by reaction was about 12 °F. Therefore, during the first 44 minutes of shut-in, the temperature in the well was warmed back significantly. From 5:59 to 7:10, the high temperature peak was dispersed and the effect of reaction diminished. The geothermal temperature caused a relatively slower temperature warm-back from 5:59 to 7:10. The temperature behavior in the formation for the section from 5800 ft to 6000 ft is plotted in Fig. 5.19. The acid penetrated deeply in this layer. When the injection was stopped for a short time, the wellbore was surrounded by a large amount of the cold acid. Therefore, the wellbore temperature was heated slowly. After another 71 minutes of shut-in, the temperature peak caused by reaction had effect on the wellbore temperature and increased the wellbore temperature much faster.

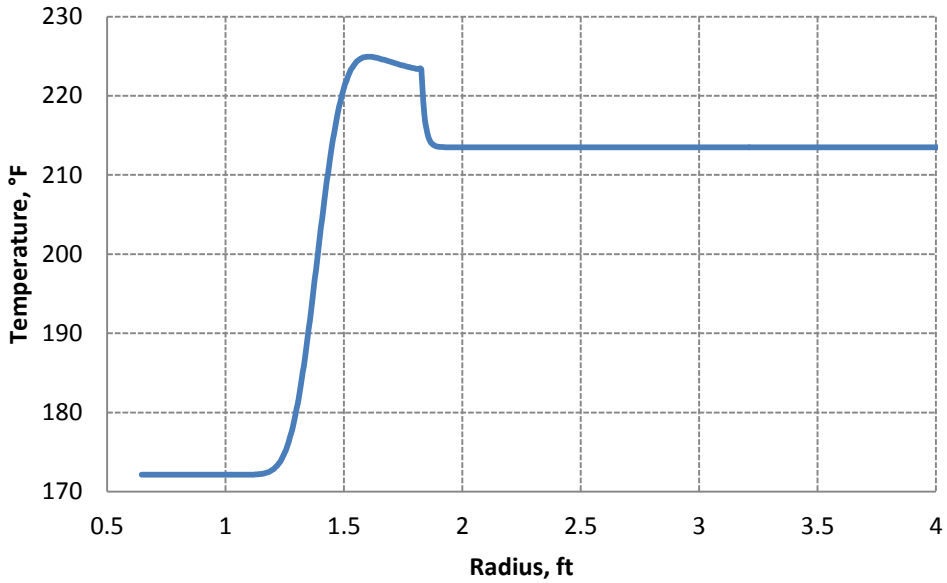

Fig. 5.19—Temperature profile inside the formation for the bottom perforated interval at the end of the main acid stage

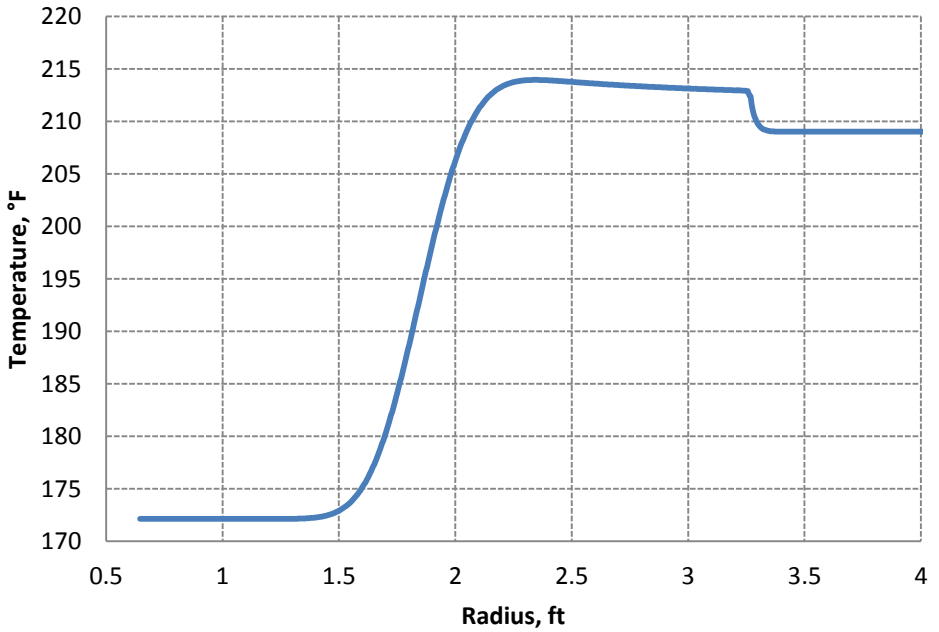

Fig. 5.20—Temperature profile inside the formation for the 5800 ft-6000 ft interval at the end of the main acid stage

6. CONCLUSIONS

We have developed thermal models to simulate the temperature behavior in the formation and along the wellbore during the entire acid treatments, including acid injection period, shut-in period and flow-back period. This forward model consists of a formation thermal model and a wellbore thermal model considering the effects of both mass and heat transfer in the wellbore and the formation. The model simulates all significant thermal processes involved during a treatment, including heat of reaction, conduction and convection. Furthermore, we extend our forward model to calculate the temperature behaviors with given layer properties, since the acid distribution is dependent on permeability, damaged permeability and damaged radius. Then, an inverse model was developed to interpret the acid injection distribution or layer properties from the measured temperature data. We evaluated both gradient-based and stochastic inversion methods and found out that for this case, stochastic methods are more reliable. Therefore, we implemented an MCMC inversion algorithm as the inversion model. The method has been applied to hypothetical examples as well as the field cases. With the inversion model, we determine the acid distribution as well as layer properties. It is concluded from this study that

1. Temperature measurements contain enough information to determine the acid distribution or layer properties during an acid treatment.
2. During acid injection, due to the fast reaction of acid and carbonate rock, a large amount of reaction heat is released, causing a temperature anomaly in the formation.

3. During shut-in or flow-back, the temperature anomaly caused by heat of reaction will change the temperature profile in the wellbore. For shut-in, the zone that has taken more acid will show a lower temperature in the wellbore at the beginning. Then, because of the temperature anomaly in the formation, the fluid in the well will be heated up much faster. For flow-back, the fluid in the formation with higher temperature will flow into the well, and mix with the fluid flowing inside the well. Although mixing will disperse the temperature signal, the temperature peak still can be detected in the wellbore. Besides, the wellbore temperature at the depth of production layers during flow-back is also related to the amount of acid that has been injected into the layer. The layer that accepts more acid will show a higher temperature in the wellbore. These unique thermal phenomena enable the interpretation of acid distribution.
4. Furthermore, layer properties can be determined from the temperature measurements as well by applying the extended forward model. This is helpful to understand the formation conditions, and can be compared with well logging results.
5. Finally, by applying this method to field examples, it can help us to quantitatively understand the acid distribution and evaluate the effectiveness of an acid treatment.

REFERENCES

Buijse, M.A. and Glasbergen, G. 2006. A Semi-Empirical Model to Calculate Wormhole Growth in Carbonate Acidizing. Paper SPE 96892 presented at the SPE Annual Technical Conference and Exhibition, Dallas, Texas, 9-12 October.

Carnahan, B.D., Clanton, R.W., Koehler, K.D., Harkins, G.O. and Williams, G.R. 1999. Fiber Optic Temperature Monitoring Technology. Paper SPE 54599 presented at the SPE Western Regional Meeting, Anchorage, Alaska, 26-28 May.

Clanton, R.W., Haney, J.A., Pruett, R., Wahl, C.L., Goiffon, J.J. and D. Gualtieri, D. 2006. Real-Time Monitoring of Acid Stimulation Using a Fiber-Optic DTS System. Paper SPE 100617 presented at the SPE Western Regional/AAPG Pacific Section/GSA Cordilleran Section Joint Meeting, Anchorage, Alaska, 8-10 May.

Economides, M.J., Hill, A.D. and Ehlig-Economides, C. 1994. *Petroleum Production Systems*. Upper Saddle River, New Jersey: Prentice Hall, Inc.

Gao, G. and Jalali, Y. 2005. Interpretation of Distributed Temperature Data During Injection Period in Horizontal Wells. Paper SPE 96260 presented at the SPE Annual Technical Conference and Exhibition, Dallas, Texas, 9-12 October.

Glasbergen, G., Gualtieri, D., Trehan, R., Van Domelen, M. and Nelson, M. 2007. Real-Time Diversion Quantification and Optimization Using DTS. Paper SPE 110707 presented at the SPE Annual Technical Conference and Exhibition, Anaheim, California, 11-14 November.

Glasbergen, G., Gualtieri, D., Van Domelen, M. and Sierra, J. 2009. Real-Time Fluid Distribution Determination in Matrix Treatments Using DTS. *SPE Prod & Oper* **24** (1): 135-146. SPE-107775-PA.

Hasan, A.R. and Kabir, C.S. 2002. *Fluid Flow and Heat Transfer in Wellbores*. Richardson, Texas: Society of Petroleum Engineering.

Hastings, W.K. 1970. Monte Carlo Sampling Methods Using Markov Chains and Their Applications. *Biometrika* **57**(1): 97-109

Huckabee, P. 2009. Optic Fiber Distributed Temperature for Fracture Stimulation Diagnostics and Well Performance Evaluation Paper SPE 118831 presented at SPE Hydraulic Fracturing Technology Conference, The Woodlands, Texas, 19-21 January.

Izgec, B., Kabir, C. S., Zhu, D. and Hasan, A. R. 2006. Transient Fluid and Heat Flow Modeling in Coupled Wellbore/Reservoir Systems. *SPE Res Eval & Eng* **10** (3): 294-301. SPE-102070-PA.

Johnson, D., Sierra, J., Kaura, J. and Gualtieri, D. 2006. Successful Flow Profiling of Gas Wells Using Distributed Temperature Sensing Data. Paper SPE 103097 presented at SPE Annual Technical Conference and Exhibition, San Antonio, Texas, USA, 24-27 September.

Johnson, D.O., Sugianto, R., Mock, P.H. and Jones, C.H. 2004. Identification of Steam-Breakthrough Invervals with DTS Technology. *SPE Prod & Oper* **19**(1): 41-48. SPE-87631-PA.

Li, Z. and Zhu, D. 2009. Predicting Flow Profile of Horizontal Wells by Downhole Pressure and DTS Data for infinite Waterdrive Reservoir. Paper SPE 124873 presented at the SPE Annual Technical Conference and Exhibition, New Orleans, Louisiana, 4-7 October.

Marquardt, D.W. 1963. An Algorithm for Least-Squares Estimation of Nonlinear Parameters. *Journal of the Society for Industrial and Applied Mathematics* **11** (2): 431-441.

McAdams, W.H. 1942. *Heat Transmission*, 135-137. New York and London: McGraw-Hill Book Co.

Medeiros, F. and Trevisan, O.V. 2006. Thermal Analysis in Matrix Acidization. *Journal of Petroleum Science and Engineering*. **51** (1-2): 85-96.

Metropolis, N., Rosenbluth, A,W., Rosenbluth, M.N., Teller, A.H. and Teller, E. 1953. Equations of State Calculations by Fast Computing Machines. *Journal of Chemical Physics* **21** (6): 1087-1092.

Ochi, I.A., Li, Z., Zhu, D. and Hill, A.D. 2008. An Interpretation Method of Downhole Temperature and Pressure Data for Flow Profiles in Gas Wells. Paper SPE 116292 presented at the SPE Russian Oil & Gas Technical Conference and Exhibition, Moscow, Russia, 28-30 October.

Ouyang, L.-B. and Belanger, D. 2004. Flow Profiling via Distributed Temperature Sensor (DTS) System-Expectation and Reality. Paper SPE 90541 presented at the SPTE Annual Technical Conference and Exhibition, Houston, Texas, 26-29 September.

Perry, R.H., Green, D.W. and Maloney, J.O. 1963. *Perry's Chemical Engineers' Handbook*, 226-231. New York: McGraw-Hill Book Co.

Ramey, H.J. Jr. 1962. Wellbore Heat Transmission. *J. Pet Tech* **14** (4): 427-435; *Trans.*, AIME, 225. SPE-96-PA.

Sui, W., Zhu, D., Hill, A. D. and Ehlig-Economides, C. A. 2008. Determining Multilayer Formation Properties From Transient Temperature and Pressure Measurements. Paper SPE 116270 presented at SPE Annual Technical Conference and Exhibition, Denver, Colorado, USA, 21-24 September.

Tolan, M., Boyle, M. and William, G. 2001. The Use of Fiber-Optic Distributed Temperature Sensing and Remote Hydraulically Operated Interval Control Valves for the Management of Water Production in Douglas Field. Paper SPE 71676 presented at the SPE Annual Technical Conference and Exhibition, New Orleans, Louisiana, 30 September-3 October.

Wang, X., Lee, J., Thigpen, B., Vachon, G., Poland, S., and Norton D. 2008. Modeling Flow Profile Using Distributed Temperature Sensor (DTS) System. Paper SPE 111790 presented at the Intelligent Energy Conference and Exhibition, Amsterdam, The Netherlands, 25-27 February.

Wadsley, A.W. 2005. Markov Chain Monte Carlo Methods for Reserves Estimation. Paper SPE 10065 presented at the International Petroleum Technology Conference, Doha, Qatar, 21-23 November.

Yoshioka, K., Zhu, D., Hill, A. D., Dawkrajai, P. and Lake, L. W. 2005. A Comprehensive Model of Temperature Behavior in a Horizontal Well. Paper SPE 95656 presented at SPE Annual Technical Conference and Exhibition, Dallas, Texas, 9-12 October.

VITA

Name: Xuehao Tan

Address: Harold Vance Department of Petroleum Engineering

Texas A&M University

3116 TAMU-Richardson Building

College Station, TX 77843

Email Address: tanxh03@gmail.com

Education: B.E., Engineering Thermal Dynamics, Tsinghua University, Beijing, China, July 2007

M.S., Petroleum Engineering, Texas A&M University, Texas, USA, May 2009

Ph.D., Petroleum Engineering, Texas A&M University, Texas, USA, August 2012